University of Neuchâtel
Faculty of Science

Centre for Hydrogeology
and Geothermics

Ph.D. Thesis

Riverbank Filtration within the Context of River Restoration and Climate Change

presented to the Faculty of Science of the University of Neuchâtel to satisfy the requirements of the degree of Doctor of Philosophy in Science

by

Samuel Diem

Thesis defense date: 20.08.2013

Public presentation date: 19.09.2013

Ph.D. Thesis evaluation committee:

Prof. Dr. Daniel Hunkeler, University of Neuchâtel (Director of the thesis)

Prof. Dr. Mario Schirmer, University of Neuchâtel (Co-director of the thesis)

Prof. Dr. Philippe Renard, University of Neuchâtel

Prof. Dr. John Molson, University Laval, Québec, Canada

IMPRIMATUR POUR THESE DE DOCTORAT

La Faculté des sciences de l'Université de Neuchâtel autorise l'impression de la présente thèse soutenue par
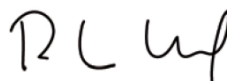
Monsieur Samuel DIEM

Titre:

"Riverbank Filtration within the Context of River Restoration and Climate Change"

sur le rapport des membres du jury:

- Prof. Daniel Hunkeler, Université de Neuchâtel, directeur de thèse
- Prof. ass. Mario Schirmer, Université de Neuchâtel, co-directeur de thèse
- Prof. Philippe Renard, Université de Neuchâtel
- Prof. John Molson, Université Laval, Québec, Canada

Neuchâtel, le 9 septembre 2013   Le Doyen, Prof. P. Kropf

Acknowledgments

Abstract

Drinking water derived by riverbank filtration is generally of high quality and is an important source of drinking water in several European countries. In the future however, riverbank-filtration systems will face two major challenges – river restoration and climate change. The goal of this Ph.D. Thesis was to deepen the understanding of physical and biogeochemical processes that occur during riverbank filtration and develop new tools in order to facilitate the assessment of potential adverse effects of river restoration and climate change on the quality of river-recharged groundwater.

River restoration measures can lead to shorter residence times between the river and the pumping well and therefore can increase the risk of drinking water contamination by bacteria or pollutants. Numerical groundwater models provide quantitative information on groundwater flow paths and residence times, but require a rigorous definition of the spatial and temporal river water level distribution. In this thesis, two new interpolation methods were developed to generate time-varying 1D and 2D river water level distributions. The methods were implemented at the partly restored Niederneunforn field site at the peri-alpine Thur River (NE-Switzerland), and were applied to a 3D groundwater flow and transport model. The results confirmed the method's suitability for accurately simulating groundwater flow paths and residence times.

The increased occurrence of heat waves due to climate change likely favors the development of anoxic conditions in the infiltration zone, which may significantly deteriorate the quality of river-recharged groundwater. Results from field sampling campaigns and column experiments suggest that particulate organic matter (POM) degradation mainly accounted for the variability of dissolved oxygen (DO) consumption during riverbank filtration. Furthermore, DO consumption was found to positively correlate with temperature and discharge. The latter was attributed to an enhanced trapping of POM within the riverbed during high-discharge conditions. To quantify the temperature and discharge dependence of DO consumption during riverbank filtration, a new semi-analytical model was developed and successfully applied to the Niederneunforn field site. The modeling approach can be transferred to other riverbank-filtration systems to efficiently estimate groundwater DO concentrations under various climatic and hydrologic conditions and, hence, to assess the risk of arising anoxic conditions.

Kurzfassung

Mittels Uferfiltration gewonnenes Trinkwasser ist generell von hoher Qualität und stellt eine wichtige Trinkwasserressource für mehrere europäische Länder dar. In der Zukunft werden Uferfiltrationssysteme jedoch mit zwei bedeutenden Herausforderungen konfrontiert – Flussrevitalisierung und Klimaänderung. Das Ziel dieser Doktorarbeit war es, das Verständnis physikalischer und biogeochemischer Prozesse während der Flussinfiltration zu vertiefen und Instrumente zu entwickeln, um potentielle negative Auswirkungen von Flussrevitalisierung und Klimaänderung auf die Qualität des Uferfiltrats besser zu erfassen.

Massnahmen der Flussrevitalisierung können zu verkürzten Fliesszeiten zwischen Fluss und Trinkwasserfassung führen, was das Risiko einer Trinkwasserkontamination mit Bakterien und Schadstoffen erhöhen kann. Numerische Grundwassermodelle liefern quantitative Informationen über Grundwasserfliesspfade und Fliesszeiten, benötigen aber eine genaue Definition der räumlichen und zeitlichen Flusswasserstandsverteilung. In dieser Arbeit wurden zwei neue Interpolationsmethoden entwickelt, um zeitlich variable 1D und 2D Flusswasserstandsverteilungen zu generieren. Die Methoden wurden am teilweise revitalisierten Feldstandort Niederneunforn am voralpinen Fluss Thur (Nordostschweiz) implementiert und auf ein 3D Grundwasserströmungs- und Transportmodell angewandt. Die Resultate bestätigten die Eignung der Methoden zur präzisen Simulation von Grundwasserfliesspfaden und Fliesszeiten.

Das vermehrte Auftreten von Hitzewellen aufgrund der Klimaänderung begünstigt möglicherweise die Ausbildung anoxischer Verhältnisse in der Infiltrationszone, was die Qualität des Uferfiltrats deutlich verschlechtern würde. Die Resultate aus Feldprobennahmen und Säulenversuchen deuten darauf hin, dass der Abbau von partikulärem organischem Material (POM) hauptsächlich für die Variabilität der Sauerstoffzehrung während der Flussinfiltration verantwortlich war. Zusätzlich wurde eine positive Korrelation zwischen der Sauerstoffzehrung und der Temperatur sowie dem Abfluss festgestellt. Letztere wurde einem erhöhten Eintrag von POM in das Flussbett während Hochwasserbedingungen zugeschrieben. Um die Temperatur- und Abflussabhängigkeit der Sauerstoffzehrung während der Flussinfiltration zu quantifizieren, wurde ein neues semi-analytisches Modell entwickelt und erfolgreich am Feldstandort Niederneunforn angewandt. Der Modellansatz lässt sich auf weitere Uferfiltrationssysteme übertragen, um Sauerstoffkonzentrationen im Grundwasser effizient abzuschätzen, und somit das Risiko aufkommender anoxischer Bedingungen zu beurteilen.

Résumé

L'eau de consommation provenant de la filtration sur berge est généralement de bonne qualité et constitue une source d'eau potable dans plusieurs pays de l'Union Européenne. A l'avenir pourtant, la filtration sur berge devra faire face à deux défis majeurs: les programmes de restauration de rivière et les changements climatiques. La présente thèse vise, d'une part, à approfondir la compréhension des processus physiques et biogéochimiques liés à la filtration sur berge et, d'autre part, à développer de nouveaux outils pour évaluer les impacts potentiels des programmes de restauration et des changements climatiques sur la qualité de l'eau souterraine provenant de ces techniques de filtration.

Les mesures de restauration de rivière peuvent conduire à un raccourcissement des temps de résidence de l'eau entre la rivière et le puits de pompage, et ainsi augmenter les risques de contamination chimique et microbiologique. La modélisation hydrodynamique est une approche quantitative privilégiée pour identifier les chemins d'écoulements souterrains et quantifier les temps de résidence; elle requiert cependant une définition rigoureuse de la variabilité spatiale et temporelle des niveaux de rivière. Dans cette thèse, deux méthodes d'interpolation sont développées pour générer une représentation temporelle adéquate des niveaux de rivières en 1D et 2D. Ces méthodes sont testées sur le site expérimental et partiellement restauré de Niederneunforn (NE de la Suisse), situé sur la rivière préalpine Thur, et sont implémentées dans un modèle numérique d'écoulement et de transport souterrain 3D. Les résultats confirment la pertinence de ces méthodes pour la simulation précise des chemins d'écoulements et des temps de résidence.

Avec les changements climatiques, l'augmentation de la fréquence des vagues de chaleur favorisera probablement le développement de conditions anoxiques dans les zones d'infiltration de la rivière, ce qui tendra à détériorer la qualité de l'eau souterraine rechargée par filtration de berge. Les résultats de campagnes d'échantillonnage et d'expériences sur colonne suggèrent que la dégradation de la matière organique particulaire (MOP) est la principale cause de variabilité de la consommation en oxygène dissous (OD) liée au processus de filtration sur berge. En outre, la consommation de l'OD apparaît positivement corrélée à la température et au débit de la rivière. Cette seconde corrélation est attribuée au piégeage accru de la MOP dans le lit du cours d'eau pendant les périodes de hauts débits. Finalement, afin de quantifier l'influence de la température et du débit sur la consommation en OD dans un contexte de filtration sur berge, un modèle semi-analytique original est développé et évalué, avec succès, sur les données du site de Niederneunforn. Cette approche de modélisation est

transférable à d'autres sites de filtration sur berge où des outils performants sont nécessaires pour estimer les teneurs en OD dans diverses conditions climatiques et hydrologiques, et évaluer ainsi le risque de développement de conditions anoxiques.

Keywords

Stichwörter

Mots clés

Content

Chapter 1

Introduction

1.1 Motivation and background

Riverbank filtration provides an inexpensive, sustainable and yet effective means to improve the quality of surface water (Tufenkji et al., 2002). During passage through the riverbed and the aquifer, the infiltrated river water is exposed to processes like sorption, physicochemical filtration and biodegradation. These natural attenuation processes efficiently remove suspended particles, bacteria, viruses, parasites, micropollutants, and other organic and inorganic compounds usually present in surface waters, such as natural organic matter and ammonium (Kuehn and Mueller, 2000; Sacher and Brauch, 2002). The effectiveness of riverbank filtration has long been recognized in Europe, where several countries cover considerable fractions of their drinking water demand by riverbank filtration (~50% in France and Slovak Republic, ~48% in Finland, ~45% in Hungary, ~25% in Switzerland and ~16% in Germany (Hiscock and Grischek, 2002; Tufenkji et al., 2002)). Hence, riverbank filtration provides an important drinking water resource, which needs to be maintained and protected, especially within the context of upcoming challenges such as river restoration and climate change. Even though experience of more than a century in the operation of riverbank-filtration systems exists, the current understanding of bank-filtration schemes is primarily based on empirical knowledge (Hiscock and Grischek, 2002). Therefore, the adequate management of riverbank-filtration systems in a changing environment requires a better understanding of the physical and biogeochemical processes that occur during riverbank filtration (Hoehn and Meylan, 2009), which is the motivation for this Ph.D. Thesis.

1.1.1 Riverbank filtration

Riverbank filtration can occur under natural conditions or can be induced by a lowering of the groundwater table below surface water levels either by hydraulic boundaries such as side channels, or by groundwater abstraction at pumping wells (Fig. 1.1). Infiltration occurs mostly under saturated conditions, in direct hydraulic connection to the groundwater table (Hiscock and Grischek, 2002). If the groundwater table is more than a few decimeters below the riverbed, the hydraulic connection is lost and river water infiltrates through an unsaturated zone, which is aerated (Brunner et al., 2009; Hoehn and Meylan, 2009). Riverbank-filtration systems are typically positioned in alluvial valley aquifers, which predominantly consist of

gravels and sands allowing for high abstraction rates. However, floodplain deposits are complex geologic systems that exhibit heterogeneity on different scales and can include highly conductive "open framework gravels" forming preferential groundwater flow paths, as well as layers of silt and clay (Huggenberger et al., 1998).

Besides the dilution of the freshly infiltrated river water with ambient groundwater at the pumping well, the residence time of the bank filtrate has been identified as one of the key factors determining the removal efficiency of riverbank filtration. Several studies have shown that concentrations of natural organic matter and organic contaminants decreased with increasing travel time (Sontheimer, 1980; Grünheid et al., 2005). Also, the removal of pathogenic microbes was found to be strongly related to the residence time. A breakthrough of *E. Coli* at a pumping station at the Rhine River was observed after a flood event, due to shortened groundwater residence times (Eckert and Irmscher, 2006). Therefore, to ensure an adequate quality of produced water, minimal residence times are often required by law and are regulated via the definition of protection zones (FOEN, 2012b). The required minimal groundwater residence time between the river and a pumping well is 10 d in Switzerland (BUWAL, 2004) and 50 d in Germany (DVGW, 2000).

Infiltrating river water is subject to strong geochemical changes that are related to redox reactions, dissolution/precipitation of minerals, ion exchange and gas exchange (Jacobs et al., 1988; Tufenkji et al., 2002). Numerous studies have demonstrated that the most significant geochemical changes were associated with the biodegradation of natural organic matter (Jacobs et al., 1988; Bourg and Bertin, 1993; Brugger et al., 2001b; Sobczak and Findlay, 2002; Tufenkji et al., 2002). These degradation reactions were found to occur dominantly within the first meters of infiltration, where the microbial abundance and activity was highest (von Gunten et al., 1994; Brugger et al., 2001a). This interface between the river and alluvial groundwater, the hyporheic zone, has been identified as a distinct environment playing a crucial functional role in the biogeochemical cycling of nutrients and organic matter (Brunke and Gonser, 1997; Boulton, 2007).

Natural organic matter (NOM) in river systems originates from both allochthonous (terrestrially-derived) sources and generally more biodegradable autochthonous sources (periphyton) (Pusch et al., 1998; Leenheer and Croue, 2003). NOM is composed of dissolved organic matter (DOM) and particulate organic matter (POM). During infiltration of river water, DOM is transported through the riverbed as a "mobile substrate", whereas POM is retained in the riverbed sediments as a "stationary substrate" (Pusch et al., 1998). The

retention and storage of POM within the riverbed was found to depend on the grain-size distribution of the riverbed sediments and the hydrologic conditions (Brunke and Gonser, 1997).

The microbial degradation of NOM in riverbed sediments leads to a consumption of dissolved or solid terminal electron acceptors such as oxygen (O_2), nitrate (NO_3^-) and Mn(III/IV)-/Fe(III)(hydr)oxides. In case of oxygen depletion, the redox sequence proceeds to denitrification followed by reductive dissolution of manganese and ferric oxyhydroxides releasing dissolved Mn(II) and Fe(II). These species are undesired and need to be removed from pumped water by additional cost-intensive treatment steps (Kuehn and Mueller, 2000). Furthermore, re-oxidation of dissolved Mn(II) and Fe(II) when mixing with aerobic water at the pumping well can cause clogging of the well screen. It also has been recognized that redox conditions can significantly influence the removal efficiency of riverbank filtration. The degradation of DOM and several organic micropollutants was found to be less effective under anoxic conditions (Schwarzenbach et al., 1983; Grünheid et al., 2005; Massmann et al., 2006; Maeng et al., 2010).

The temperature dependence of the microbially mediated NOM degradation is well known (O'Connell, 1990; Kirschbaum, 1995). As a result, redox conditions at various bank-filtration systems were observed to undergo seasonal variations with the occurrence of anoxic conditions in summer (von Gunten et al., 1991; Greskowiak et al., 2006; Massmann et al., 2006; Massmann et al., 2008). Besides temperature, the redox conditions in the infiltration zone are also influenced by the availability of electron donors (NOM, ammonium) and electron acceptors (dissolved oxygen, nitrate). During industrialization in the 1950s and 1960s, rivers in urban catchments carried higher loads of organic substances and ammonium (Eckert and Irmscher, 2006). Combined with lower oxygen concentrations in river water, strongly reducing conditions prevailed in the infiltration zones of many riverbank-filtration systems, which caused the mobilization of manganese and iron. Since the 1970s, river water quality has improved significantly and oxic conditions in infiltration zones re-established (Kuehn and Mueller, 2000).

The retention of fine suspended particles (<2 mm) during riverbank filtration contributes to the clogging of the riverbed and the development of a colmation layer (Fig. 1.1), which is characterized by a reduced permeability causing lower infiltration rates and higher residence times of infiltrated river water (Brunke, 1999). The colmation layer may be subject to strong spatial heterogeneity and temporal variability. Bed-moving floods can rework the riverbed

3

and cause a decolmation with an inherent increase in riverbed permeability (Schubert, 2002; Doppler et al., 2007). The higher permeability during floods was found to promote the import of POM into gravelly riverbed sediments, which in turn enhanced the microbial respiration rate (Naegeli et al., 1995). The colmation of the riverbed can have a positive effect on the removal of organic and inorganic pollutants and bacteria due to higher residence times (Hiscock and Grischek, 2002). On the other hand, a colmation layer may adversely affect groundwater quality, as higher residence times also favor the development of anoxic conditions and the mobilization of Mn(II) and Fe(II) (Tufenkji et al., 2002).
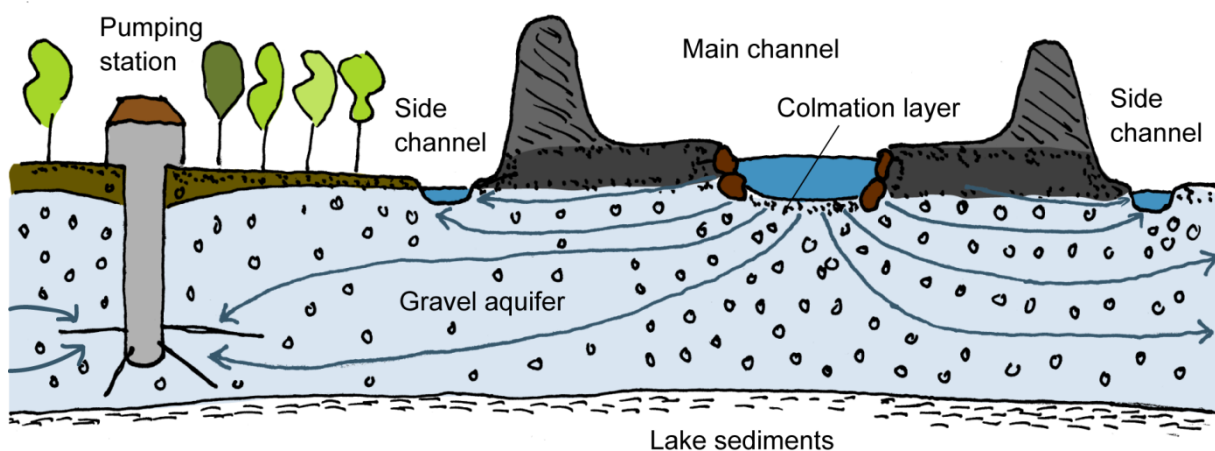
Fig. 1.1. Schematic illustration of riverbank filtration. Infiltrated river water passes the riverbed and the aquifer and is extracted at a pumping station, where it mixes with ambient groundwater and may undergo secondary treatment steps before being supplied to the drinking water distribution system. Adapted from Schirmer (2013).

1.1.2 Challenge 1: River restoration

Over the past few decades, there has been a shift in perspective of water authorities from river corridor channelization toward restoration. As a consequence, several laws have been established such as the European Water Framework Directive (European-Commission, 2000) or the Swiss Water Protection Law (GSchG, 2011; GSchV, 2011) that require engineering tasks in river courses to jointly improve flood protection, ecological status and water quality. In Switzerland, 15000 km of river length are strongly engineered, channelized and in a bad ecological condition, of which 4000 km will undergo river restoration during the next 80 years (FOEN, 2012c).

River restoration measures may comprise removal of the bank stabilization and the colmation layer, widening of the riverbed, as well as the establishment of braided river sections, re-meandering stream reaches and gravel bars (Fig. 1.2). These actions enhance the exchange between the river and the hyporheic zone and increase the habitat diversity, both being essential for the ecological health of a river system (Brunke and Gonser, 1997; Baumann et al., 2009). The higher exchange with the hyporheic zone is thought to increase the interstitial microbial activity and therefore the removal of various contaminants. However, the widening of the riverbed and the higher riverbed permeability might decrease groundwater residence times and therewith increase the risk of drinking water contamination by pollutants or bacteria (Hoehn and Scholtis, 2011). Due to a lack of process understanding and following the precautionary principle, river restoration measures are not allowed within the protection zones of drinking water wells (FOEN, 2012b).

To mitigate this conflict of interest between river restoration and drinking water protection, a good knowledge of the physical and biogeochemical processes is needed. More specifically, the well-capture zone, groundwater flow paths, flow velocities, groundwater residence times and the fraction of freshly infiltrated river water need to be known (Hoehn and Meylan, 2009). Several methods based on natural tracers such as temperature and electrical conductivity were developed to quantify exchange rates (Anderson, 2005; Kalbus et al., 2006; Vogt et al., 2010b), travel times and the fraction of riverbank filtrate in abstracted water (Hoehn and Cirpka, 2006; Cirpka et al., 2007; Vogt et al., 2010a). However, these methods are not able to provide information on groundwater flow paths and flow velocities. To this end, groundwater flow and transport modeling is a powerful tool, as it provides a quantitative link between groundwater residence times, flow paths and flow velocities (Wondzell et al., 2009).

It is well known from modeling studies and field observations that riverbed morphology affects the river water level distribution, which in turn affects or drives the exchange with groundwater (Harvey and Bencala, 1993; Woessner, 2000; Cardenas et al., 2004; Cardenas, 2009; Käser et al., 2009). Accordingly, one of the prerequisites for the setup of a groundwater flow model of a real river-groundwater system is an accurate description of the water level distribution in the river (Käser et al., 2013). However, restored river systems may have complex water level distributions that need to be characterized by their full spatial (i.e. two horizontal dimensions) and temporal extent (i.e. for any discharge condition). Ideally, such water level information is extracted from hydraulic models (Doppler et al., 2007; Derx et al., 2010; Engeler et al., 2011), but their setup is time consuming and requires a considerable amount of data input, that is, the riverbed's bathymetry and water level information for the

calibration and validation process. Therefore, there is a need for alternative methods to describe surface water level distributions of dynamic rivers that allow for reliable simulations of the groundwater flow field and accurate predictions of groundwater residence times. Additionally, the sensitivity of these predictions on the method selection and the level of detail in the water level distribution related to these methods should be assessed.
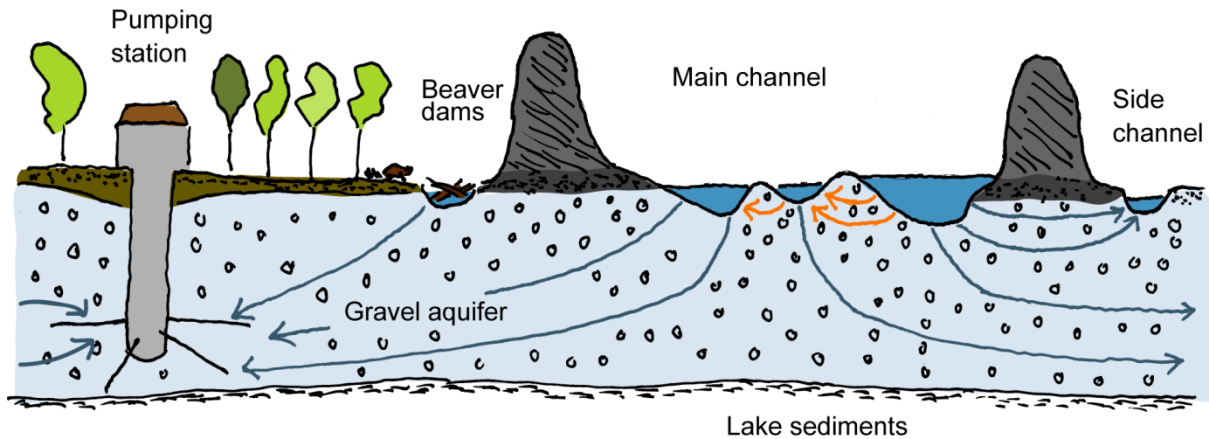
Fig. 1.2. Schematic illustration of a restored riverbank-filtration system. The riverbed was widened, the colmation layer removed and gravel bars were established. These river restoration measures promote hyporheic exchange (orange arrows) and the development of new habitats. On the other hand, flow paths between the river and the pumping well may be shortened, which can cause a contamination of the drinking water by pollutants or bacteria. Beaver dams in side channels can lead to higher water levels that may reverse the hydraulic gradient. Adapted from Schirmer (2013).

1.1.3   Challenge 2: Climate change

Today, most peri-alpine alluvial gravel-and-sand aquifers are oxic owing to the low loads of organic matter and nutrients in rivers. Oxic conditions allow a beneficial minimal treatment of pumped groundwater before supplying it as drinking water to the distribution system. However, during the hot summer of 2003, which was accompanied by low river discharges and river temperatures of more than 25°C (OcCC, 2005), the redox conditions in numerous riverbank-filtration systems turned anoxic over a period of up to three months (Eckert et al., 2008) and the onset of denitrification was observed (Sharma et al., 2012). Denitrification may result in elevated concentrations of nitrite (NO_2^-), which is of concern due to its toxicity. Hoehn and Scholtis (2011) even reported a case where the redox sequence proceeded to Mn(IV)- and Fe(III)-reducing conditions. As mentioned in Section 1.1.1, the appearance of dissolved Mn(II) and Fe(II) in the abstracted water requires additional treatment processes, and precipitation of Mn(IV)-/Fe(III)(hydr)oxides can lead to clogging of the filter screen.

Furthermore, compounds that are better degraded under oxic conditions such as DOM, ammonium and certain micropollutants are more persistent under anoxic conditions and may appear at the pumping well in elevated concentrations (Section 1.1.1).

For Europe, climate models predict an increase in air temperature, a decrease in summer rainfall and an increase in winter rainfall, as well as an increased frequency and intensity of weather extremes such as heat waves or flood events (IPCC, 2007), which is consistent with the climate-change scenarios for Switzerland (CH2011, 2011). River discharges are expected to decrease in summer and increase in winter. River water temperature, which is decisive for the degradation processes within the riverbed, is likely to increase by the same extent as air temperature, especially during low-flow conditions (FOEN, 2012a).

The effects of climate-related changes in temperature and discharge on the quality of surface water and groundwater are manifold (Murdoch et al., 2000; Zwolsman and van Bokhoven, 2007; Park et al., 2010; Green et al., 2011). Riverbank-filtration systems are most vulnerable to changes in residence time and redox conditions (Section 1.1.1). An increased occurrence of flood events may raise the risk of drinking water contamination by pathogenic bacteria or other pollutants. However, flood events are temporally limited to a few days, facilitating their management.

Low discharges are expected to increase groundwater residence times, as well as the loads of organic matter and nutrients in rivers due to less dilution of wastewater effluent (Sprenger et al., 2011). Combined with higher temperatures, summer heat waves tend to promote the development of anoxic conditions in the infiltration zone, as observed in summer 2003. An increased frequency and intensity of long-lasting heat waves is therefore likely to increase the risk for riverbank-filtration systems to become denitrifying or even Mn(IV)- or Fe(III)-reducing (Fig. 1.3) over periods of several months (Sprenger et al., 2011). Such long-lasting anoxic conditions would require complementary drinking water treatment technologies, the implementation of which is expensive and needs to be planned in advance to ensure the supply of high-quality drinking water. To assess the risk of arising anoxic conditions more accurately, it is crucial to understand the dynamics of NOM degradation during riverbank filtration and its dependence on the climate-related variables temperature and discharge. The quantification of these dependencies might allow for model-based estimates of oxygen concentrations in river-recharged groundwater, which would facilitate the anticipation of possible changes in redox conditions under various climatic and hydrologic conditions.
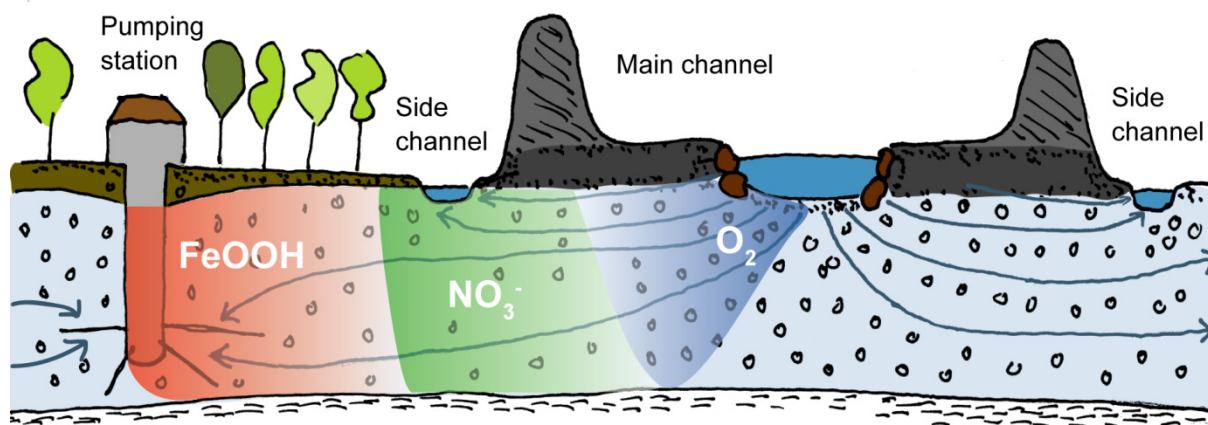
Fig. 1.3. Higher temperatures during future summer heat waves will enhance the microbial degradation of NOM, which might lead to a complete consumption of oxygen. In case of anoxic conditions, denitrification and eventually reductive dissolution of manganese and ferric oxyhydroxides can take place. The occurrence of nitrite and especially dissolved manganese and iron would require additional drinking water treatment steps. Furthermore, the re-oxidation of dissolved manganese and iron at the pumping well can lead to a clogging of the filter screen. Adapted from Schirmer (2013).

1.2   Objectives and structure of this thesis

The overall goal of this Ph.D. Thesis is to deepen the understanding of physical and biogeochemical processes affecting the quality of river-recharged groundwater, and to develop tools that may help to assess potential impacts of river restoration measures and climatic changes on the effectiveness of riverbank-filtration systems. This overall goal of the thesis was subdivided into four main objectives (i-iv), which will be addressed in Chapters 2-5, respectively. To achieve these objectives, an integrative approach was employed that combines field investigations, laboratory experiments, as well as groundwater flow and reactive transport modeling.

This thesis was written within the RIBACLIM project (RIverBAnk filtration under CLIMate change scenarios) in the framework of the National Research Program "Sustainable Water Management" (NRP61). Field investigations, method development and modeling work were performed at a partly restored field site in Niederneunforn (northeastern Switzerland) at the peri-alpine Thur River. Chapters 2-5 contain detailed descriptions of the field site.

Within the context of river restoration, the objectives of this Ph.D. Thesis were (i) to develop alternative methods to generate water level distributions of dynamic rivers for the application in groundwater models, and (ii) to assess the predictive capability of these methods with respect to the simulated groundwater residence time.

Chapter 2 presents two new alternative interpolation methods to estimate water level distributions of highly dynamic rivers in the context of modeling riverbank-filtration systems at scales in the order of kilometers. These methods were implemented at the Niederneunforn field site and water level time series at multiple locations within the river reach were generated. These water level predictions were compared with those of a third reference method, which is based on an existing hydraulic model, to test the accuracy of the alternative interpolation methods.

Chapter 3 investigates the impact of the method selection and the considered level of detail in the river water level distribution on the simulated groundwater residence time. Thereto, steady-state surface water level distributions were generated using both alternative methods, the reference method, as well as two simplified methods, and were assigned to a 3D groundwater flow and transport model of the field site. After calibration against groundwater heads, each of the models was used to predict the spatial groundwater residence time distribution within the modeling domain.

Within the context of climate change, the objectives of this Ph.D. Thesis were (iii) to investigate the dependence of NOM degradation during riverbank filtration on the climate-related variables temperature and discharge and (iv) to develop a model that simulates oxygen consumption during riverbank filtration as a function of river temperature and discharge.

Chapter 4 elucidates the contribution of DOM consumption to the overall consumption of electron acceptors and its dependence on the climate-related variables temperature and discharge. Two detailed groundwater sampling campaigns were performed during typical summer and winter conditions to capture different temperature ranges. The results were compared to those of laboratory column experiments that were conducted at temperatures that span the range of the field conditions. Additionally, data of periodic field samplings that covered a wide range of temperature and discharge conditions over a period of five years were evaluated.

Chapter 5 presents a newly developed semi-analytical model that allows estimating oxygen concentrations in river-recharged groundwater under various climatic and hydrologic conditions. The model is based on the stochastic-convective reactive approach and incorporates a dependence of the oxygen consumption rate on river temperature and discharge. These dependencies were inferred from high-resolution oxygen time series measured in the Thur River and an adjacent observation well.

Chapter 2

New methods to estimate 2D water level distributions of dynamic rivers

Abstract

River restoration measures are becoming increasingly popular and are leading to dynamic riverbed morphologies that in turn result in complex water level distributions in a river. Disconnected river branches, nonlinear longitudinal water level profiles and morphologically induced lateral water level gradients can evolve rapidly. The modeling of such river-groundwater systems is of high practical relevance in order to assess the impact of restoration measures on the exchange flux between a river and groundwater or on the residence times between a river and a pumping well. However, the model input includes a proper definition of the river boundary condition, which requires a detailed spatial and temporal river water level distribution. In this study, we present two new methods to estimate river water level distributions that are based directly on measured data. Comparing generated time series of water levels with those obtained by a hydraulic model as a reference, the new methods proved to offer an accurate and faster alternative with a simpler implementation.

2.1 Introduction

Over the past few decades there has been a shift in focus from river corridor channelization toward restoration. It has been recognized that rivers need more space for the purpose of flood protection (Woolsey et al., 2007). Furthermore, restoration measures such as widening of the riverbed, re-meandering stream reaches, and constructing gravel bars, should increase the exchange between rivers and groundwater, which is essential for the ecological health of a river (Brunke and Gonser, 1997). On the other hand, riverbed widening can decrease travel times between rivers and pumping wells, which may increase the risk of drinking water contamination by pollutants or bacteria (Hoehn and Scholtis, 2011).

Groundwater flow and transport modeling is a valuable tool to obtain a process-based understanding of (restored) surface water-groundwater systems. Compared to tools developed to work with artificial and natural tracers, a calibrated model provides quantitative conclusions on flow paths, mixing ratios and travel times (Wondzell et al., 2009). It is well known that riverbed morphology affects the river water level distribution, which in turn affects or drives the exchange with groundwater (Woessner, 2000; Cardenas et al., 2004; Cardenas, 2009). Therefore, one of the prerequisites for the setup of a groundwater flow model of a real river-groundwater system is an accurate description of the water level distribution in the river.

Restored river systems may have complex water level distributions that need to be characterized by their full spatial (i.e. two horizontal dimensions) and temporal extent (i.e. for any discharge condition). Past small-scale field and modeling studies (10 to 100 m) applied one or two sets of detailed water level measurements in one or two dimensions (Wroblicky et al., 1998; Storey et al., 2003; Lautz and Siegel, 2006; Wondzell et al., 2009). On the scale in the order of kilometers, which is more relevant for practical problems, this approach is not applicable. Instead, the extraction of river water level information from a hydraulic model might be a proper solution (Doppler et al., 2007; Derx et al., 2010; Engeler et al., 2011). However, the setup of a hydraulic model is time consuming and requires a large amount of data input, that is, the riverbed bathymetry and water level information for the calibration and validation process.

In this study, we present two alternative methods to estimate water level distributions of highly dynamic rivers in the context of modeling river-groundwater systems at scales in the order of kilometers. The two methods combine continuous and periodic water level measurements from different locations in order to account for the spatial and temporal

variability of the water level distribution. We predicted water levels at several locations at a restored reach of the peri-alpine Thur River and compared them with water level predictions of a reference method, which is based on an existing hydraulic model. Finally, we point out the advantages and disadvantages of the different methods and discuss the optimal use of each method when assigning the water level distribution of restored and dynamic river systems to groundwater flow and transport models.

2.2 Interpolation methods to estimate river water levels

2.2.1 Problem setup

Instrumentation of a 1 km river reach is typically comprised of two water level gauges, one upstream and one downstream of the field site. For groundwater flow modeling, river water levels need to be estimated at each river boundary node between the two gauging stations. The simplest method assumes a constant gradient (linear interpolation) in the longitudinal direction and a zero gradient in the lateral (transverse) direction. Although this might be adequate for a channelized system, for restored corridors the dynamic riverbed morphology might lead to a nonlinear longitudinal water level profile and to lateral water level gradients. Furthermore, the water level distribution might change as a function of the discharge.

The basic idea of the two new interpolation methods is to combine continuous water level records from water level gauges with water levels measured periodically under different discharge conditions. The latter are measured at "fixpoints", which are distributed throughout the river reach to refine the water level distribution at locations where the installation of a water level gauge is technically difficult or simply too expensive. A fixpoint is defined as a reference point in the river, for example, a point on a construction rock or a steel rod, whose altitude is known. By establishing a mathematical relationship between the water level data at the gauging stations and the fixpoint, the water level at the fixpoint can be estimated for any measured water level at the gauging station.

We consider the river as a two-dimensional (2D) domain, which is discretized by multiple lines parallel to the main flow direction of the river and several sections of support points (S) perpendicular to the flow direction (Fig. 2.1). The key task of the interpolation methods is to estimate a water level h^S at each support point from any water level measured at the gauging station (i.e. for any discharge condition). Support points are placed at a location where a fixpoint (F) or a gauging station (G) exists. One fixpoint per section is enough unless lateral water level gradients are observed, in which case a fixpoint must be defined on both sides of

the river (Fig. 2.1). The periodic water level measurements at the fixpoints are denoted as h^F, while the continuous water level measurements at the gauging station are denoted as h^G. The estimation of h^S consists of three steps:

1. Establish a mathematical relationship ϕ between the measurements h^F and h^G
2. Use ϕ to compute h^F for any time step or time series: $h^F \approx \phi[h^G]$
3. Estimate the water levels or water level time series h^S for the support points located on the same section as the fixpoint F.

Different options for these steps have been considered for the two new methods, which are referred to as alternative methods. In order to compare these alternative methods with a reference, we developed a third method that is based on a hydraulic model and is referred to as the reference method. These three methods are described in the following sections. The explanation is descriptive in order to convey the main idea. A thorough mathematical development of the methods and their application to real data is presented in the Supporting information (Section 2.6).
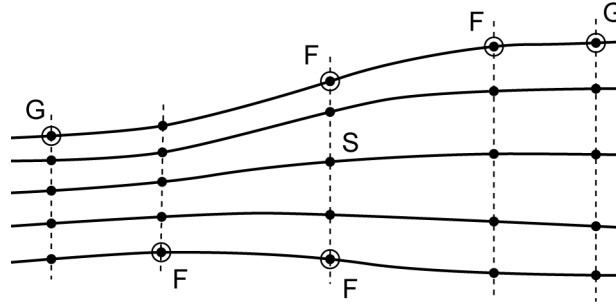
Fig. 2.1. Schematic representation of a river system with multiple lines and sections of support points (S, black dots). Gauging stations (G) and fixpoints (F) are shown as black circles.

Once the set of lines and support points with water levels h^S has been obtained using one of the three methods, the final interpolation of the water levels from the support points to the river boundary nodes of the numerical model has to be performed. This step is identical for all three methods and is accomplished by a one-dimensional linear interpolation along the lines, which implies that each of the lines is mapped by a curvilinear system of longitudinal coordinates to account for different curvatures of the lines. More precisely, each of the river boundary nodes of the groundwater model is projected perpendicularly onto the closest line and the water level is linearly interpolated between the upstream and downstream support point. Some simulation codes (e.g. FEFLOW) offer tools to accomplish this final interpolation step.

2.2.2 Method 1: Regression of measured data (RM)

The first alternative method uses a polynomial regression technique to obtain the mathematical relationship ϕ. The method requires a continuous water level time series at one gauging station G and periodic water level measurements at a fixpoint F (Fig. 2.2). Each time a measurement is made at the fixpoint, the corresponding water level at the gauging station can be extracted from the continuous water level time series. A polynomial equation is then fitted to the data pairs, which constitutes the mathematical relationship ϕ. The polynomial order has to be chosen according to the range and the characteristics of the data. A guideline to defining the polynomial order is given in the Supporting information (Section 2.6). Applying ϕ to any water level time series measured at the gauging station produces predictions of corresponding water level time series at the fixpoint. If there are two fixpoints on the same section to capture lateral gradients, a separate polynomial equation is fitted to the corresponding data pairs. The gauging station G is denoted as determining gauging station G^d, as its water level uniquely defines the water level at the fixpoint.
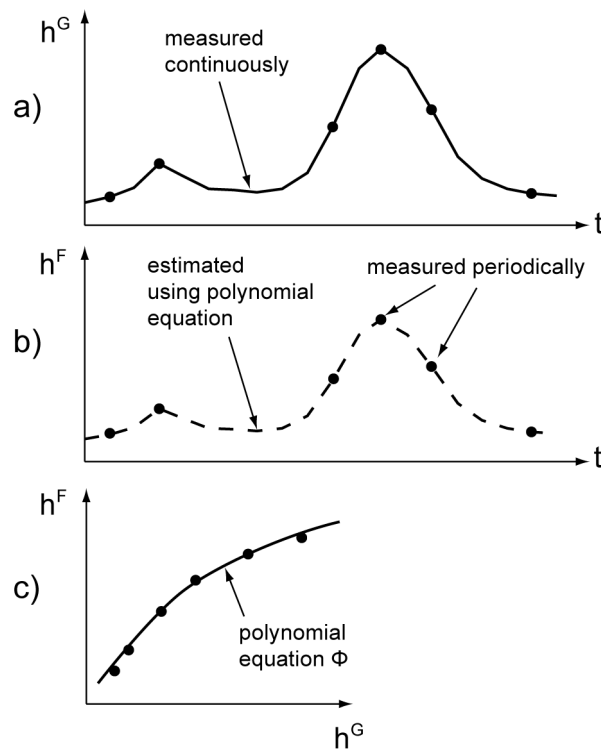
Fig. 2.2. Illustration of the regression approach. (a) Continuous water level time series h^G measured at the gauging station. (b) Periodic water level measurements h^F at a fixpoint (black dots). For the same measurement times, water levels at the gauging station are extracted in (a). (c) ϕ is established between h^G and h^F by polynomial regression and is used to estimate the water level time series (dashed line) at the fixpoint in (b).

The estimation of the water level at the support points from the water level at the fixpoint is made in the simplest possible manner. If no lateral gradients exist, the water level of the fixpoint is assigned to all of the support points located on the same section. However, if a second fixpoint was installed on the same section to capture a lateral gradient, assigning the water levels to the support points should be based on field observations. For example, if a discrete step forms the lateral gradient, the water level at each support point can be determined from the most representative fixpoint. Otherwise, a linear interpolation between the two fixpoints might be an appropriate solution.

2.2.3 Method 2: Interpolation of measured data (IM)

The second alternative method uses an interpolation approach that requires two gauging stations. One of them has to be defined as determining gauging station G^d. The fixpoints can be located between or outside of the two gauging stations.

This IM method is based on a conceptual behavior model. According to the model, the riverbed morphology exerts a high influence on the river water level distribution under low-flow conditions, potentially leading to nonlinear longitudinal water level profiles or lateral water level gradients. As the water level rises, the influence of the riverbed morphology on the water level distribution decreases, and at some point lateral water level gradients disappear and a linear longitudinal water level profile is reached. In general, the IM method describes the water level at a fixpoint by an interpolation function (ϕ) that consists of a linear interpolation term l between the water levels at the two gauging stations (h^G and h^{Gd}) and a deviation D from the linear trend (Fig. 2.3). Following the conceptual behavior model, the deviation D is at a maximum, $D = a$, when water levels at the determining gauging station h^{Gd} are smaller than h^a. On the other hand, the deviation goes to zero for water levels higher than a threshold water level h^{thresh}. Between h^a and h^{thresh}, the deviation D is assumed to decrease linearly (Fig. 2.3). Similarly, we can describe the water level at a second fixpoint on the same section by the water level of the first fixpoint plus a lateral difference D^L. Again, D^L is at a maximum for low water levels and goes to zero above a threshold water level.

To estimate the parameters a, h^a and h^{thresh}, the deviation from the linear trend has to be calculated for each measurement at a fixpoint and plotted against the corresponding water level at the determining gauging station. More details on how to estimate the parameters for the IM method are given in the Supporting information (Section 2.6). The estimation of the water level at the support points is identical to the procedure described in the previous section for the RM method.
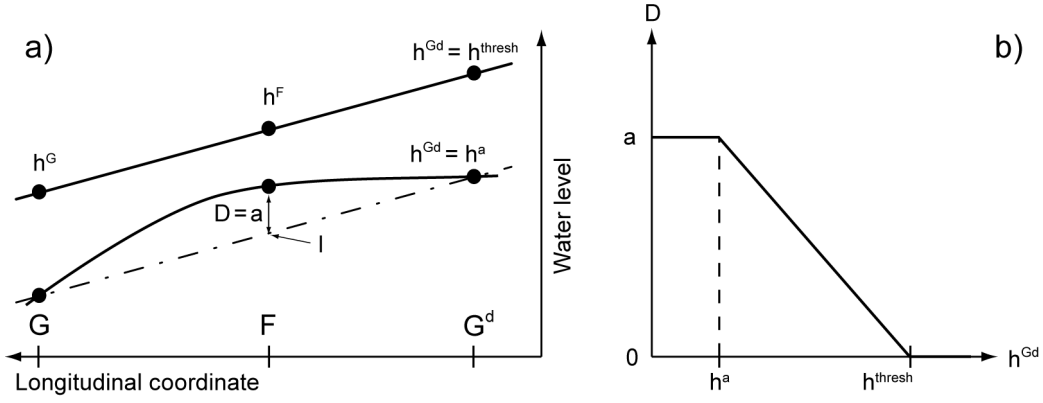
Fig. 2.3. Illustration of the interpolation approach. (a) Two longitudinal water level profiles for the conditions $h^{Gd} = h^a$ and $h^{Gd} = h^{thresh}$. (b) Deviation from the linear trend (D) as a function of h^{Gd}.

2.2.4 Method 3: Regression of hydraulic model data (RH)

To compare the two alternative methods with an independent reference, we developed a third method that is based on data from an existing hydraulic model of the main river channel in the section of interest. The hydraulic model output consists of 2D water level distributions, each corresponding to a specific discharge condition. Similar to the RM method, the RH method applies a polynomial regression technique to obtain the mathematical relationship ϕ. However, the relationships are based on water levels extracted from the hydraulic model output at each support point and at the location of the determining gauging station, and not on measured water levels.

2.3 Application to the Niederneunforn field site

2.3.1 Field site

The peri-alpine Thur River drains a catchment area of 1730 km^2 and originates in an alpine region that reaches its highest point on Mount Säntis (2502 m above sea level, m asl). The Thur River is the largest river in Switzerland without a retention basin. This leads to a very dynamic discharge regime ranging from 3 to 1100 m^3/s with an average of 47 m^3/s. The field site (Fig. 2.4) is located approximately 12 km upstream of the confluence with the Rhine River. In the western part of the field site, restoration measures were realized in 2002. Restoration measures were forbidden in the upstream section to protect the water quality at the nearby pumping station, where a pumping well supplies the community of Nieder- and Oberneunforn with drinking water. The field site was instrumented with more than 80 piezometers (2'') during the interdisciplinary RECORD project (Restored corridor dynamics, http://www.cces.ethz.ch/projects/nature/Record; Schneider et al. (2011)). The aquifer has a

17

thickness of 5.3±1.2 m and its hydraulic conductivities were estimated to range from 4×10^{-3} to 4×10^{-2} m/s (Diem et al., 2010; Doetsch et al., 2012). The silty sand of the alluvial fines on top of the aquifer has a much lower hydraulic conductivity and can be regarded as the semi-confining unit, with a thickness of 0.5-3 m.

The Thur River has a width of 50-100 m (Fig. 2.4). In the restored section a large gravel bar has evolved during the past few years. To the north, a disconnected branch of the river exists, which is only flooded at high river stages (>200 m^3/s). The longitudinal river water level profile does not have a linear shape for low-flow conditions. In the upstream 400 m of the river the gradient is 0.5‰ and in the downstream 800 m it is 2‰. In the middle of the river reach, lateral water level gradients occur during low-flow conditions. These lateral surface water level differences exist due to the asymmetrical riverbed morphology and can reach up to 0.4 m. Two side channels (north and south) flow parallel to the river and have an average width of 4-8 m. Two beaver dams are located in the northern side channel. The upstream dam has a significant effect on water levels, creating differences of up to 0.5 m.

A 2D hydraulic model of the Thur River was developed by Pasquale et al. (2011) and forms the basis for the reference RH method (Section 2.2.4). Riverbed cross sections measured in September 2009 with an average spacing of 50 m were interpolated using the technique presented by Schäppi et al. (2010) to obtain the river bathymetry. The hydrodynamic simulations were performed using the 2D model BASEMENT, which applies the finite volume method to integrate the shallow water equations (Pasquale et al., 2011). The model deals with both sub- and supercritical flow regimes, thus providing a suitable tool to simulate 2D water level distributions of dynamic rivers. The modeling results comprise 19 steady-state simulations for flows ranging between 10 and 650 m^3/s, and provide water level altitudes at each raster cell (2×2 m). The hydraulic model does not include the side channels and the disconnected branch and is considered to be valid until the major flood events of June 2010.
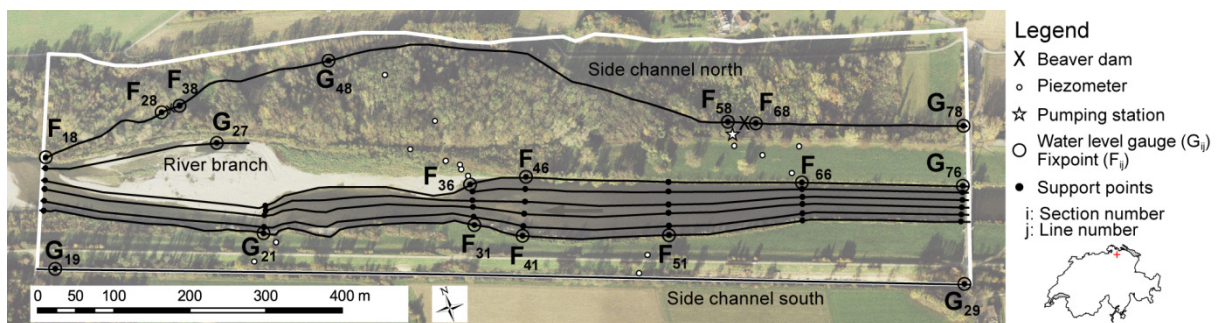

Fig. 2.4. Field site located in Niederneunforn at the Thur River with indicated lines, support points, fixpoints and gauging stations. Selected piezometers are shown as well. The white polygon shows the perimeter of method implementation.

2.3.2 Data collection and method implementation

We installed two water level gauges in the main channel of the river, as well as in both side channels, and one in the river branch (Fig. 2.4). Three of these water level gauges are maintained by the Agency for the Environment of the canton Thurgau. The sensors (DL/N 70, STS AG, Switzerland) have been continuously measuring pressure, temperature and electrical conductivity (EC) at 15-min intervals since April 2010 (error of single measurement: ±0.1% for pressure, ±0.25% for temperature and ±2% for EC, according to the manufacturer's manual). We installed sensors of the same type in selected piezometers shown in Fig. 2.4. The raw data were processed in order to remove outliers, to subtract the barometric air pressure and to transform the pressure data to absolute water levels (m asl). To have more information on the water level distribution between the water level gauges, we installed several fixpoints along the river and the northern side channel. We chose the fixpoint positions according to the location of piezometer transects and visibly steep water level gradients (e.g. hydraulic jumps at beaver dams) or lateral gradients (central part of the river). We defined an indexing system that allows a distinct identification of each point. The first index refers to the section number and the second index to the line number. We leveled the absolute height of the fixpoints using a high-precision differential GPS (Leica GPS1200, Leica Geosystems AG, Switzerland) and a leveling device (Sprinter 100M, Leica Geosystems AG, Switzerland). We measured water levels at these fixpoints periodically between February and May 2011 covering a discharge range of 10 to 100 m^3/s.

Based on the resulting data set, we implemented both alternative methods and the reference method, each of which covered the three steps described in Section 2.2.1. As the hydraulic model did not include the disconnected branch and the side channels, we coupled the RH method to the RM method. More details on the method implementation can be found in the Supporting information (Section 2.6).

2.3.3 Comparison of the interpolation methods

To evaluate the performance of the two alternative methods, we applied each of the interpolation methods (RM, IM, and RH) to generate water levels for a 1-month period (May 26, 2010 to June 30, 2010, vertical lines in Fig. 2.5) at each fixpoint and gauging station within the river domain. The upstream gauging station G_{76} was used as the determining gauging station for each of the methods. We plotted the generated time series of water levels (30-min intervals) of the reference method (RH) against the time series of both alternative methods (RM and IM). Fig. 2.6 shows examples for one gauging station and two fixpoints. If

the generated water levels were the same for each time step, the dots of the scatter plots would be located on a line with a slope of one. Deviations from this line correspond to deviations of the RM/IM methods from the RH method and were quantified by a mean and a standard deviation (Fig. 2.6, Table 2.1).
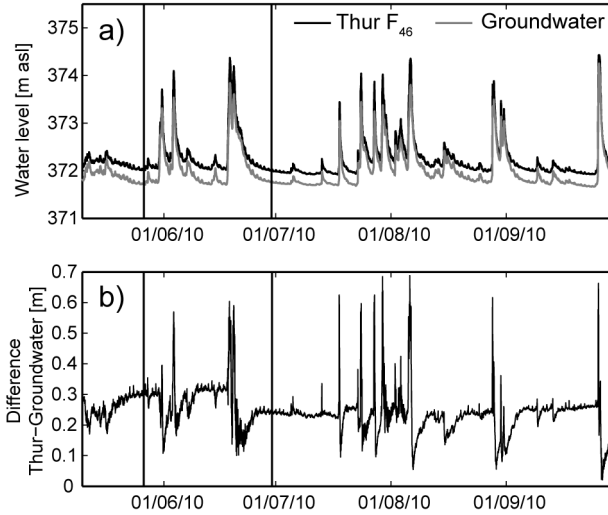
Fig. 2.5. (a) Water level time series in the Thur River at fixpoint F_{46} predicted with the RH method and measured groundwater heads in a nearby piezometer between May and October 2010. (b) Calculated water level difference between the river and groundwater. The vertical lines indicate the 1-month period used for creating the scatter plots of Fig. 2.6.

The scatter plots for the gauging station G_{21} are identical for the RM and the IM method, which both used the gauging station data directly for this point. The water levels of the RH method however, were generated based on the hydraulic model. Therefore, these two plots actually compare the measured water level data with the water level predictions of the hydraulic model. The match was good for lower water levels but deviations of up to 0.5 m occurred for the peak flows during flood events. As only a small portion of the data was subject to such large errors, the mean error of water level prediction with the RH method was small (1 cm). The uncertainty of the water level prediction is reflected in the standard deviation of 10 cm (Table 2.1).

The scatter plots of the fixpoint F_{41} revealed a difference in the behavior of the two alternative methods. The water level predictions for the study period (Fig. 2.5) exceeded the range of water levels measured at F_{41} (371.6-372.5 m asl). Depending on the polynomial fit, the RM method is likely to fail for predictions outside of the measured range, as there are no data points constraining the polynomial equation. In our case, the parabola that was fitted to the data at the fixpoint F_{41} was obviously too narrow in order to reliably predict water levels beyond the measured range. Correspondingly, the deviations with respect to the RH method

showed a mean error of -11 cm and a standard deviation of 42 cm. The IM method performed better for the peak flow water levels. As the water level predictions at a fixpoint are always bounded by two measured water levels at the upstream and downstream gauge, the stability beyond the measured range was better for the IM method. For the fixpoint F_{66}, both the RM and the IM method performed well despite the systematic positive offset for the RM method at high water levels. This offset might be attributed to the problem described above for the fixpoint F_{41}.

Most of the mean errors and their standard deviations for the fixpoints within the river domain varied between 1 and 10 cm (Table 2.1). We considered this level of error to be acceptable as the reference RH method itself had an accuracy of ± 10 cm at G_{21}. As G_{76} was the determining gauging station for all fixpoints in the river, predictions were identical for all methods, explaining the values of zero in Table 2.1. The high standard deviations for the fixpoints F_{41} and F_{46} for the RM method can be blamed on the failure of the regression approach beyond the measured data.
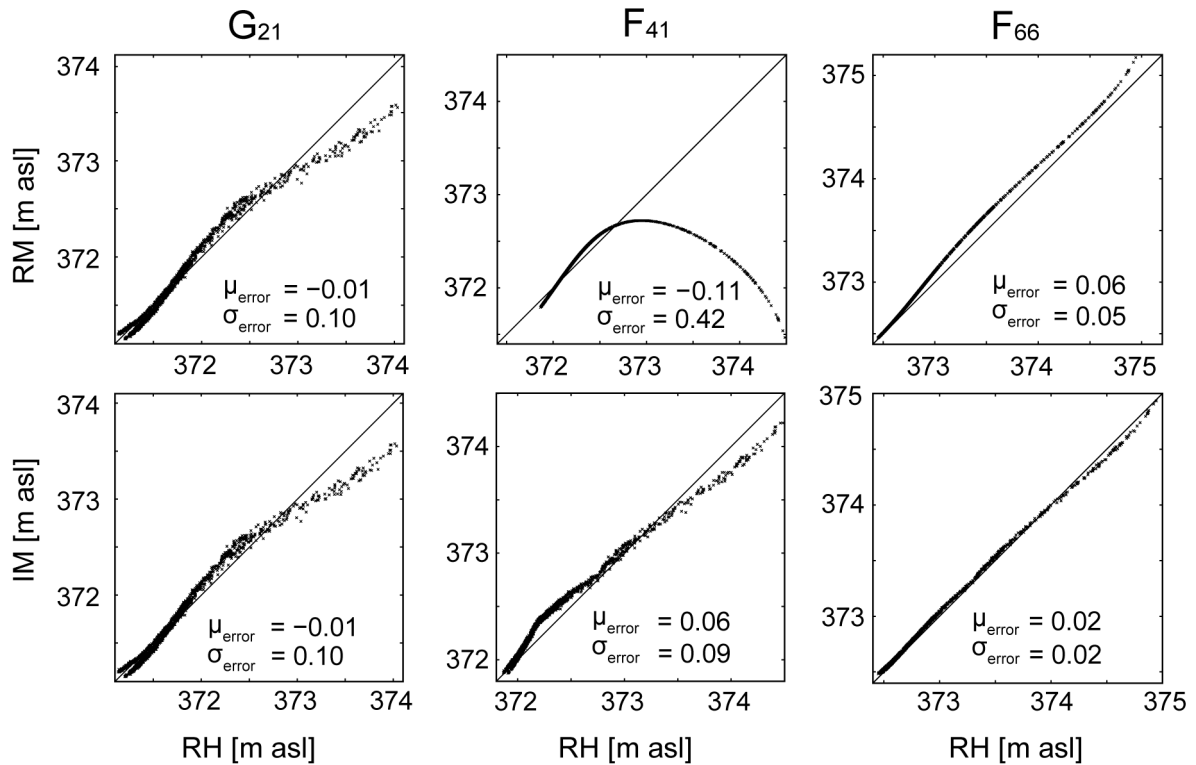
Fig. 2.6. Scatter plots for one gauging station (G_{21}) and two fixpoints (F_{41}, F_{66}) within the river domain. The time series of water levels generated by the reference method RH are plotted against the time series of water levels generated by the RM (top three figures) and the IM method (bottom three figures). Mean (μ_{error}) and standard deviations (σ_{error}) of the residuals between the alternative methods and the reference method are indicated.

The alternative methods – especially the IM method – tend to show higher deviations (>10 cm) from the RH method at the fixpoints on sections 1 to 4, which are located in the restored part of the river. We found evidence that the major flood event on June 17 through 24, 2010 (Fig. 2.5) led to a change in the riverbed morphology in the restored river section and to a corresponding change in the relationship between the water levels at the determining gauging station and at the fixpoints. First, the scatter plot for the gauging station G_{21} (Fig. 2.6) reveals two distinct regimes at the lower end of the water level spectrum for the 1-month period that covers the major flood event. Second, after the flood event there is a clear and permanent decrease (~10 cm) in the difference between the water levels at F_{46} predicted with the RH method, and groundwater heads measured at a nearby piezometer (Fig. 2.5). The drop in the water level difference could be due to a change in the riverbed morphology after the flood, resulting in an underprediction of water levels by the RH method, which assumed a constant morphology. Because the data for the RM and the IM method were collected after this morphologically active flood event, they might have captured the higher water levels and accordingly led to an overestimation of water levels compared to the RH method. Therefore, the differences in predicted water levels among the different methods were presumably not only caused by structural artifacts, but also by real differences due to morphology changes in the river.

Table 2.1. Mean (μ_{error}) and standard deviations (σ_{error}) of the residuals [m] between the time series of water levels generated by both alternative methods and the reference method at the gauging stations and fixpoints within the river domain.

RM	F_{18}	G_{21}	F_{36}	F_{31}	F_{46}	F_{41}	F_{51}	F_{66}	G_{76}
μ_{error}	0.07	-0.01	0.05	0.06	-0.08	-0.11	-0.01	0.06	0.00
σ_{error}	0.12	0.10	0.04	0.04	0.42	0.42	0.07	0.05	0.00
IM	F_{18}	G_{21}	F_{36}	F_{31}	F_{46}	F_{41}	F_{51}	F_{66}	G_{76}
μ_{error}	0.11	-0.01	0.16	0.17	0.12	0.06	-0.04	0.02	0.00
σ_{error}	0.16	0.10	0.09	0.08	0.08	0.09	0.04	0.02	0.00

2.4   Discussion

A hydraulic model has the advantage of being physically based, which allows a wide range of discharge conditions to be simulated. This makes water level predictions by the RH approach very robust. However, setting up a hydraulic model is time consuming, and needs both a large data set and to be thoroughly calibrated. At our field site, the hydraulic model was not able to include the water levels of the disconnected river branch, because during low-flow conditions this branch is fed by groundwater. Furthermore, the hydraulic model did not cover the side

channels. The RH method had to be coupled to the RM method in order to include the full surface water level distribution required for the assignment of boundary conditions in a groundwater model.

Compared to the RH method, both alternative methods presented in this chapter (RM and IM) provide a more efficient way of predicting water level distributions in a hydraulically and morphologically varying environment. First, the accuracy of the water level predictions with the alternative methods was in the same range as the accuracy of the reference RH method itself. Second, the alternative methods require minimal data and computational effort, making them simpler and faster to implement than the hydraulic model.

In comparison to the IM method, the RM method benefits from the regression approach, which is fast and straightforward in its implementation and its application. However, the RM method does not provide reliable water level predictions when they exceed the range of water levels measured at the fixpoints. This in turn is the strength of the IM method, whose water level predictions are always bounded by water levels measured at two gauging stations. Furthermore, the IM method is based on a conceptual behavior model that is physically consistent. Even though the IM method is empirical and more complex in its implementation, the measured data at most of the fixpoints supported the method's underlying assumptions.

2.5 Conclusions

Several field and modeling studies have shown that the water level distribution in rivers exerts an important influence on the exchange between rivers and groundwater. In this study, we presented two new methods to define spatial and temporal river water level distributions for the purpose of modeling surface water-groundwater systems. The basic idea is to record water levels continuously at water level gauges and measure water levels periodically under different discharge conditions at fixpoints to refine the water level distribution at locations where it is technically difficult or too expensive to install a gauging station. The RM method applies a polynomial regression approach for the prediction of water levels at fixpoints as a function of the corresponding water levels at the determining gauging station, while the IM method uses an interpolation approach between two gauging stations. To compare these alternative methods to a reference method, we developed a third method, which is based on water level data from a 2D hydraulic model and also applies a regression approach (RH). The hydraulic model has the clear advantage of being physically based and covering a wide range of discharge. On the other hand, the alternative methods are simpler and faster in their implementation, while still being able to account for typical hydromorphological features of

dynamic (restored or natural) river sections (e.g. nonlinear longitudinal water level distributions, lateral water level gradients, disconnected river branches and hydraulic jumps).

We compared water level time series generated by both alternative methods with those generated by the reference method at all of the fixpoints located in the 1.2 km long river reach of our field site. For most cases, the accuracy of the water level predictions of the alternative methods was comparable to the accuracy of the reference method itself. In addition, we found evidence that the riverbed, and hence the water level distribution for a given discharge condition, changed between the implementation of the reference and the alternative methods. This change in riverbed morphology might have contributed to some of the larger deviations among water level predictions.

The results of this study allow us to recommend both alternative methods for the river water level assignment in future modeling studies of river-groundwater systems at scales in the order of kilometers. The RM method is straightforward in its implementation, but is limited to water level predictions within the range of measurements made at the fixpoints. If discharge conditions beyond the measured range have to be simulated, we recommend the use of the IM method instead.

Each of the presented methods has limitations in terms of accuracy in water level predictions. Even though we consider each of the methods to be accurate, water level predictions will differ for a specific discharge condition. The impact of the river water level uncertainty on key predictions of groundwater models as exchange flux or groundwater residence time, both in steady state and transient conditions, could be the basis for future research.

Acknowledgments

2.6 Supporting information

This section contains a detailed description of the interpolation methods and their implementation at the Niederneunforn field site.

2.6.1 Problem setup

At our field site, we considered the river as a two-dimensional domain and the two side channels as a one-dimensional domain, based on their different widths. The river geometry was represented by a set of six lines for the main channel plus one line for the disconnected branch. Both side channels were represented by one line (Fig. 2.7). A more general and schematic river system is illustrated in Fig. 2.8. We consider now that each of the lines is mapped by a curvilinear system of longitudinal coordinates x_l. The lines were numbered with an index $j = 1, 2, .., 6$ for the main river channel in our example. Similarly, sections perpendicular to the main course of the river were considered and numbered with another index $i = 1, 2, .., 7$. The same numbering system was used for the river branch and the side channels with the line indices $j = 7, 8, 9$.
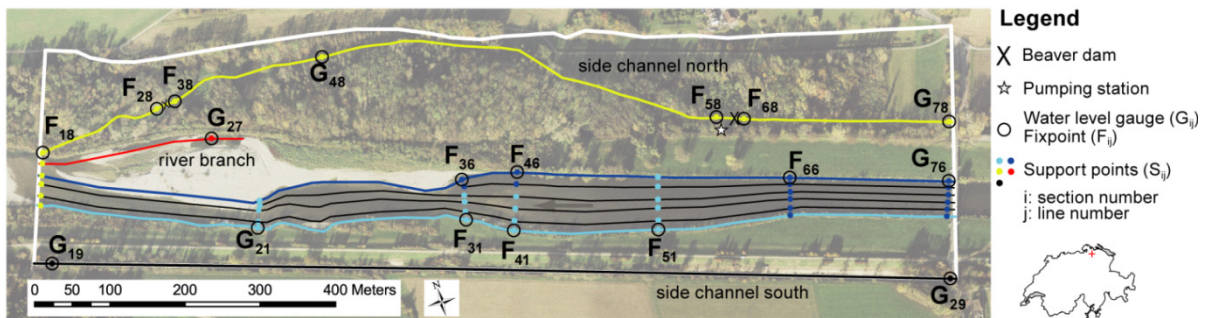
Fig. 2.7. Field site located in Niederneunforn at the Thur River with indicated lines, support points, fixpoints and gauging stations. The colors of the support points indicate the line/fixpoint, from which the water level was transferred. The general flow direction in the river and the side channels is from right to left.

The intersections between the lines and the sections (Fig. 2.8) define the locations of support points where water levels will be estimated using the interpolation methods described below. Support points are identified in this coordinate system with a letter and two indices, S_{ij}. The first index always refers to the section number and the second index always refers to the line number.

25
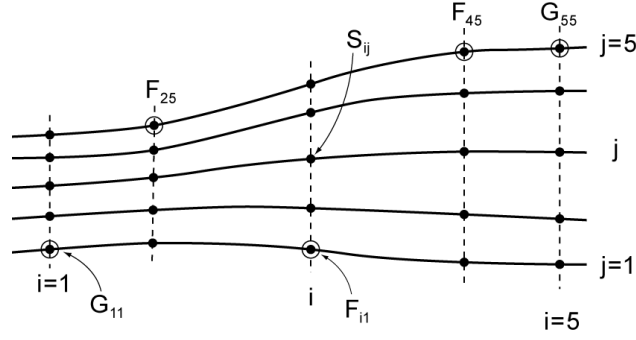
Fig. 2.8. Schematic representation of a curvilinear coordinate system with the lines $j = 1, 2, .., 5$ and the sections $i = 1, 2, .., 5$. The dots at intersections between the lines and the sections represent support points S_{ij} and the circles represent gauging stations G_{ij} or fixpoints F_{ij}.

G_{ij} represents a gauging station located on section i and line j where water levels are measured continuously. F_{ij} represents a fixpoint on section i and line j with periodic manual measurements. Their curvilinear coordinates are denoted $x_l(G_{ij})$ and $x_l(F_{ij})$, respectively. The measured water levels are denoted as $h_{ij}^G(t)$ for those continuously recorded at G_{ij}, and $h_{ij}^F(t^p)$ for those recorded periodically at fixed times t^p at F_{ij}. The longitudinal position of the sections perpendicular to the main river axis are chosen such that each section contains at least one fixpoint or gauging station.

The aim of the interpolation methods is to estimate the water levels at any support point $h_{mn}^S(t)$, where only limited or no water level data is available, by combining the measured water levels at a gauging station $h_{kl}^G(t)$ with those at a fixpoint $h_{ij}^F(t^p)$. The indices kl and mn have the same meaning as ij but refer to a different location within the coordinate system.

The estimation of $h_{mn}^S(t)$ is comprised of three steps.

1. Establish a mathematical relationship ϕ, such that $h_{ij}^F(t^p) \approx \phi[h_{kl}^G(t^p)]$.
2. Use ϕ to compute $h_{ij}^F(t)$ for any time step t: $h_{ij}^F(t) \approx \phi[h_{kl}^G(t)]$.
3. Estimate the water levels $h_{in}^S(t)$ for the support points located on section $m = i$ and lines $n = j$ and $n \neq j$, based on $h_{ij}^F(t)$.

Different options for these steps have been considered for the two new methods, which are both based on measured data at gauging stations and fixpoints and are referred to as alternative methods. In order to compare these alternative methods with a reference, we developed a third method, which is based on a hydraulic model and is referred to as reference method. These three methods are described in the following sections. All three methods have been implemented in a MATLAB program. The final interpolation of the water levels from

26

the support points to the river boundary nodes of the numerical model is identical for all the methods and is accomplished by a one-dimensional linear interpolation along the lines j.

2.6.2   Method 1: Regression of measured data (RM)

This first method is based on using a polynomial regression technique to obtain the mathematical relationship ϕ. For each fixpoint F_{ij}, we identify the gauging station G_{kl}^d (Fig. 2.9, Fig. 2.10) whose extracted water levels $h_{kl}^{Gd}(t^p)$ for the measurement times t^p correlate best with the water levels $h_{ij}^F(t^p)$.
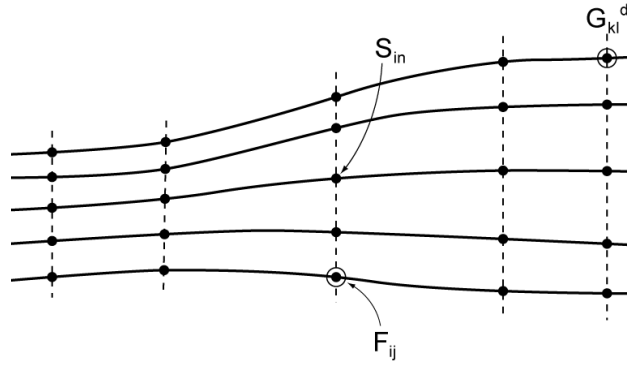
Fig. 2.9. Illustration of the notations used for describing the RM ("Regression of measured data") method.

The polynomial regression is expressed as follows:

$$h_{ij}^F = \phi\left[h_{kl}^{Gd}\right] = \sum_{u=0}^{v} b_u \left(h_{kl}^{Gd}\right)^u \tag{2.1}$$

The gauging station G_{kl}^d is denoted as the determining gauging station as its water level uniquely determines the water level at F_{ij}. The coefficients b_u are obtained by standard least-square fitting to the measured data for the times t^p. To determine the maximum order v of the polynomial Eq. (2.1), we conducted a systematic analysis. We increased the polynomial order step by step and chose the one for which the following increase would have led to a RMSE (root mean square error (Mayer and Butler, 1993)) reduction of less than 0.001 m. This procedure led to a second-order (quadratic) and a first-order (linear) polynomial equation for the fixpoints in the river and in the northern side channel, respectively (Fig. 2.11).

Applying ϕ to any measured time series $h_{kl}^{Gd}(t)$ allows estimating the time series $h_{ij}^F(t)$.

$$h_{ij}^F(t) = \phi\left[h_{kl}^{Gd}(t)\right] = \sum_{u=0}^{v} b_u \left(h_{kl}^{Gd}(t)\right)^u \tag{2.2}$$
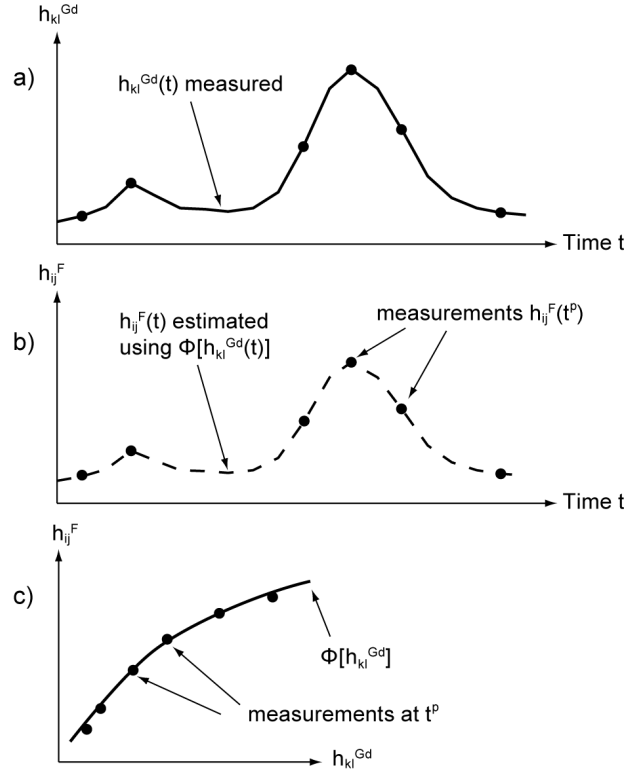
Fig. 2.10. Schematic representation of the regression approach. (a) Continuous water level time series measured at the determining gauging station. (b) Measured water levels at a fixpoint at the times t^p, for which the water levels at the determining gauging station are extracted in (a). (c) ϕ is established between h_{kl}^{Gd} and h_{ij}^{F} by polynomial regression. ϕ is used to estimate the time series $h_{ij}^{F}(t)$ in (b).

At section three and four, the water levels were measured at two fixpoints (F_{31}, F_{36} and F_{41}, F_{46}) on both shores to capture the lateral gradients. The lateral water level differences vary depending on the river stage. These differences are in the order of 0.4 m for low water levels and gradually decrease as the water level rises (Fig. 2.11). This suggests an asymmetric riverbed morphology inducing lateral water level gradients for low-flow conditions. As the water level rises, the influence of the riverbed morphology decreases until the lateral differences are negligible.

The estimation of the water level $h_{in}^{S}(t)$ at the support points of section i (Fig. 2.9) based on the water level $h_{ij}^{F}(t)$ (or $h_{ij}^{G}(t)$) is made in the simplest possible manner. In general, it is assumed that there is no lateral gradient and therefore we have the following expression:

$$h_{in}^{S}(t) = h_{ij}^{F}(t), \quad n = j \ and \ n \neq j \tag{2.3}$$

For the support points S_{3n} and S_{4n} at section three and four however, we assigned the water levels of the northern fixpoints to the support points of the lines $n = 5, 6$ and the water levels

28

of the southern fixpoints to the support points on the lines $n = 1..4$, based on field observations.
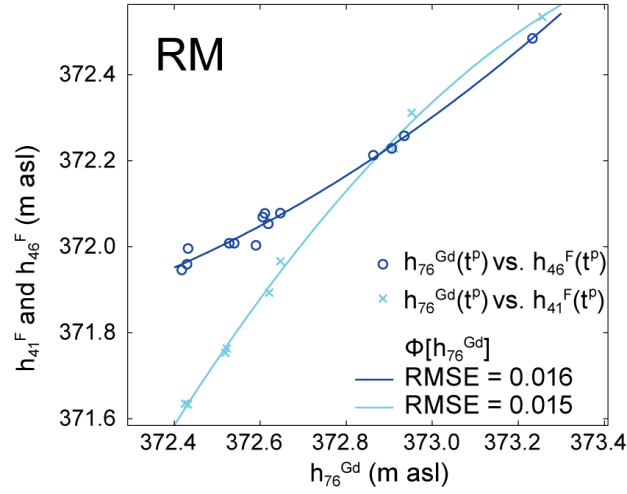
Fig. 2.11. Application of the regression approach to establish ϕ between the water levels at the determining gauging station h_{76}^{Gd} and the water levels at the fixpoints h_{41}^{F} and h_{46}^{F} according to the RM ("Regression of measured data") method. The RMSE of the polynomial equations are indicated.

2.6.3   Method 2: Interpolation of measured data (IM)

The second method uses an interpolation function ϕ that estimates the water level at a fixpoint F_{ij}, located between a determining gauging station G_{kl}^{d} and a second gauging station G_{mn}. The identification of the determining gauging station is not strictly defined; it can be either the upstream or the downstream gauging station. We assume for the development of the equations that the upstream gauging station is the determining gauging station and that F_{ij}, G_{kj}^{d} and G_{mj} are located on the same line j but on different sections i, k and m (Fig. 2.12).
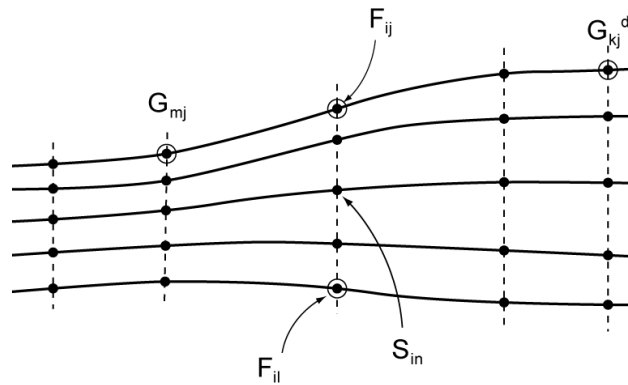
Fig. 2.12. Illustration of the notations used for describing the IM ("Interpolation of measured data") method.

According to the IM method, the water levels $h_{ij}^F(t)$ at a fixpoint between G_{kj}^d and G_{mj} can generally be described by a linear interpolation term $l_{ij}(t)$ plus a deviation from this linear trend $D_{ij}(t)$.

$$h_{ij}^F(t) = \phi\left[h_{kj}^{Gd}(t)\right] = l_{ij}(t) + D_{ij}(t) \tag{2.4}$$

with

$$l_{ij}(t) = h_{kj}^{Gd}(t) - \frac{x_l(F_{ij}) - x_l(G_{kj}^d)}{x_l(G_{mj}) - x_l(G_{kj}^d)}\left(h_{kj}^{Gd}(t) - h_{mj}^G(t)\right) \tag{2.5}$$

According to the conceptual behavior model, on which the IM method relies, $D_{ij}(t)$ is at a maximum a_{ij} for water levels $h_{kj}^{Gd}(t)$ smaller than a specific water level h^a due to a strong influence of the riverbed morphology (Fig. 2.13a).

$$D_{ij}(t) = a_{ij}, \qquad h_{kj}^{Gd}(t) < h^a \tag{2.6}$$

As the water level rises, the influence of the riverbed morphology decreases and the longitudinal water level distribution approaches a linear shape, with $D_{ij}(t)$ being zero (Fig. 2.13a) for water levels $h_{kj}^{Gd}(t)$ higher than a threshold water level h^{thresh}.

$$D_{ij}(t) = 0, \qquad h_{kj}^{Gd}(t) > h^{thresh} \tag{2.7}$$

To account for the decrease of $D_{ij}(t)$ between h^a and h^{thresh}, a_{ij} is multiplied by an "inhibition term", which is assumed to decrease linearly from one to zero (Fig. 2.13b).

$$D_{ij}(t) = a_{ij}\left(1 - \frac{h_{kj}^{Gd}(t) - h^a}{h^{thresh} - h^a}\right), \qquad h^a \le h_{kj}^{Gd}(t) \le h^{thresh} \tag{2.8}$$
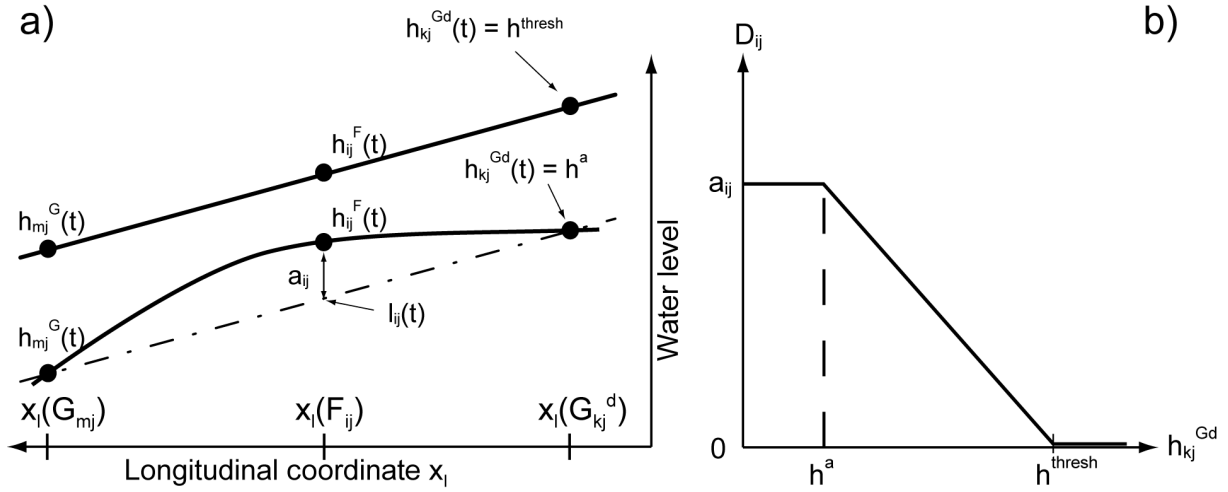
Fig. 2.13. Schematic illustration of the interpolation approach. (a) Two hypothetical longitudinal water level profiles for the situations $h_{kj}^{Gd}(t) = h^a$ and $h_{kj}^{Gd}(t) = h^{thresh}$. (b) D_{ij} as a function of h_{kj}^{Gd}.

To estimate $h_{ij}^F(t)$ according to Eq. (2.4), the parameters a_{ij}, h^a and h^{thresh} have to be obtained at each fixpoint. To obtain these parameters, we calculate the deviation from the linear trend $D_{ij}(t^p)$ for each measurement $h_{ij}^F(t^p)$.

$$D_{ij}(t^p) = h_{ij}^F(t^p) - l_{ij}(t^p) = a_{ij}\left(1 - \frac{h_{kj}^{Gd}(t^p) - h^a}{h^{thresh} - h^a}\right) \qquad (2.9)$$

According to Eq. (2.9), plotting $D_{ij}(t^p)$ against $h_{kj}^{Gd}(t^p)$ should reveal a linear dependence between the water levels h^a and h^{thresh} (Fig. 2.13b), which was confirmed by the data at most of our fixpoints (Fig. 2.14). The parameters can then be estimated according to Fig. 2.13b. Typically, we use the maximum value of $D_{ij}(t^p)$ for a_{ij} and the corresponding value of $h_{kj}^{Gd}(t^p)$ for h^a. The threshold value h^{thresh} can be determined by using the value $h_{kj}^{Gd}(t^p)$ for which $D_{ij}(t^p)$ is zero. In case the measured water level spectrum did not include high enough values of $h_{kj}^{Gd}(t^p)$ for $D_{ij}(t^p)$ going to zero, the linear trend can be extrapolated to the intersection with the abscissa to estimate h^{thresh}.

To account for lateral water level gradients in a two-dimensional river system, the IM method extends the conceptual behavior model, which is described above for the longitudinal direction, to the lateral direction. Accordingly, the water level at a fixpoint F_{il} located on a second line l (Fig. 2.12) can be described by the water level at the fixpoint F_{ij} plus a lateral difference D_{il}^L.

$$h_{il}^F(t) = \phi\left[h_{kj}^{Gd}(t)\right] = h_{ij}^F(t) + D_{il}^L(t) \qquad (2.10)$$

31

D_{il}^{L} is at a maximum a_{il}^{L} for water levels $h_{kj}^{Gd}(t)$ smaller than a specific water level h^{aL}, due to the influence of an asymmetric riverbed.

$$D_{il}^{L}(t) = a_{il}^{L}, \qquad h_{kj}^{Gd}(t) < h^{aL} \tag{2.11}$$

For water levels $h_{kj}^{Gd}(t)$ higher than a threshold water level $h^{threshL}$, the lateral gradients disappear.

$$D_{il}^{L}(t) = 0, \qquad h_{kj}^{Gd}(t) > h^{threshL} \tag{2.12}$$

In between, a linear decrease of $D_{il}^{L}(t)$ is assumed.

$$D_{il}^{L}(t) = a_{il}^{L}\left(1 - \frac{h_{kj}^{Gd}(t) - h^{aL}}{h^{threshL} - h^{aL}}\right), \qquad h^{aL} \leq h_{kj}^{Gd}(t) \leq h^{threshL} \tag{2.13}$$

The measured lateral difference

$$D_{il}^{L}(t^{p}) = h_{il}^{F}(t^{p}) - h_{ij}^{F}(t^{p}) = a_{il}^{L}\left(1 - \frac{h_{kj}^{Gd}(t^{p}) - h^{aL}}{h^{threshL} - h^{aL}}\right) \tag{2.14}$$

can be plotted against the water level $h_{kj}^{Gd}(t^{p})$ in order to estimate the required parameters by Eq. (2.10). The same procedure can be applied as described above for estimating the parameters required for Eq. (2.4) (Fig. 2.13b). The linear dependence of D_{il}^{L} on h_{kj}^{Gd} as expected by Eq. (2.14) was confirmed by our data (Fig. 2.14).

In our example, we determined the water levels at almost all fixpoints by using the formulation for $h_{ij}^{F}(t)$ according to Eq. (2.4). The determining and the second gauging stations as well as the parameters describing $D_{ij}(t)$ are listed in Table 2.2.

Eq. (2.4) assumes that both gauging stations are located on the same line as the fixpoint, which is not the case for our river system. However, as we assume equal water levels across each section (Eq. (2.3)) except at section three and four, this assumption is still valid. At section three and four, we determined the water levels at the southern fixpoints F_{31} and F_{41} by using the formulation for $h_{il}^{F}(t)$ according to Eq. (2.10). In Table 2.2, the parameters describing $D_{il}^{L}(t)$ are written in italic. The estimation of the water level at the support points $h_{in}^{S}(t)$ is identical to the procedure described for the RM method in the previous section.
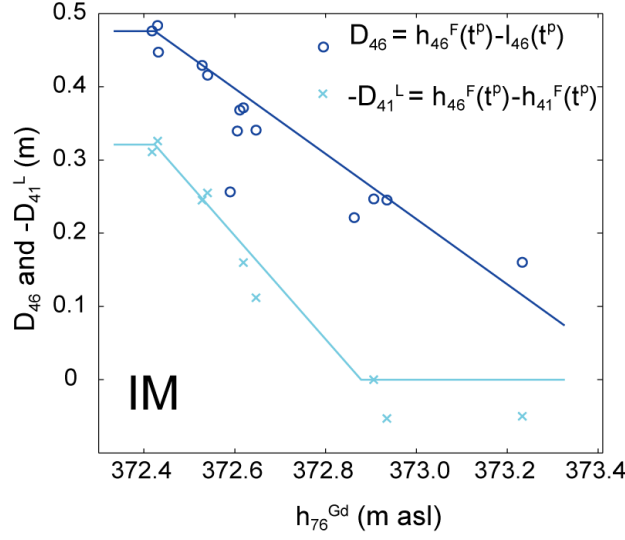
Fig. 2.14. Application of the interpolation approach to estimate the required parameters to establish ϕ according to the IM ("Interpolation of measured data") method. Dark blue: Measured deviations from the linear trend for the fixpoint F_{46}. Light blue: Measured water level differences between the fixpoints F_{46} and F_{41}. The lines indicate the linear trend as expected by Eqs. (2.8) and (2.13).

Table 2.2. Determining gauging stations G_{kl}^d of each fixpoint and gauging station along the lines $j = 1, 6$ (river main channel) and $j = 8$ (northern side channel) for all methods. For the IM method, the second gauging station G_{mn} and the resulting parameters of Eqs. (2.4) and (2.10) are also given. The dashes indicate that the data of the gauging station are used directly. The italic numbers refer to the description of lateral gradients according to Eq. (2.10). The brackets for the fixpoints and gauging stations in the northern side channel for the reference RH method (see next section) indicate the coupling to the RM method.

	RM G_{kl}^d	IM G_{kl}^d	G_{mn}	a_{ij} / a_{ij}^L [m]	h^a / h^{aL} [m asl]	h^{thresh} / $h^{threshL}$ [m asl]	RH G_{kl}^d
F_{18}	G_{76}	G_{76}	G_{21}	-0.20	372.43	373.20	G_{76}
G_{21}	-	-	-	-	-	-	G_{76}
F_{36}	G_{76}	G_{76}	G_{21}	0.47	372.43	373.60	G_{76}
F_{31}	G_{76}	G_{76}	G_{21}	*-0.25*	*372.43*	*372.90*	G_{76}
F_{46}	G_{76}	G_{76}	G_{21}	0.47	372.43	373.60	G_{76}
F_{41}	G_{76}	G_{76}	G_{21}	*-0.32*	*372.43*	*372.90*	G_{76}
F_{51}	G_{76}	G_{76}	G_{21}	0.44	372.43	373.60	G_{76}
F_{66}	G_{76}	G_{76}	G_{21}	0.28	372.43	373.60	G_{76}
G_{76}	-	-	-	-	-	-	-
F_{28}	G_{48}	F_{18}	G_{48}	0.46	370.35	371.31	(G_{48})
F_{38}	G_{48}	F_{18}	G_{48}	0.48	370.35	371.60	(G_{48})
G_{48}	-	-	-	-	-	-	$(-)$
F_{58}	G_{48}	G_{48}	G_{78}	-0.29	371.57	373.00	(G_{48})
F_{68}	G_{78}	G_{48}	G_{78}	0.20	371.57	371.83	(G_{78})
G_{78}	-	-	-	-	-	-	$(-)$

2.6.4 Method 3: Regression of hydraulic model data (RH)

To compare the two alternative methods with an independent reference, we developed a third method that is based on data from an existing hydraulic model of the main river channel in the section of interest. This reference method applies a polynomial regression technique to obtain the mathematical relationship ϕ, as the RM method does. In contrast to the RM method however, the RH method allows the extraction of water level information directly at each support point within the river domain $h_{ij}^{S}(Q)$ from the hydraulic model output, each corresponding to one specific discharge condition Q. We identify the determining support point S_{kl}^{d} that is located at the position of the determining gauging station G_{kl}^{d} (Fig. 2.15), whose water levels correlate best with the water levels within the river domain.
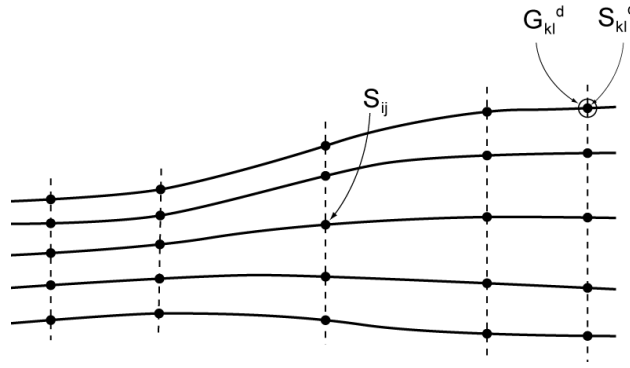
Fig. 2.15. Illustration of the notations used for describing the RH ("Regression of hydraulic model data") method.

The polynomial regression is performed by standard least-square fitting in order to obtain the parameters b_u according to the following equation:

$$h_{ij}^{S} = \phi\left[h_{kl}^{Sd}\right] = \sum_{u=0}^{v} b_u \left(h_{kl}^{Sd}\right)^{u}$$

(2.15)

Applying the systematic analysis described in the section of the RM method, we determined a maximal order $v = 4$ for the polynomial Eq. (2.15) (Fig. 2.16). The range of extracted water levels from the hydraulic model (Fig. 2.16) is much bigger than the range of measured water levels used for the RM method (Fig. 2.11). This difference explains the different polynomial order for the RH and RM method as a second-order polynomial approximates a fourth-order polynomial over a small range. The hydraulic model confirmed the existence of lateral water level gradients and their decrease for increasing water levels (Fig. 2.16), as included in the RM and IM method.

The application of ϕ to a measured time series $h_{kl}^{Gd}(t)$ allows estimating the time series $h_{ij}^{S}(t)$.

$$h_{ij}^{S}(t) = \phi\left[h_{kl}^{Gd}(t)\right] = \sum_{u=0}^{v} b_u \left(h_{kl}^{Gd}(t)\right)^u \qquad (2.16)$$

As the hydraulic model did not include the disconnected branch and the side channels, we coupled the RH method to the RM method (Table 2.2).
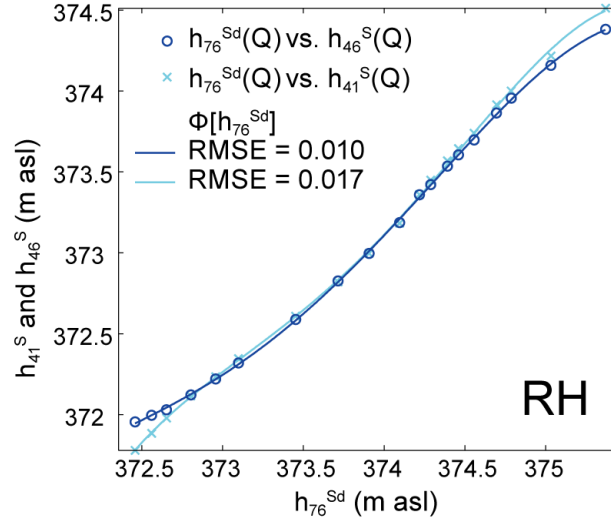
Fig. 2.16. Application of the regression approach to establish ϕ between the water levels at the determining support point h_{76}^{Sd} and the water levels h_{41}^{S} and h_{46}^{S} according to the RH method ("Regression of hydraulic model data"). The RMSE of the polynomial equations are indicated.

Chapter 3

Assessing the effect of different river water level interpolation schemes on modeled groundwater residence times

Abstract

Modeling river-groundwater interactions requires knowledge of the river's spatiotemporal water level distribution. A quantitative understanding of these interactions is of particular importance in the context of river restoration. The dynamic nature of riverbed morphology in restored river reaches might result in complex river water level distributions, including disconnected river branches, nonlinear longitudinal water level profiles and morphologically induced lateral water level gradients. Recently, two new methods were proposed to accurately and efficiently capture 2D water level distributions of dynamic rivers. In this study, we assessed the predictive capability of these methods with respect to simulated groundwater residence times. Both methods were used to generate surface water level distributions of a 1.2 km long partly restored river reach of the Thur River in northeastern Switzerland. We then assigned these water level distributions as boundary conditions to a 3D steady-state groundwater flow and transport model. When applying either of the new methods, the calibration-constrained groundwater flow field accurately predicted the spatial distribution of groundwater residence times; deviations were within a range of 30% when compared to residence times obtained using a reference method. We further tested the sensitivity of the simulated groundwater residence times to a simplified river water level distribution. The negligence of lateral river water level gradients of 20-30 cm on a length of 200 m caused errors of 40-80% in the calibration-constrained groundwater residence time distribution compared to results that included lateral water level gradients. The additional assumption of a linear water level distribution in longitudinal river direction led to deviations from the complete river water level distribution of up to 50 cm, which caused wide-spread errors in

simulated groundwater residence times of 200-500%. For an accurate simulation of groundwater residence times, it is therefore imperative that the longitudinal water level distribution is correctly captured and described. Based on the confirmed predictive capability of the new methods to estimate 2D river water level distributions, we can recommend their application to future studies that model dynamic river-groundwater systems.

3.1 Introduction

Groundwater flow and transport modeling is a valuable and frequently applied tool to gain a process-based understanding of surface water-groundwater systems, providing quantitative information on flow paths, mixing ratios and residence times (Wondzell et al., 2009). It is well known from synthetic modeling studies that riverbed morphology affects the river water level distribution, which in turn drives the exchange with groundwater (Woessner, 2000; Cardenas et al., 2004; Cardenas, 2009). Therefore, an important prerequisite for the setup of a groundwater flow and transport model of a real surface water-groundwater system is an accurate description of the water level distribution along the surface water boundary conditions.

A quantitative assessment of groundwater flow paths and residence times is of particular interest at riverbank filtration systems (Tufenkji et al., 2002). Groundwater residence time is an important parameter in determining the effectiveness of the natural attenuation processes that occur during riverbank filtration (Eckert and Irmscher, 2006). River restoration measures, such as riverbed enlargements, potentially lead to reduced groundwater residence times, and hence, to an increased risk of drinking water contamination (Hoehn and Scholtis, 2011) that competes with the original purpose of river restoration (Brunke and Gonser, 1997; Woolsey et al., 2007). Groundwater flow and transport modeling could help to mitigate this conflict of interest, by providing a quantitative assessment of the groundwater flow paths and residence times (Hoehn and Meylan, 2009).

Restored river systems may have complex water level distributions characterized by nonlinear longitudinal water level distributions, morphologically induced lateral water level gradients, disconnected river branches and hydraulic jumps. Such water level distributions need to be characterized by their full spatial (i.e. two horizontal dimensions) and temporal extent (i.e. for any discharge condition) and ideally are extracted from hydraulic models (Doppler et al., 2007; Derx et al., 2010; Engeler et al., 2011). However, the setup of a hydraulic model is time consuming and requires a considerable amount of data input. In Chapter 2, we proposed two new alternative interpolation methods to estimate time-varying one- and two-dimensional (1D,

2D) surface water level distributions of dynamic rivers based directly on measured water level data. Even though transient water level predictions with the alternative methods are considered to be accurate when compared to those of a third reference method, water level predictions will differ for a specific discharge condition (Chapter 2).

In this study, we assess the predictive capability of the new alternative methods with respect to the simulated groundwater residence time and the effect of reducing the considered level of detail in the surface water level distribution. Thereto, steady-state surface water level distributions at a partly restored riverbank filtration system are generated with both alternative methods and the reference method, as well as with two simplified methods. The resulting water level distributions are then assigned to a 3D groundwater flow and transport model. After calibration against groundwater heads, each of the model scenarios is used to predict the spatial groundwater residence time distribution within the modeling domain.

3.2 Interpolation methods

The interpolation methods used in this study are based on those established in Chapter 2. A brief description of the methods is provided in this section, but for a more detailed description the reader is referred to Chapter 2. The alternative methods and the reference method are referred to as "complete interpolation methods", as they cover the full level of detail including lateral water level gradients and nonlinear longitudinal water level distributions.

3.2.1 Complete interpolation methods

Both new alternative interpolation methods are based on the concept of combining continuous water level records (h^G) from water level gauges (G) with periodic water level measurements (h^F) at fixpoints (F) in between. By combining this data, the water level distribution between the water level gauges is obtained at a higher resolution. Fixpoints are defined as reference points in the river whose altitude is known. The first alternative "RM method" (Regression of measured data) applies a polynomial regression technique to predict water levels at fixpoints from any measured water level at a specific water level gauge, while the second alternative "IM method" (Interpolation of measured data) uses a nonlinear interpolation approach between two water level gauges.

Depending on the lateral extent, the river might be considered as a 1D or a 2D domain. In the latter case, the river is discretized by multiple lines parallel to the main flow direction of the river and several sections of support points (S) perpendicular to the flow direction (Fig. 3.1). Sections of support points are defined at locations where a water level gauge or a fixpoint

exists. One fixpoint per section is enough unless lateral water level gradients are observed, in which case a fixpoint should be defined on both shorelines.

The water levels at the support points (h^S) are estimated from the water levels at the fixpoint in the simplest possible manner. If no lateral water level gradient exists, the water level of the fixpoint is assigned to all support points on the same section. If a second fixpoint was defined to capture lateral gradients, assigning water levels to the support points should be based on field observations. The final interpolation of water levels from the support points to the river boundary nodes of the numerical model is identical for all the interpolation methods and is performed by a linear interpolation along the set of lines.

The third complete "RH method" (Regression of hydraulic model data) applies a polynomial regression technique, similar to the RM method, but is based on water levels extracted from a hydraulic model at each support point directly. The RH method is therefore considered as reference method among the complete interpolation methods.

3.2.2   Simplified interpolation methods

In addition to the predictive comparison of the complete interpolation methods described above, we assessed the error in residence time prediction that evolves when the water level distribution of the river is simplified. Thereto, we applied two progressively simplified methods, both based on the complete IM method. The first simplified method ignores lateral water level gradients and is denoted as "Interpolation of measured data without lateral gradients" (IM_wo_lat). The second simplification additionally assumes a linear interpolation between the river water level gauges and is called "Interpolation of measured data assuming a linear interpolation" (IM_lin).
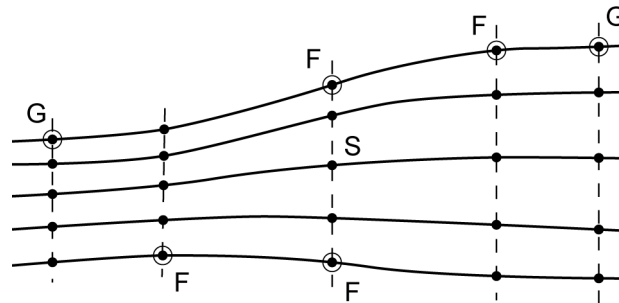
Fig. 3.1. Schematic illustration of a river system with multiple lines and sections of support points (S, filled black circles). The open black circles indicate the water level gauges (G) and fixpoints (F).

3.3   Method implementation

This section provides a description of the Niederneunforn field site (Section 3.3.1) and a review of the implementation of the interpolation methods at this field site (Section 3.3.2). Section 3.3.3 presents the generated surface water level distributions, which we assigned to the groundwater flow and transport model (see Section 3.4) to simulate the spatial groundwater residence time distribution.

3.3.1   Field site

The Niederneunforn field site (Fig. 3.2) is located at the Thur River in NE-Switzerland, approximately 12 km upstream of the confluence with the Rhine River. The Thur River is a peri-alpine river draining a catchment area of 1730 km^2. It is the largest river in Switzerland without a retention basin and therefore has a very dynamic discharge regime. Discharges range from 3 to 1100 m^3/s, with an average discharge of 47 m^3/s.
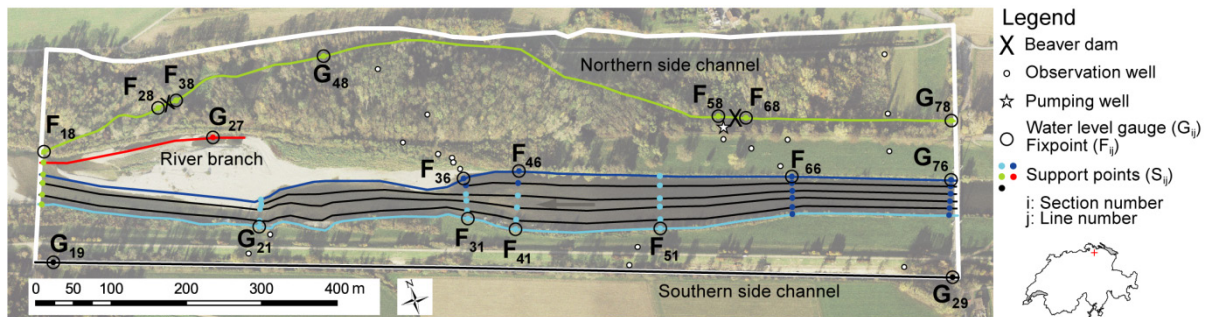
Fig. 3.2. Niederneunforn field site at the Thur River in NE-Switzerland. Fixpoints and water level gauges in the river and the side channels are shown as open black circles. Based on their position, the set of lines and sections of support points (filled circles) were defined for the implementation of the interpolation methods. The colors of the lines will be used in Fig. 3.4 again. The colors of the support points in the river indicate the shore line or the fixpoint/water level gauge on that shore line from which the water levels were transferred. The white polygon represents the modeling domain. The general flow direction of the river and the side channels is from right to left.

The field site was instrumented with more than 80 piezometers (2'') during the interdisciplinary RECORD project (Restored corridor dynamics, http://www.cces.ethz.ch/projects/nature/Record; Schirmer (2013); Schneider et al. (2011)) in the context of restoration measures that were realized in 2002. The river restoration was constrained to the northwestern part of the river reach (Fig. 3.2). Restoration measures were forbidden in the northeastern part in order to protect the water quality of the nearby pumping station, which supplies the community of Nieder- and Oberneunforn with drinking water. This vertical well produces a total of 36 m^3, split into two daily periods of 1 h and 2 h. At the

southern bank of the Thur River, the bank stabilization was maintained to protect the 4 m-high dam, which prevents flooding of nearby farms and agricultural land.

Based on 57 drilling profiles, the gravel-and-sand aquifer has a thickness of 5.3±1.2 m at the field site. Hydraulic conductivities were estimated to range from 4×10^{-3} to 4×10^{-2} m/s by slug tests, a pumping test and a salt tracer test (Diem et al., 2010; Doetsch et al., 2012). The aquifer is underlain by a lacustrine clay layer, which forms the lower hydraulic boundary. On top of the aquifer is a 0.5-3 m thick layer of silty sand from the alluvial fines that can be regarded as the semi-confining unit. The aquifer varies both spatially and temporally between confined and unconfined. Cross-borehole georadar travel-time tomography revealed an average porosity of 20±3% (Schneider et al., 2011).

At the field site, the width of the Thur River varies between 50 and 100 m (Fig. 3.2). After the completion of the restoration measures, a large gravel bar has evolved at the downstream end of the river reach. At the same time, a partly disconnected branch of the river developed, which is only flooded at high river stages (>200 m^3/s) and is otherwise fed by groundwater. During low-flow conditions, the river water level profile in the longitudinal direction is nonlinear. In the upstream 400 m, the gradient is 0.5‰ and in the downstream 800 m, it is 2‰. In the central part of the river reach, lateral water level gradients occur during low-flow conditions. These lateral surface water level differences are caused by the asymmetrical riverbed morphology and can reach up to 0.4 m. Two side channels (north and south) flow parallel to the river with widths ranging between 4 and 8 m. Two beaver dams are located in the northern side channel. The upstream dam has a more pronounced effect on water levels, resulting in changes of up to 0.5 m.

3.3.2 Data collection

Two water level gauges were installed in the main channel of the river, two in each side channel, and one in the river branch (Fig. 3.2). Several fixpoints were added between the water level gauges to increase the spatial resolution of the water level distribution. In the northern side channel, the fixpoints were placed upstream and downstream of both beaver dams to capture the hydraulic jumps. Fixpoints in the river were placed close to piezometer transects, either on the northern or on the southern shore. In the central portion of the river reach, where lateral water level gradients were observed, a fixpoint was added on either shore. The southern side channel is very straight, has a uniform width, and does not have any obstacles. Therefore, a linear water level distribution was assumed between the water level gauges, which was confirmed by one set of measurements along the channel.

Water levels were measured periodically at the fixpoints between February and May 2011 covering a discharge range of 10 to 100 m³/s. The sensors of the water level gauges (DL/N 70, STS AG, Switzerland) have been continuously measuring pressure, temperature and electrical conductivity (EC) at 15-min intervals since April 2010 (error of single measurement: ±0.1% for pressure, ±0.25% for temperature and ±2% for EC, according to the manufacturer's manual). For model calibration, the same type of sensor was placed in each of the observation wells shown in Fig. 3.2. The raw data of the water level gauges and the observation wells were processed to correct for the barometric air pressure, and to transform the pressure data to absolute water levels (m asl).

The system of lines and support points was defined based on the location of water level gauges and fixpoints. Each point can be identified by a uniquely defined indexing system. The first index i refers to the section number and the second index j to the line number (G_{ij}, F_{ij}, S_{ij}). The river was considered to be a 2D domain, described by a set of six lines for the main channel, and one additional line for the disconnected branch. Sections of support points were defined wherever a water level gauge or a fixpoint was located. The colors of the support points in Fig. 3.2 indicate the shore line or the fixpoint/water level gauge on that shore line, from which the water levels were transferred. A zero lateral gradient was assumed everywhere except for the river sections $i = 3, 4$, where the generally lower water levels of the southern fixpoints were assigned to the support points on lines $j = 1..4$ and the generally higher water levels of the northern fixpoints to the support points on lines $j = 5, 6$ (Fig. 3.2). Because the width of the northern and southern side channel is much smaller relative to the river width, they were considered as a 1D domain and described by a single line.

For the implementation of the RH method, an existing 2D hydraulic model of the Thur River was used, which was developed based on the bathymetry measured in September 2009 and covered a discharge range of 10-650 m³/s (Schäppi et al., 2010; Pasquale et al., 2011). The hydraulic model did not include the side channels and the disconnected river branch. Therefore, the RH method was coupled to the RM method to cover the full surface water level distribution at the Niederneunforn field site.

Fig. 3.3a shows a 3-month water level time series at the support point S_{46}, determined using the reference RH method (black line). The time series of measured groundwater head at an observation well located 100 m from S_{46} (gray line, Fig. 3.3a) illustrates the quasi-instantaneous reaction of the groundwater heads to changes in the river water level, with a propagation speed of about 0.2 m/s or 19600 m/d. Minima in EC, which corresponded with

peak flows in the river, were caused by the diluting effect of rain events (Fig. 3.3b). The characteristic EC signal was identified in all observation wells close to the river, both on its northern and its southern side, which indicates losing conditions. The EC signal in the river was transported into groundwater and was used as a natural tracer. By analyzing the EC time series with nonparametric deconvolution (Cirpka et al., 2007; Vogt et al., 2010a), we obtained estimates of local residence time distributions, characterized by a mean and a standard deviation (Supporting information; Section 3.7: Fig. 3.9, Fig. 3.10, Table 3.2).
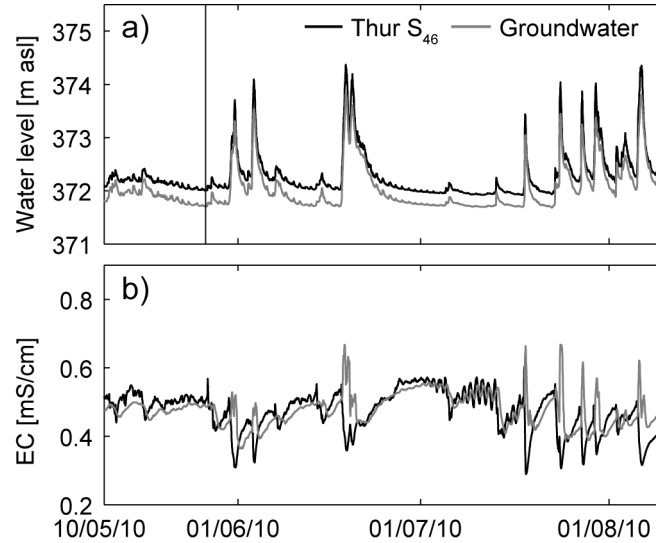
Fig. 3.3. (a) Water level time series (May to August 2010) generated by the RH method at support point S_{46} in the Thur River (black line) and measured groundwater head time series at a nearby observation well (gray line). The black vertical line indicates the point in time (May 26, 2010, 17:00) for which the surface water level distribution at the field site was generated using each of the five methods (Fig. 3.4). (b) Time series of electrical conductivity (EC) measurements in the Thur River at the same observation well used in (a).

3.3.3 Generated water level distributions

The surface water level distributions used for the steady-state model simulations were generated with all interpolation methods for the conditions on May 26, 2010 (vertical line in Fig. 3.3a), which was at the end of a relatively short period of low flow (23 m^3/s). As groundwater heads are highly correlated with the river water levels (Fig. 3.3a), a steady-state assumption is reasonable.

Fig. 3.4a shows the spatial water level distributions generated by the three complete methods. For better clarity, we only plotted the results from one line in the main river channel ($j = 6$, dark blue), which illustrates the nonlinear longitudinal water level distribution. The southern side channel ($j = 9$, black line) had a much lower water level than the river and therefore complied with its purpose of draining groundwater. Water levels in the northern side channel

($j = 8$, green line) were considerably higher because the northern channel flows back to the river at the western end of the field site (river section $i = 1$). The northern side channel could only drain groundwater in one ~400 m segment, where water levels were below river water levels. This segment was located downstream of the 50 cm water level drop caused by the eastern beaver dam (S_{58}). The disconnected branch of the river ($j = 7$, red line) showed slightly lower water levels than the main river channel. The disconnected branch and the exfiltrating segment of the northern side channel seemed to be responsible for the river infiltration that occurred to the northern side of the river.

Even though the alternative methods are considered to be accurate in their water level predictions (Chapter 2), single realizations of the spatial water level distribution showed deviations from the reference RH method of mostly 10 to 20 cm (Fig. 3.4a). However, errors of more than 30 cm occurred at the river section $i = 1$. As this section was located on a bend in the river, the section did not cross the river perpendicularly. The RH method accounted for the water level gradient across this section by assigning a water level to each of the support points individually, based on the hydraulic model. In contrast, the alternative methods assumed a constant water level across section $i = 1$, as water level information was only available from one fixpoint (F_{18}).

Other deviations in the output from the complete methods were caused by a different data basis (hydraulic model vs. measured data) and/or the different structure of the interpolation methods. The coupling of the RH method to the RM method for the northern and the southern side channel led to identical water level distributions for lines $j = 8, 9$. The IM method showed an identical water level distribution for the southern side channel as well, while deviations from the RM/RH method in the northern side channel reached a maximum of 10 cm at S_{58}.

In Fig. 3.4b, water level distributions determined from the complete IM method and from the two simplified versions are depicted. The main river channel is now represented by the southern shoreline ($j = 1$, light blue). The IM method considered lateral water level gradients across sections $i = 3, 4$ where water levels on the southern shoreline $j = 1$ (representative for lines $j = 1..4$, see Fig. 3.2) were 20-30 cm lower than on the northern shoreline $j = 6$ (representative for lines $j = 5, 6$, see Fig. 3.2). The first simplified IM method (IM_wo_lat) ignored these lateral water level gradients and the water levels of the northern fixpoints were assigned to all support points on sections $i = 3, 4$. As a consequence, water levels on the southern lines $j = 1..4$ increased by 20 and 30 cm, respectively (Fig. 3.4b, Fig. 3.2). The

second simplification of the IM method (IM_lin) additionally assumed a linear interpolation between the two water level gauges, which are located at river sections $i = 2, 7$. This assumption caused deviations in water levels of 30-50 cm at the support points in between ($i = 3..6$).
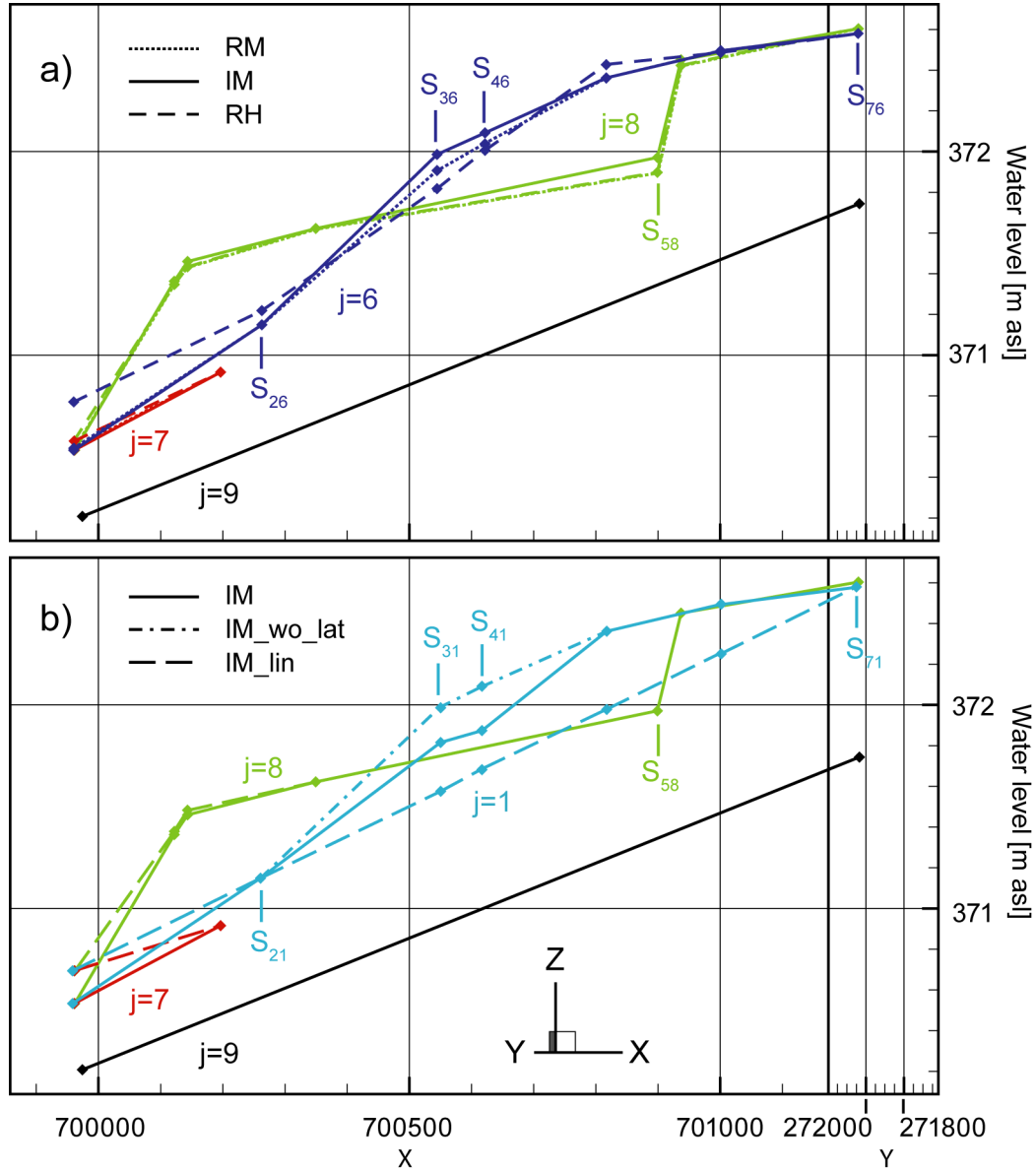
Fig. 3.4. (a) Spatial water level distribution along the lines $j = 6..9$, generated with the three complete interpolation methods. The figure is orientated for a viewer looking towards NNE, with the flow from right to left. (b) Spatial water level distribution along the lines $j = 1, 7..9$, generated with the IM method and its two simplified versions. The water level distributions were generated for the conditions on May 26, 2010, 17:00 (vertical line in Fig. 3.3a, discharge 23 m^3/s). The colors of the lines correspond to those of Fig. 3.2 and textures of the lines correspond to the different interpolation methods (see legend).

3.4 Groundwater flow and transport model

3.4.1 Numerical model setup

We set up a 3D finite-element groundwater flow and transport model using FEFLOW (version 6.0, DHI-WASY GmbH). The modeling domain is shown in Fig. 3.2. The northern boundary is defined by the northern end of the aquifer and the southern boundary by the southern side channel. The vertical model extent was restricted to the gravel-and-sand aquifer, whose top and bottom elevations were determined from 26 drilling profiles, from which the entire model domain was interpolated using a kriging technique. The horizontal discretization length of the triangular elements varied between 1 and 5 m around observation wells and along boundaries, including the river and the side channels. In the remaining model domain, the maximal horizontal length of the elements was 10 m. In the vertical direction, the aquifer was subdivided into five layers. The top four layers had a thickness of 1 m and the bottom layer had a variable thickness.

The definition of the boundary conditions is depicted in Fig. 3.5. We applied an influx boundary condition on the eastern and northern borders (q1 = 0.18 m/d, q2 = 0.0043 m/d), and an outflux boundary condition on the western border (q3 = -0.57 m/d, q4 = -2.3 m/d). These 2nd Type boundary conditions were applied to all layers. We determined the absolute groundwater flux from measured hydraulic gradients and estimated hydraulic conductivities. Recharge was neglected, as no rainfall occurred for ~10 d before the simulation time (Fig. 3.3a). At the location of the pumping well we assigned an average extraction rate of 36 m^3/d (0.4 L/s).

Within the modeling domain, the southern side channel is exfiltrating along its entire length due to water levels well below those in the river (Fig. 3.4a). The channel bed sediments are gravelly and tracer tests revealed a good connection to groundwater. We therefore chose a 1D fixed-head boundary condition (1st Type) for the top layer along the southern side channel.

A colmation layer of unknown thickness was identified in the bed of the Thur River (Hoehn and Meylan, 2009; Schneider et al., 2011). The bed of the northern side channel was covered by a thick (0.5-1 m) silt and clay colmation layer, except in the middle exfiltrating segment located downstream of the eastern beaver dam, where the bed sediments were gravelly. To account for the effect of colmation, we assigned a Cauchy boundary condition (3rd Type) to the river and the northern side channel. In FEFLOW, the colmation layer is characterized by a transfer rate $L = K_r/d_r$. K_r corresponds to the hydraulic conductivity of the colmation layer

and d_r to its thickness. The river was described by a 2D Cauchy boundary condition on the top layer, which we subdivided into two zones of transfer rates. Zone L1 (Fig. 3.5) covered the restored part of the river, including the disconnected branch. The remaining channelized part was covered by zone L2. We split the 1D Cauchy boundary condition along the northern side channel into three zones of transfer rates (L3-L5) to separate the middle exfiltrating segment (L4) (with its gravelly bed sediment) from the upstream and downstream heavily clogged segments.

FEFLOW describes each transfer rate zone by a transfer rate for infiltration (L_{in}) and exfiltration (L_{out}). Our system of Cauchy boundary conditions (L1-L5) was therefore characterized by 10 parameters ($L_{in}1$-$L_{in}5$, $L_{out}1$-$L_{out}5$). L_{out} is typically larger than L_{in}, as the exfiltrating clean groundwater "flushes" the pore space. This effect probably explains the gravelly bed sediments in the southern side channel as well as in the exfiltrating segment of the northern side channel (L4). On the other hand, suspended particles in infiltrating surface water tend to clog the pore space, as was the case in the main river channel (L1, L2) and in the upstream and downstream part of the northern side channel (L3, L5).
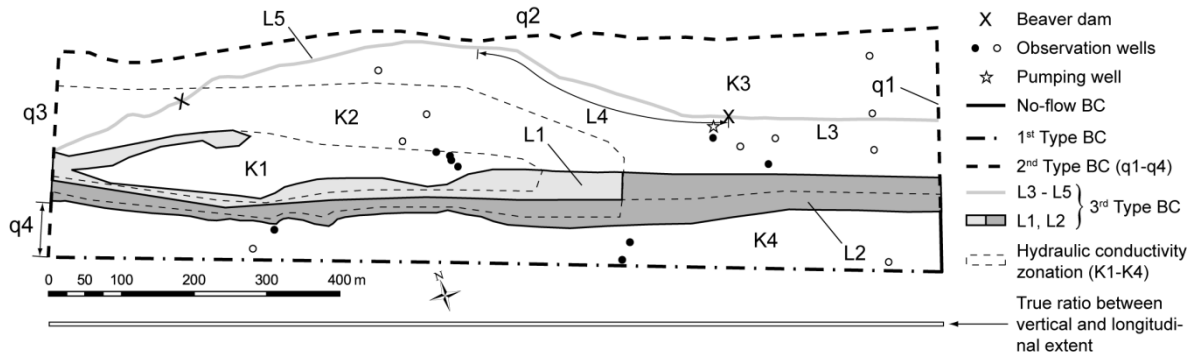
Fig. 3.5. Spatial definition of the boundary conditions (BCs) and the hydraulic conductivity zonation within the modeling domain. Groundwater head observations were available at all 19 observation wells, while experimentally determined residence times were restricted to 9 observation wells (black filling). The rectangle at the bottom of the figure illustrates the true ratio between the vertical and the longitudinal extent of the model.

3.4.2 Calibration procedure

To initially obtain a realistic spatial groundwater residence time distribution when using the reference RH water level distribution (Fig. 3.4a), we jointly estimated the transfer rates and the hydraulic conductivity distribution by fitting both, measured groundwater heads and experimentally determined groundwater residence times from nonparametric deconvolution of EC time series (Section 3.3.2, Fig. 3.5). A list of these residence times together with their standard deviations is presented in the Supporting information (Table 3.2, Fig. 3.9). To reduce the number of 10 adjustable transfer rates, pilot model runs were performed using estimated parameter values from field observations. These model runs revealed that the infiltrating main river channel ($L_{in}1$, $L_{in}2$), the exfiltrating disconnected river branch ($L_{out}1$) and the exfiltrating segment of the northern side channel ($L_{out}4$) were responsible for most of the groundwater flux at the Cauchy boundary conditions. $L_{out}1$ was additionally tied to $L_{in}1$ with a factor of 10 to eliminate parameter correlation. For each manual adjustment of the hydraulic conductivity distribution, the remaining three adjustable transfer rates were estimated using PEST (Doherty, 2005) by fitting measured groundwater heads (i.e. minimizing the sum of squared errors between simulated and measured heads). This procedure was iterated until the simulated groundwater residence times (see Section 3.4.3) were within ±1 standard deviation of the experimentally determined residence times. The resulting hydraulic conductivity distribution comprised four different zones (Fig. 3.5) and their hydraulic conductivities were within a range of 4×10^{-3} - 6×10^{-2} m/s (Table 3.1), which corresponds well to the measured values (Section 3.3.1).

Based on this initial parameterization for the reference RH model scenario (Table 3.1), the water level distributions generated with both alternative and both simplified methods (Fig. 3.4a, b) were assigned to the river and the side channel boundary conditions of the model. For each of the four model scenarios, the three adjustable transfer rates were calibrated against measured groundwater heads using PEST to ensure that the basis of the groundwater residence time simulation was a calibration-constrained groundwater flow field. The remaining transfer rates and the hydraulic conductivity distribution were kept constant. Fig. 3.11 (Supporting information) visually summarizes the initial and the subsequent calibration procedure by a flow chart.

Table 3.1. Hydraulic conductivities and transfer rates of the corresponding parameter zones (Fig. 3.5) resulting from the initial model calibration using the RH water level distribution. The transfer rates in bold were estimated using PEST. The remaining transfer rates were kept at their initial values, which in turn were estimated from field observations. $L_{out}1$ (in brackets) was tied to $L_{in}1$ with a factor of 10. The three adjustable transfer rates were estimated for the remaining four model scenarios as well (Fig. 3.6), while the hydraulic conductivity distribution was kept constant.

K1 [m/s]	6×10^{-2}		
K2 [m/s]	2×10^{-2}		
K3 [m/s]	1×10^{-2}		
K4 [m/s]	4×10^{-3}		
$L_{in}1$ [1/d]	**11.9**	$L_{out}1$ [1/d]	**(119)**
$L_{in}2$ [1/d]	**2.1**	$L_{out}2$ [1/d]	70.0
$L_{in}3$ [1/d]	0.5	$L_{out}3$ [1/d]	5.0
$L_{in}4$ [1/d]	1.0	$L_{out}4$ [1/d]	**24.7**
$L_{in}5$ [1/d]	0.5	$L_{out}5$ [1/d]	5.0

3.4.3 Simulation of groundwater age

Based on the calibration-constrained groundwater flow field, we simulated the spatial distribution of groundwater residence time, hereafter referred to as groundwater age. We performed a steady-state transport simulation of a tracer with a zero-order source term. According to Goode (1996), the groundwater age (i.e. the time since entering the model domain) is obtained by a steady-state transport simulation of a tracer with an appropriate definition of the boundary conditions and a zero-order source term equal to the porosity. A fixed age (concentration) of zero was defined at inflowing boundaries and a natural 2nd Type boundary condition at outflowing boundaries. The latter is described by $n \cdot (D \nabla A) = 0$, i.e. the age (A) in normal direction (n) to the boundary does not change. The zero-order source term was set to 0.2 mg L^{-1} d^{-1} for each element according to the mean porosity of 0.2 (Section 3.3.1).

We set the longitudinal dispersivity to 10 m for our model on the scale of 1000 m, according to Gelhar et al. (1992). We assigned a value of 1 m to both the horizontal and vertical transverse dispersivity, as differentiating the two was not possible in FEFLOW. As a result, the vertical transverse dispersivity was obviously too high, which caused an excessive vertical dispersion and hence, small vertical age differences. However, as the vertical extent of the modeling domain was very small compared to its horizontal extent (Fig. 3.5), the groundwater age was mainly controlled by horizontal transport.

To visualize and compare the spatial age distributions from the different model scenarios, we first calculated vertically averaged age distributions, weighted by the element thickness. Additionally, we produced spatial distributions of relative age differences to highlight spatial differences among the age distributions. The relative age difference ΔA_{rel} between a mean age A and a reference mean age A_{ref} was calculated at each node position as follows:

$$\Delta A_{rel} = \frac{A - A_{ref}}{A_{ref}} \cdot 100 \qquad\qquad (3.1)$$

3.5 Results and discussion

3.5.1 Calibration results

The estimated adjustable transfer rates for all the model scenarios are plotted in Fig. 3.6. Model scenarios that used the new alternative methods (RM, IM) had small changes in the estimated transfer rates compared to results of the reference RH model scenario (10-40%). Neglecting lateral water level gradients in the first simplified IM method (IM_wo_lat) led to adjustments of the transfer rates by a factor of 2-3 compared to the complete IM method. The largest changes, at 1-2 orders of magnitude, were made during model calibration of the linear river water level distribution scenario for the second simplified method (IM_lin).

The post-calibration root mean square error (RMSE) between measured and simulated groundwater heads was 7.7 cm for the reference RH method and varied between 7.2-7.3 cm for the RM, the IM as well as for the IM_wo_lat model scenario. The model efficiencies (Mayer and Butler, 1993) were 0.98 for all of the complete methods and the IM_wo_lat method. The IM_lin model scenario resulted in a RMSE of 11 cm and a model efficiency of 0.95. The improvement of the pre-calibration RMSE (using the estimated transfer rates of the RH model scenario; Table 3.1) over the post-calibration RMSE was small (0.1-0.3 cm) for the alternative methods (RM, IM). For the simplified IM_wo_lat and IM_lin methods, the RMSE was reduced by 2 and 5 cm, respectively.

The inspection of the inversion statistics revealed that the inversion problem was well posed and not infected by a high degree of non-uniqueness. First, the three eigenvalues of the parameter covariance matrix had a maximum to minimum ratio of 10^2, well below the maximum acceptable value of 10^7 (Doherty, 2005). Second, the ratio of the maximum and the minimum composite sensitivity was 9, while the acceptable maximum is 100. The highest correlation of 0.8 was found between $L_{in}2$ and $L_{out}4$. The remaining two correlation coefficients were less than 0.5.
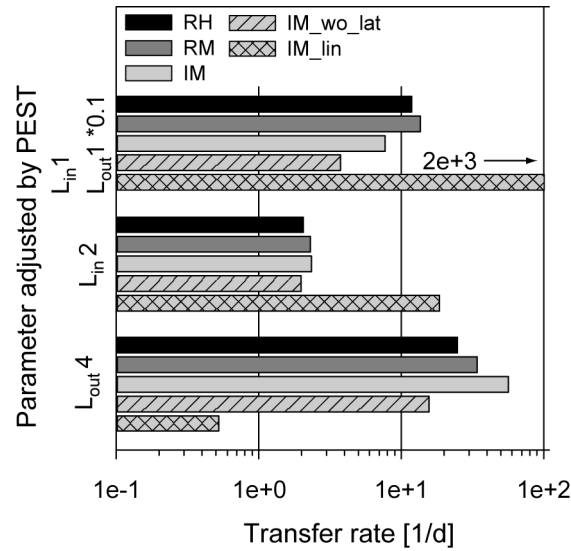
Fig. 3.6. Post-calibration transfer rates of the reference (RH), the alternative (RM, IM) and the simplified (IM_wo_lat, IM_lin) model scenarios.

3.5.2 Groundwater flow field and absolute age distribution

Before being able to compare the age distributions of different model scenarios, we have to become familiar with the general characteristics of the groundwater flow field at our field site. Fig. 3.7 presents the calibration-constrained groundwater flow field and the corresponding groundwater age distribution from the reference RH model scenario (Fig. 3.4a). For groundwater recharged by the river or the northern side channel, which was mostly the case within the modeling domain, the groundwater age reflects the "real" age since infiltration. Along the northern and northeastern inflow boundaries (Fig. 3.5) however, where a fixed age of zero was assigned as well, the groundwater age rather refers to the time since entering the modeling domain.

Infiltration at the main river channel occurred to both the northern and the southern sides, with an overall infiltration rate of 300 L/s. Most of the infiltrated water (about 80%) flowed towards the southern side, due to the high water level gradient between the river and the southern side channel. The corresponding exfiltration rate along the southern side channel (240 L/s) was validated by the measured discharge difference between the water level gauges G_{19} and G_{29} (Fig. 3.2). Only about 20% of the river infiltration occurred to the northern side, induced by the exfiltrating segment of the northern side channel (L4) and the disconnected branch of the river (Fig. 3.4a). The model estimated an exfiltration rate of 25 L/s at the exfiltrating segment of the northern side channel, which was consistent with the measured difference in discharge downstream and upstream of the beaver dam. Exfiltration at the disconnected branch occurred at a rate of about 30 L/s.

52

The groundwater flow field on the southern side of the river was relatively uniform. Infiltration occurred at a steep angle to the river and the groundwater age reached a maximum of 4-8 d. The high water level difference between the river and the southern side channel caused an asymmetric groundwater flow field underneath the river, which significantly contributed to the much higher infiltration towards the southern side.

On the northern side of the river, the flow field was more complex. In the upstream part at river sections $i = 5..7$, infiltration occurred at a relatively steep angle and groundwater flow was directed towards the exfiltrating segment (L4) of the northern side channel. To the north of L4, the low groundwater head gradients and the long flow paths led to groundwater ages of up to 90 d. On the southern side of L4, the groundwater age reached only 10-20 d due to the presence of direct pathways linking the river with the side channel. The pumping well had no significant impact on the groundwater flow field due to its low average pumping rate (Section 3.4.1).

Further downstream, at river sections $i = 4..5$, the groundwater flow field on the northern side of the river became parallel to the river as the water levels in the northern side channel became higher than those in the main river channel (Fig. 3.4a). Therefore, groundwater that was not drained by the exfiltrating segment of the northern side channel (L4) was deflected towards and drained by the disconnected branch of the river. The further upstream infiltration at river sections $i = 1..5$ occurred, the longer and the more arc-shaped the flow paths became. Accordingly, the groundwater age increased from the river towards the northern side channel, reaching a maximum of 50 d.
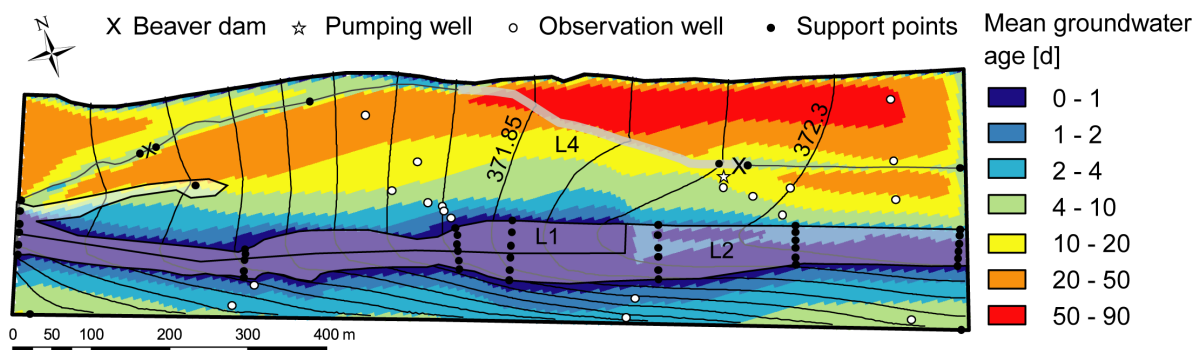

Fig. 3.7. Calibration-constrained groundwater flow field (shown as groundwater isopotentials with an equidistance of 15 cm) and vertically averaged groundwater age from the reference model scenario using the RH surface water level distribution (Fig. 3.4a). The three adjustable transfer rate zones are indicated.

3.5.3 Predictive comparison of the complete interpolation methods

To assess the predictive capability of both new alternative methods (RM, IM), we calculated the spatial distribution of the relative age difference ΔA_{rel} according to Eq. (3.1), using the age distribution of the RH method (Fig. 3.7) as a reference (A_{ref}). Both the RM and the IM model scenario showed similar results (Fig. 3.8a, b). To the north of the river, two zones with lower ages (10-20%) relative to the RH model scenario were identified between the river sections $i = 2, 3$ and $i = 6, 7$. These small deviations were caused by a combination of minor water level differences with respect to the RH method at river sections $i = 2..5$ (Fig. 3.4a) and the related changes in transfer rates that occurred during calibration, mostly within 10-40%. These changes actually provided a slightly better fit to the measured groundwater heads (Section 3.5.1). As an example, the higher water levels of the IM method along river sections $i = 3, 4$ were compensated by a 40% reduction in the $L_{in}1$ transfer rate relative to the RH model scenario (Fig. 3.6).

The highest adjustment during calibration of the IM model scenario was made for $L_{out}4$, which was doubled to balance the higher water levels in the exfiltrating segment of the northern side channel (Fig. 3.4a, Fig. 3.6). A zone of higher groundwater age remained between the river and the northern side channel (Fig. 3.8b), but deviations were restricted to an upper bound of 30%.

An additional common element of both alternative model scenarios was the zone between the main river channel and the disconnected branch, where groundwater age differed from the reference model scenario by 40-100%. These deviations can be blamed on the failure of the zero lateral gradient assumption at river section $i = 1$ for both the RM and the IM method (Section 3.3.3). The too low water levels compared to the RH method could not be compensated during calibration of the transfer rates as no observations were available in this region, and therefore led to a pronounced increase in groundwater age. The failure of the zero lateral gradient assumption was also responsible for the positive deviations in groundwater age at the western part of the southern side of the river. Apart from that, errors in groundwater age on the southern side of the river were generally small (<10%) because river water level deviations were small compared to the difference in water level between the river and the southern side channel.

Besides the large differences between the main river channel and the disconnected branch, both alternative methods (RM, IM) were able to predict the groundwater age within 30% of the reference RH method. The error of 30% is small compared to the uncertainty (standard

deviation) of the experimentally determined residence times of 60-80% (Supporting information: Table 3.2). The calibration of the transfer rates compensated for minor differences among the surface water level distributions and the resulting flow fields provided an accurate prediction of groundwater age. These results confirm the capability of the new alternative methods to efficiently capture the relevant characteristics of the surface water level distribution allowing for a reliable simulation of the groundwater age distribution.
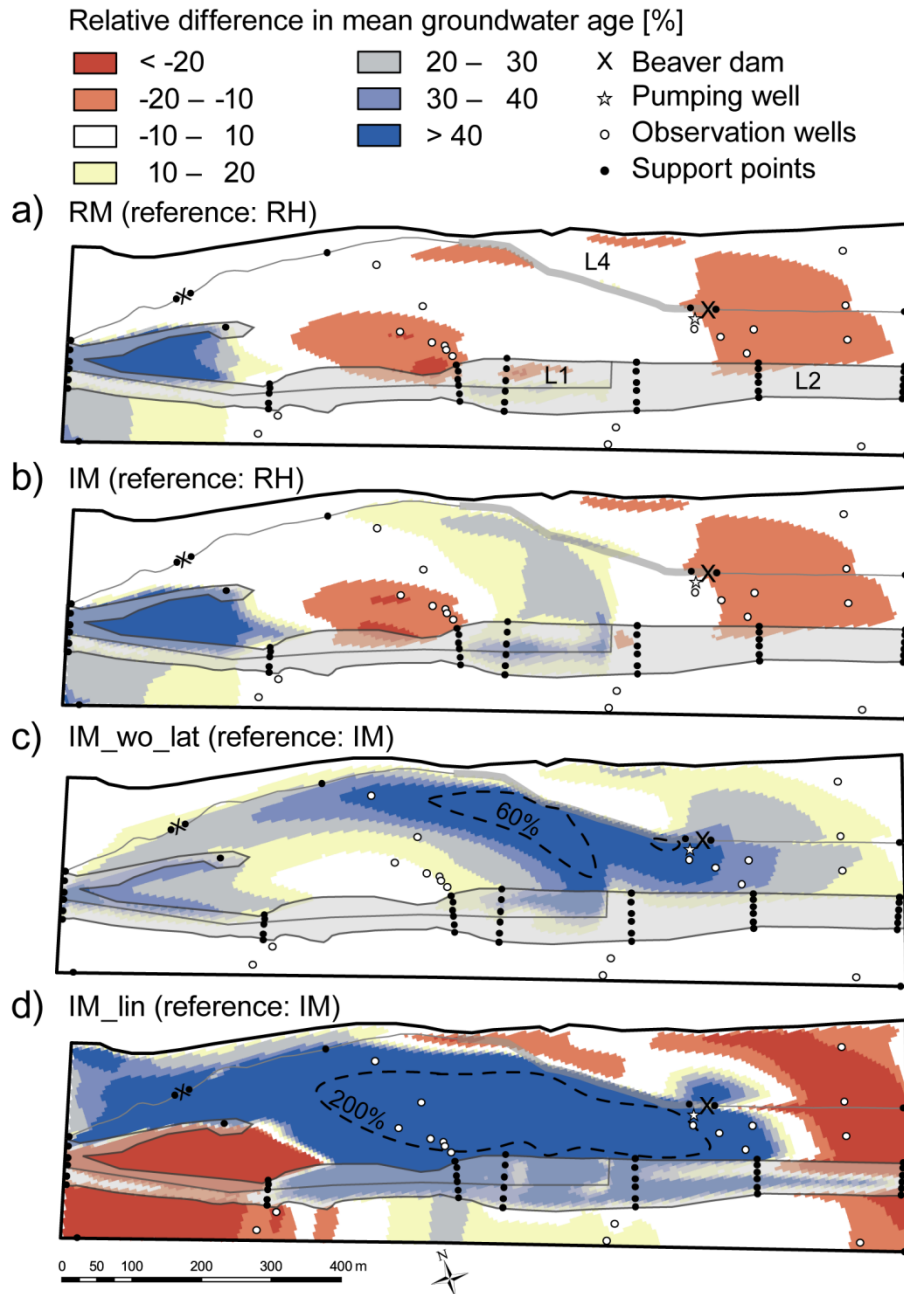
Fig. 3.8. Spatial distribution of the relative difference in mean groundwater age (Eq. (3.1)), for the two alternative methods (RM, IM) with respect to the RH method (a, b), and for the two simplified versions of the IM method with respect to the complete IM method (c, d). (c) and (d) contain an additional isoline (black dashed line) of relative age difference of 60% and 200%, respectively. The three adjustable transfer rate zones are indicated.

3.5.4 Predictive comparison of the simplified interpolation methods

We used the groundwater age distribution from the IM model scenario as a reference (A_{ref}) to compare the groundwater age distributions of the two simplified model scenarios. Fig. 3.8c shows the results for the model scenario that applied the first simplified river water level distribution, which ignored lateral water level gradients (IM_wo_lat). The only difference in the water level distribution compared to the full IM implementation was water levels 20-30 cm higher at the support points on river sections $i = 3, 4$ on the southern lines $j = 1..4$ (Fig. 3.4b, Fig. 3.2). Even though these changes in the water level distribution seem to be small, the effect on the calibration-constrained groundwater age distribution was considerable. To the north of the river, a band of higher age was identified that extended from the river at sections $i = 4..6$, along the northern side channel, to the disconnected river branch, with deviations of up to 40-80% compared to the IM model scenario.

As described in Section 3.5.2, the groundwater flow field underneath the river was generally asymmetric because groundwater was largely withdrawn by the strong gradient between the river and the southern side channel. This effect was intensified by the lateral gradient at sections $i = 3, 4$, which was also directed towards the south. Therefore, the negligence of the lateral gradient reduced the asymmetric characteristics and more water infiltrated to the northern side of the river. To counteract this additional groundwater flux and the higher groundwater heads, the $L_{in}1$ transfer rate was lowered by 50% during the calibration procedure (Fig. 3.6). However, groundwater heads at the upstream observation wells were affected as well, which in turn was compensated by a reduction of the $L_{out}4$ transfer rate by a factor of 3. On the one hand, these adjustments reduced the RMSE to nearly the same level as for the complete IM method (Section 3.5.1). On the other hand, the direction of the resulting flow field on the northern side of the river was slightly more parallel to the river direction, which caused longer flow paths and longer travel times at the nodes identified by the bluish domain in Fig. 3.8c.

Fig. 3.8d depicts the spatial distribution of the relative age difference for the second simplified model scenario that used the IM_lin water level distribution. The assumed linear interpolation between the two water level gauges at river sections $i = 2, 7$ led to lower water levels by up to 50 cm relative to the complete IM implementation (Fig. 3.4b). Accordingly, the gradient between the river and the exfiltrating segment of the northern side channel decreased substantially, which led to a more river-parallel groundwater flow field on the northern side of the river and a widespread increase of 200-500% in groundwater age. In

attempt to compensate for the errors in river water levels during calibration against groundwater heads, the $L_{in}1$ and $L_{in}2$ transfer rates were increased by 2 and 1 orders of magnitude, respectively. Additionally, the $L_{out}4$ transfer rate was decreased by 2 orders of magnitude compared to the IM model scenario. Even though the RMSE was reduced from 16 cm to 11 cm, the groundwater flow field and hence the errors in groundwater age prediction could not be improved on the northern side of the river. Instead, the very high $L_{in}1$ transfer rate caused a 20-80% decrease in groundwater age between the river and the disconnected river branch, where the water level differences were similar compared to the complete IM method (Fig. 3.4b).

The errors in the prediction of groundwater age on the southern side of the river were <10% for the IM_wo_lat model scenario and ranged from -30% in the western part to 30% in the middle part for the IM_lin model scenario. These small changes in groundwater age compared to those on the northern side of the river can be attributed to the high absolute water level difference between the river and the southern side channel, compared to which the errors in river water levels were small. For instance, the error of 30 cm at the river section $i = 6$ for the simplified IM_lin method reduced the water level gradient between the river and the southern side channel by 30%, compared to the complete IM method (Fig. 3.4b). In contrast, the same error of 30 cm reduced the water level gradient between the river and the exfiltrating segment of the northern side channel by about a factor of 2.5. This clearly demonstrates that uncertainty in surface water levels has the highest impact on the simulated groundwater age in zones where the water level gradients between infiltrating and exfiltrating boundaries are small.

The description of the river as a 2D domain allowed for including lateral water level gradients. Lateral gradients in river water levels were described in the literature, but were explained by stream curvature and the centrifugal force (Cardenas et al., 2004). In restored river reaches, morphologically induced lateral water level gradients are likely to occur quite frequently. At our field site, lateral water level differences of 20-30 cm were restricted to a ~200 m long section (Fig. 3.4b) and their negligence caused errors in groundwater age prediction of 40-80% (Fig. 3.8c). When compared to the uncertainty of the experimentally determined residence times of 60-80% (Supporting information: Table 3.2), the errors associated with neglecting lateral gradients might be acceptable, depending on the purpose and requirements of the study. At other field sites, however, lateral water level gradients can be more pronounced and their inclusion might be crucial for an accurate groundwater age prediction.

The explicit consideration of the river as a 2D domain was also essential to reliably represent the river's lateral extent and therewith the length of the groundwater flow paths as well as the groundwater residence times. Furthermore, the 2D representation of the river in its full lateral extent allowed us to account for asymmetric groundwater flow underneath the river, which was identified as an important feature influencing the infiltration rates towards the northern and the southern side of the river (Fig. 3.7, Section 3.5.2). In previous modeling studies, the river was described as a 2D domain as well, but was cut in approximately the middle where a no-flow boundary condition was assumed (Derx et al., 2010). This assumption suppresses potential asymmetric groundwater flow underneath the river and might lead to a bias in the flow field and the water budget.

Linearly interpolating water levels between water level gauges separated by one or several kilometers is common practice when assigning river water levels to models of river-groundwater systems. Our results revealed that assuming a linear water level distribution can lead to considerable errors in the river water level distribution that translate into inacceptable errors in the simulated groundwater age of >200%. Hence, the accurate description of the longitudinal water level distribution is of major importance for a reliable groundwater age prediction.

3.6   Conclusions

In this study, we assessed the predictive capability of two new alternative methods for the estimation of 1D and 2D river water level distributions of dynamic rivers (RM, IM), with respect to the simulated groundwater residence time (groundwater age). Surface water levels generated with both alternative methods and with a reference method (RH) were assigned to the river and side channel boundary conditions of a 3D groundwater flow and transport model of a partly restored riverbank-filtration system in NE-Switzerland. Steady-state model calibration against measured groundwater heads was performed for each of these model scenarios by an automated adjustment of selected transfer rates using PEST. The age predictions of the calibration-constrained groundwater flow fields lay within a range of 30% compared to the reference RH model scenario. This relatively low error confirmed the predictive capability of the alternative methods when applied to real and complex river-groundwater systems.

We also investigated the sensitivity of the modeled groundwater age distribution to reduced complexity in the river water level distribution. For the first scenario, we modified the IM method to ignore lateral gradients, which led to errors in groundwater age prediction of 40-80%

over a considerable area to the north of the river. In the second scenario, we further simplified the IM method by assuming a linear longitudinal water level distribution. As a result, errors in groundwater age of 200-500% were widespread, which demonstrates the importance of an accurate longitudinal water level distribution for the modeled groundwater age.

The results of this study allow us to recommend both alternative approaches presented in Chapter 2 for the river water level assignment in future modeling studies of river-groundwater systems at the kilometer scale. To implement either of the alternative methods at a specific river-groundwater system, the placement of the water level gauges and the fixpoints should be carefully assessed. First, it is important to note that an accurate description of the surface water levels is most important in zones where the gradients between infiltrating and exfiltrating boundaries are small. Second, our results indicate that the longitudinal water level distribution should be captured in detail to reliably simulate the groundwater flow field and the groundwater age distribution. We suggest that, if feasible, water level gauges should be installed at 1 km intervals. In between, fixpoints (e.g. an armor stone or a steel rod) should be installed and leveled with a spacing that is inversely proportional to the change in surface water level gradient and might range from 50-200 m. For instance, a segment with a linear water level profile can be captured by two fixpoints, while a segment with a changing gradient requires three or more fixpoints. Additionally, fixpoints should be installed upstream and downstream of a hydraulic jump, for example at beaver dams or weirs. To maximize the accuracy in groundwater age prediction, we recommend the inclusion of lateral water level gradients by defining two fixpoints on the same section.

This study demonstrates that a reduced level of detail in the river water level distribution can lead to considerable errors in simulated groundwater flow paths and residence times. Therefore, it is essential to capture the river water level distribution in its full spatial and temporal extent. To this end, the new methods proposed in Chapter 2 proved to offer an accurate and efficient alternative compared to using a hydraulic model. The application of these interpolation methods when modeling riverbank-filtration systems will, for instance, help to reliably assess the impact of river restoration measures on groundwater residence times and hence, to mitigate the conflict of interest between river restoration and drinking water protection.

Acknowledgments

3.7   Supporting information

Fig. 3.9. Vertically averaged spatial groundwater age distribution of the calibrated RH model scenario. At the labeled observation wells, estimates of the local groundwater residence time distribution were obtained by nonparametric deconvolution of EC time series (Table 3.2).
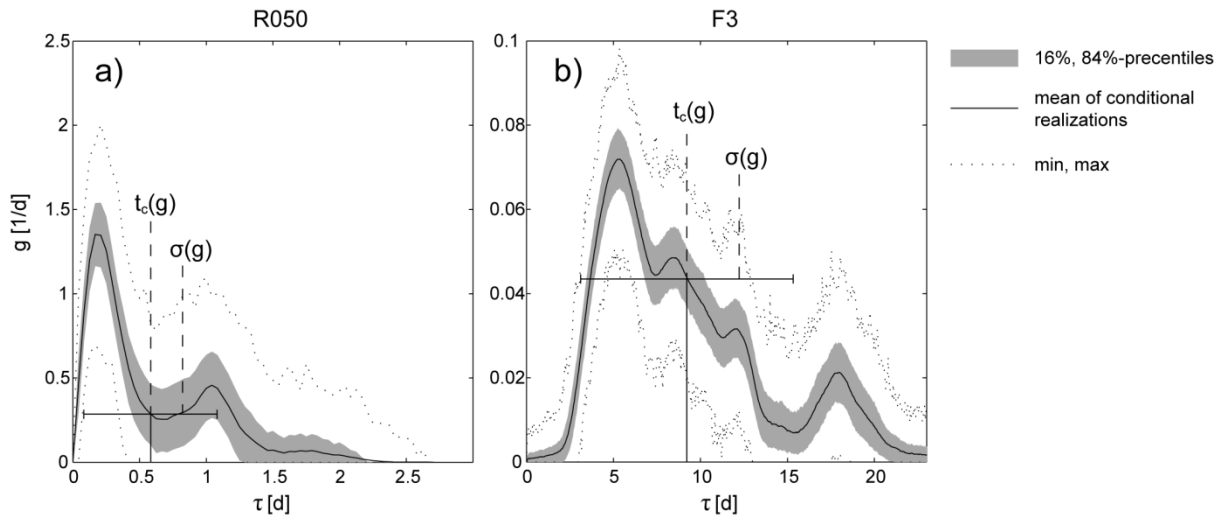
Fig. 3.10. Estimated residence time distributions $g(\tau)$ from nonparametric deconvolution of the EC time series measured in the Thur River and in groundwater (a) at an observation well close to the river (R050) and (b) at an observation well close to the pumping well (F3) (Fig. 3.9). Solid line: mean of 1000 conditional realizations, gray area: 16 and 84 percentiles of the conditional statistical distributions, dotted lines: minimum and maximum values obtained in all realizations. The mean residence time (center of gravity, $t_c(g)$) and the standard deviation ($\sigma(g)$) of both residence time distributions are indicated.

Table 3.2. Mean residence times (center of gravity, $t_c(g)$) and standard deviations ($\sigma(g)$) of the residence time distributions obtained by nonparametric deconvolution of the EC time series at the labeled observation wells in Fig. 3.9 (Froyland, 2011). These residence times were used as observations for the initial model calibration (Section 3.4.2). The standard deviations ($\sigma(g)$) typically amounted to 60-80% of the mean residence times ($t_c(g)$).

	$t_c(g)$ [d]	$\sigma(g)$ [d]
R050	0.6	0.5
R073	1.1	0.7
R051	3.5	2.4
R059	3.8	3.5
R006	3.2	1.8
F3	8.9	6.0
R069	1.5	1.3
R081	2.3	1.8
R049	4.5	3.8

Groundwater head measurements and determination of experimental groundwater residence times at observation wells

↓

Generation of surface water level distribution using complete (RH, RM, IM) and simplified (IM_wo_lat, IM_lin) interpolation methods

↓

Pilot model runs to reduce number of adjustable transfer rates

↓

Initial model calibration using the RH (reference) surface water level distribution to initially obtain reasonable spatial groundwater residence time distribution

Manual adjustment of hydraulic conductivity distribution

Automated estimation of the three adjustable transfer rates by fitting measured groundwater heads using PEST

Simulation of spatial groundwater residence time distribution

Are the simulated groundwater residence times at observation wells within ±1 standard deviation of experimentally determined residence times?

No

Yes

Assign surface water level distributions of alternative methods (RM, IM) and of simplified methods (IM_wo_lat, IM_lin) to the model

↓

Estimation of the three adjustable transfer rates by fitting measured groundwater heads using PEST, while keeping the hydraulic conductivity distribution constant

↓

Simulation of spatial groundwater residence time distribution for each calibration-constrained model scenario
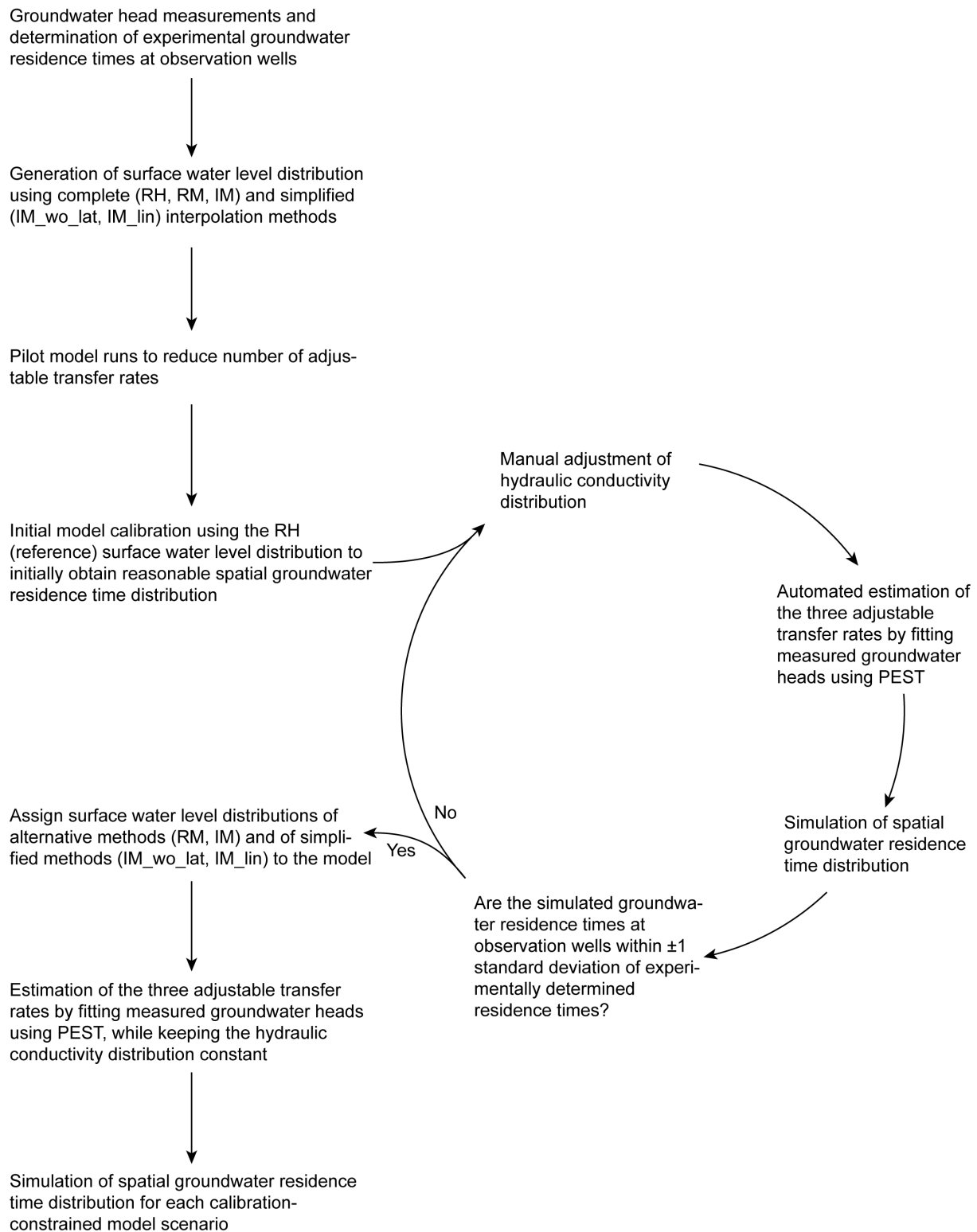
Fig. 3.11. Flow chart describing the initial model calibration using the reference RH water level distribution and the subsequent model calibration using the water level distributions of the alternative and the simplified methods.

63

Chapter 4

NOM degradation during river infiltration: Effects of the climate variables temperature and discharge

Abstract

Most peri-alpine shallow aquifers fed by rivers are oxic and the drinking water derived by riverbank filtration is generally of excellent quality. However, observations during past heat waves suggest that water quality may be affected by climate change due to effects on redox processes such as aerobic respiration, denitrification, reductive dissolution of manganese(III/IV)- and iron(III)(hydr)oxides that occur during river infiltration. To assess the dependence of these redox processes on the climate-related variables temperature and discharge, we performed periodic and targeted (summer and winter) field sampling campaigns at the Thur River, Switzerland, and laboratory column experiments simulating the field conditions. Typical summer and winter field conditions could be successfully simulated by the column experiments. Dissolved organic matter (DOM) was found not to be a major electron donor for aerobic respiration in summer and the DOM consumption did not reveal a significant correlation with temperature and discharge. It is hypothesized that under summer conditions, organic matter associated with the aquifer material (particulate organic matter, POM) is responsible for most of the consumption of dissolved oxygen (DO), which was the most important electron acceptor in both the field and the column system. For typical summer conditions at temperatures >20°C, complete depletion of DO was observed in the column system and in a piezometer located only a few meters from the river. Both in the field system and the column experiments, nitrate acted as a redox buffer preventing the release of manganese(II) and iron(II). For periodic field observations over five years, DO consumption showed a pronounced temperature dependence (correlation coefficient r = 0.74) and therefore a seasonal pattern, which seemed to be mostly explained by the temperature dependence of

the calculated POM consumption (r = 0.7). The river discharge was found to be highly and positively correlated with DO consumption (r = 0.85), suggesting an enhanced POM input during flood events. This high correlation could only be observed for the low-temperature range (T<15°C). For temperatures >15°C, DO consumption was already high (almost complete) and the impact of discharge could not be resolved. Based on our results, we estimate the risk for similar river-infiltration systems to release manganese(II) and iron(II) to be low during future average summer conditions. However, long-lasting heat waves might lead to a consumption of the nitrate buffer, inducing a mobilization of manganese and iron.

4.1 Introduction

Riverbank filtration is a widely applied technique to produce drinking water and contributes substantially to the overall drinking water production in several European countries (France ~50%, Germany ~16% (Tufenkji et al., 2002), Switzerland ~25%). Natural attenuation processes during river infiltration efficiently remove particles, bacteria, viruses, parasites and, to a lesser extent, organic contaminants, such as pharmaceuticals (Kuehn and Mueller, 2000; Sacher and Brauch, 2002; Grünheid et al., 2005). During river infiltration, biogeochemical processes can alter the composition of the infiltrating water significantly (Jacobs et al., 1988).

The most important biogeochemical process during river infiltration is the biodegradation of natural organic matter (NOM), which occurs within bacterial biofilms in riverbed sediments (Pusch et al., 1998). NOM in river systems originates from both allochthonous (terrestrially-derived) sources and generally more biodegradable autochthonous sources (periphyton) (Pusch et al., 1998; Leenheer and Croue, 2003). NOM is composed of dissolved organic matter (DOM) and particulate organic matter (POM), usually quantified as dissolved organic carbon (DOC) and particulate organic carbon (POC), respectively (Leenheer and Croue, 2003). During infiltration of river water, DOM is transported through the riverbed as a "mobile substrate", whereas POM is retained in the riverbed sediments as a "stationary substrate" (Pusch et al., 1998).

The biodegradation of NOM in riverbed sediments leads to a consumption of dissolved or solid terminal electron acceptors, such as oxygen (O_2), nitrate (NO_3^-), Mn(III/IV)- and Fe(III)(hydr)oxides and sulfate (SO_4^{2-}). Redox conditions in riverbank-filtration and artificial-recharge systems were observed to undergo seasonal variations with the formation of anoxic conditions during summer due to the temperature dependence of NOM degradation (Greskowiak et al., 2006; Massmann et al., 2006; Sharma et al., 2012).

In the Swiss context, riverbank filtration is often the only barrier between river water and drinking water. This is possible because of the usually high dilution of wastewater effluents in receiving rivers and the generally oxic conditions of shallow groundwater. However, during the hot summer of 2003, the redox conditions in several riverbank-filtration systems turned anoxic. Hoehn and Scholtis (2011) reported a case at the Thur River, where the redox sequence even proceeded to Mn(IV)- and Fe(III)-reducing conditions. The subsequent re-oxidation of dissolved Mn(II) and Fe(II) at the pumping station led to clogging of the filter screen and to rusty water.

Climate models predict an increase in summer air temperatures (4-5 K) and a decrease in precipitation (25%) inducing lower discharges in rivers during summer months in northern Switzerland by 2085 (CH2011, 2011; FOEN, 2012a). Lower discharges may give rise to less dilution of wastewater effluents and accordingly to higher DOC concentrations. Combined with higher temperatures, the risk for riverbank-filtration systems to become anoxic or even develop Mn(IV)- or Fe(III)-reducing conditions is likely to increase (Sprenger et al., 2011). To assess this risk more accurately, the dynamics of NOM degradation and its dependence on climate variables need to be better understood (Eckert et al., 2008; Green et al., 2011).

Besides the direct influence of temperature and discharge, the biogeochemical processes during river infiltration and hence the redox conditions in the infiltration zone might also be affected by indirect climate-related changes in river water quality. The effect of climate change on river water quality (e.g. dissolved oxygen, nutrients (nitrate, ammonium), DOC and major ions) in relation to hydrologic, terrestrial and resource-use factors has been addressed in many studies (Murdoch et al., 2000; Zwolsman and van Bokhoven, 2007; Park et al., 2010). However, Senhorst and Zwolsman (2005) conclude that the impact of climate change on surface water quality is quite site specific and cannot be generally transferred to other watersheds and hence, should be assessed case by case. Therefore, we focused on the direct effect of the climate-related variables temperature and discharge on NOM degradation and the related consumption of electron acceptors during river infiltration.

The objectives of the present study were to assess the contribution of DOM consumption to the overall consumption of electron acceptors and to examine the effects of the climate-related variables temperature and discharge by means of field investigations and column experiments. To capture different temperature ranges, the field investigations consisted of two detailed sampling campaigns performed during typical summer and winter conditions at the peri-alpine Thur River. The column experiments were performed at temperatures that span the

range of typical field conditions. Additionally, the data of periodic field samplings that covered a wide range of temperature and discharge conditions over a period of five years were evaluated.

Firstly, we assessed the temperature dependence of the consumption of dissolved oxygen (DO) and DOM by comparing the data of the field campaigns with those of column experiments and verified the findings by a correlation analysis of the periodic data. Secondly, we investigated the impact of the discharge conditions on DO and DOM consumption using the periodic field data. Finally, we discuss the implications of our findings on the redox-related groundwater quality at riverbank-filtration systems in a changing climate.

4.2 Materials and methods

4.2.1 Field site

The field site of our investigation is located in NE-Switzerland (Niederneunforn) at the peri-alpine Thur River, which drains a catchment of 1700 km^2 (Fig. 4.1a). As no retention basin is located along the whole course of the river, the discharge behaves very dynamically with a range of 3-1100 m^3/s. During the interdisciplinary RECORD project (Restored corridor dynamics, http://www.cces.ethz.ch/projects/nature/Record; Schneider et al. (2011); Schirmer (2013)), 80 piezometers were installed (Fig. 4.1b). To the northern side of the river, the piezometers are arranged in two transects, the forest transect and the pumping station transect. Most of the piezometers are fully screened, covering the full aquifer thickness (5.3±1.2 m). The gravel-and-sand aquifer, which is underlain by lacustrine clay and overlain by 0.5-3 m alluvial fines, is highly conductive with hydraulic conductivities between 4×10^{-3} and 6×10^{-2} m/s (Chapter 3). The pumping well at the pumping station transect is operated during a daily period of only 3 h extracting a total volume of 36 m^3.

A groundwater flow and transport model was set up for low-flow conditions (23 m^3/s) and was calibrated against groundwater heads and experimentally determined travel times (Chapter 3). According to the resulting groundwater flow field (Fig. 4.1b, c), river water is naturally infiltrating into the aquifer, both at the forest and the pumping station transect. The low abstraction rate of the pumping well was found not to have any significant effect on the infiltration rate or the groundwater flow field. Groundwater flow velocities were in the order of 5-10 m/d at the pumping station transect and ranged between 20-50 m/d at the forest transect.
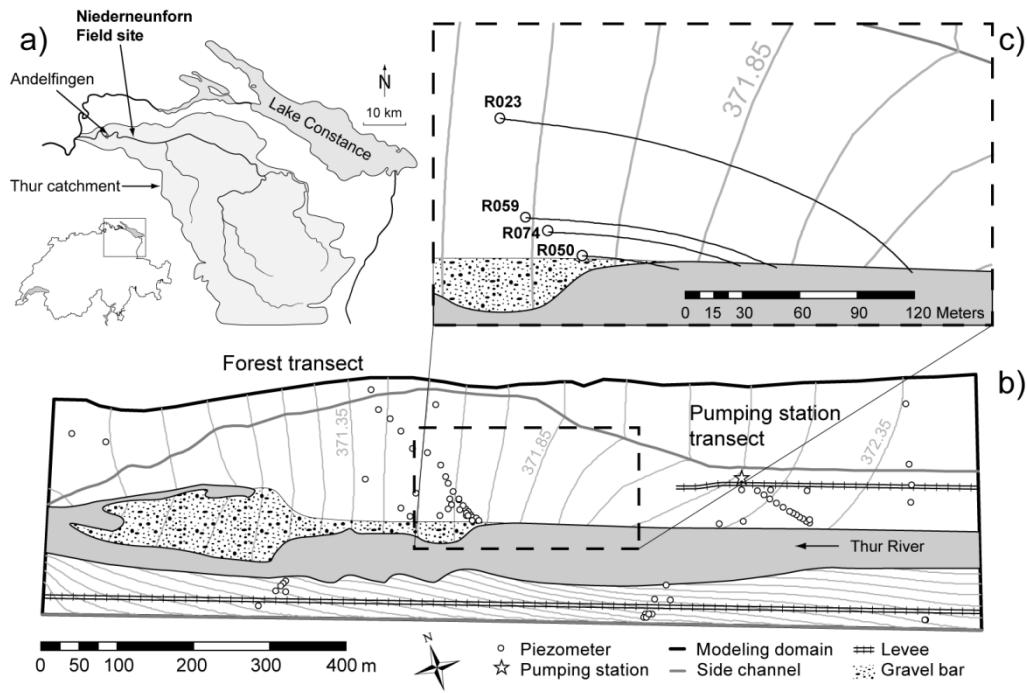
Fig. 4.1. (a) Catchment of the Thur River and location of the Niederneunforn field site, NE-Switzerland. (b) Schematic representation of the Niederneunforn field site. Groundwater head isolines (head equidistance 10 cm, light gray) were extracted from a groundwater flow model (Chapter 3). (c) Enlargement of the area indicated by the dashed rectangle in (b), which contains the locations of the piezometers used in this study. The black lines in (c) indicate the advective flow paths from the river to the piezometers according to the resulting flow field of the groundwater flow model.

Neither the pumping station transect nor the forest transect can be considered as a typical riverbank-filtration system with high abstraction rates considerably changing the groundwater flow field. Yet, both transects qualify for studying the microbial degradation processes during river infiltration and their dependencies on the climate-related variables temperature and discharge. Compared to the pumping station transect, the forest transect has the advantage of higher flow velocities and shorter residence times to the closest piezometers, which allows a more detailed assessment of the NOM degradation dynamics. Therefore, in this chapter, we focus on results from the forest transect.

4.2.2   Sampling campaigns and periodic samplings

To capture different temperature ranges, we conducted two detailed sampling campaigns during summer and winter 2011. We sampled the river and adjacent groundwater on five days between August 19-26, 2011 (summer campaign) and November 23-29, 2011 (winter campaign). The periodic samplings were carried out during a period of five years (2008-2012) and covered a wide temperature and discharge range (Supporting information; Section 4.5:

69

Fig. 4.9). Samples were taken in different piezometers at the forest transect. For better clarity, we only present results from a representative subset of the sampled piezometers (Fig. 4.1c).

The groundwater samples were pumped by a submersible electric pump (Whale®, Bangor, Northern Ireland) with an average pumping rate of 10 L/min. Before taking the in-situ measurements and the samples, we pumped at least 20 L (twice the piezometer volume) and waited until the electrical conductivity (EC) of the pumped groundwater was stable. We measured DO concentrations (LDO10115 (optical sensor), Hach Lange GmbH, Berlin, Germany, accuracy ±0.1 mg/L), pH and temperature (PHC10115, Hach Lange GmbH, Berlin, Germany, accuracy pH ±0.1, T±0.3 K) and EC (Cond 340i, WTW GmbH, Weilheim, Germany) in a 10 L bottle, which was constantly flushed with groundwater. The small opening on top of the bottle minimized the gas exchange with the atmosphere and thus guaranteed reliable DO measurements at near-zero concentrations. Groundwater and river water was filled into polypropylene bottles (1 L), filtered within 24 h through a 0.45 µm cellulose nitrate filter (Sartorius AG, Göttingen, Germany) and stored at 4°C until analysis. Concentrations of DOC (to quantify DOM), nitrate, ammonium and major ions were measured in the river water and groundwater samples (for analytical method see Section 4.2.4).

DO, as well as temperature and discharge were continuously measured (10-min intervals) in the Thur River at a gauging station of the Federal Office for the Environment (FOEN), which is located in Andelfingen, 10 km downstream of our field site (Fig. 4.1a). The river DO concentrations in Andelfingen were found to agree well with those at our field site (Hayashi et al., 2012). DO concentrations in the river underwent diurnal fluctuations. Such diurnal DO fluctuations are mainly caused by a combination of photosynthesis of periphyton during daytime and respiration during the night (Hayashi et al., 2012).

We calculated the DO consumption that occurred during infiltration by subtracting the measured DO concentration in groundwater from the daily mean DO concentration in the river. The latter was calculated based on the continuous DO time series measured at the gauging station in Andelfingen to minimize the bias in calculated DO consumption due to diurnal DO fluctuations in the river. As the diurnal fluctuations of the DOC concentrations in the river were not significant, we subtracted the measured DOC concentration in groundwater from the DOC concentration in the river to calculate the DOM consumption.

Eight grab samples were taken from the riverbed at a depth of 0-20 cm close to the first piezometer R050 (Fig. 4.1c). The samples were dried and sieved; the riverbed sediment

mainly consists of sandy gravel with little silt and clay. To quantify the POM contained in the riverbed sediment, we measured the POC concentrations for three grain-size fractions <0.25 mm. The POC concentration was highest for the fraction <0.063 mm (1.4±0.3% w/w), and lowest for the fraction 0.125-0.25 mm (0.5±0.3% w/w) (for analytical method see Section 4.2.4).

4.2.3   Column experiments

A schematic representation of the setup of the column experiments is shown in Fig. 4.2. The column casing consisted of a Plexiglas tube (length 30 cm, inner diameter 5.2 cm) and was packed with fractionated sand (0.125-0.25 mm grain size) from a gravel bar at the field site close to the forest transect. The sand was dried at room temperature and sieved afterwards before being dry-filled into the column in form of a "sand rain" (von Gunten and Zobrist, 1993). The sand was mainly composed of calcite and quartz (40% and 25%, respectively) and the POC concentration was about 0.3±0.2% (w/w). The sand fraction 0.125-0.25 mm was chosen because it is well defined and represents the available reactive surfaces with a considerable amount of POM.

Filtered Thur River water (0.45 μm, cellulose nitrate, Sartorius AG, Göttingen, Germany) was stored in a 2 L tank and was used as feed water for the column. It was pumped from the bottom to the top of the column at a flow rate of 0.4 L/d by means of an HPLC pump (Jasco PU-2080, Jasco Corporation, Tokyo, Japan) (Fig. 4.2). Every three days, the storage tank was replenished with fresh Thur River water stored at 5°C. In case of the experiment at 20°C, Thur River water was allowed to equilibrate for about 6 hours before replenishment. No measurable DOM degradation in the storage tank was observed under these conditions. To assess the hydraulics in the column, a tracer test with a 8.55 mM NaCl solution was conducted and the EC was measured at the end of the column. We estimated an effective porosity of 0.32 and a dispersivity of 0.08 cm by inverse modeling with the software CXTFIT (Toride et al., 1995). The corresponding total pore volume of the column was 0.2 L. Hence, the residence time in the column was 0.5 d at a flow rate of 0.4 L/d.

The column was first operated at 20°C in a climatised chamber for 19 days after an equilibration time of about 2 months with Thur River water taken on July 4, 2012 (composition 1, Supporting information: Table 4.1). After that, the column was operated at 5°C with the same feed water in an incubator for 26 days including an equilibration time of 20 days. Thereafter, as a control experiment, the column was operated again at 20°C in an incubator for 28 days including an equilibration time of 22 days (water composition 2,

Supporting information: Table 4.2). This control experiment was conducted to test if any of the column properties relevant for the bacterial degradation processes (sand composition, POM concentration/composition) had changed during the operation period at 5°C.
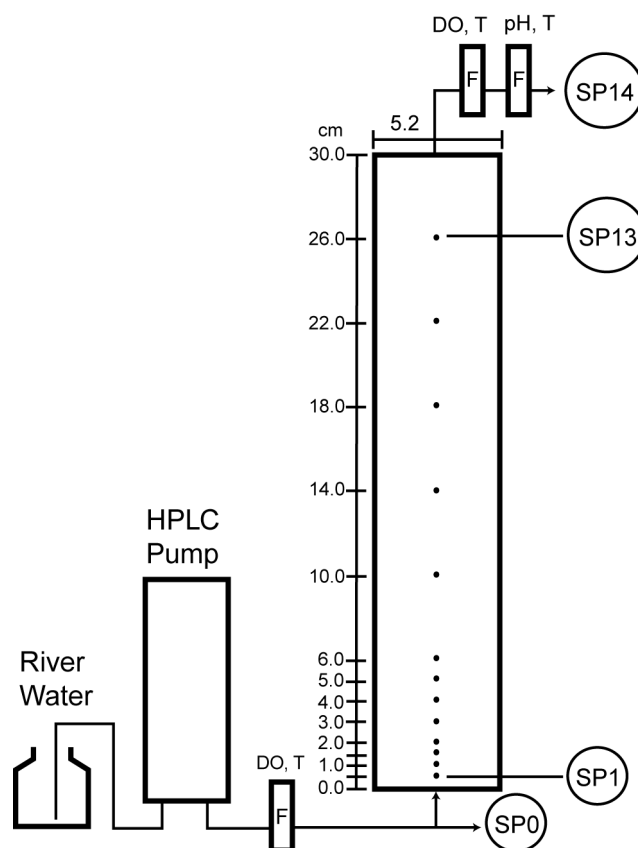

Fig. 4.2. Schematic representation of the setup of the column experiment with 13 sampling ports along the column (SP1-13) and one at the inlet (SP0) and one at the outlet (SP14). River water was pumped from the bottom to the top of the column. DO, temperature (T) and pH were measured in flow-through cells (F).

The column featured 15 sampling ports; one at the inlet, 13 along the column and one at the outlet (Fig. 4.2). DO and temperature were continuously measured at the inlet and at the outlet of the column (LDO101 (optical sensor), Hach Lange GmbH, Berlin, Germany, accuracy ±0.1 mg/L, T±0.3 K), while pH was measured after the column (PHC 301, Hach Lange GmbH, Berlin, Germany, accuracy pH ±0.1) in flow-through cells (Fig. 4.2). For each of the experiments at different temperatures, we measured three DO concentration profiles after an equilibration time of ≥20 d. DO was measured directly at each sampling port in a flow-through cell. After that, about 40 mL of sample volume was taken at the column inlet (SP0) and outlet (SP14) for the DOC and nitrate analyses by connecting a rinsed regenerated 0.45 μm cellulose filter (National Scientific Company, Rockwood, USA) to the port. The sampling procedure was conducted from the outlet to the inlet of the column, following the opposite direction of the water flow.

The DO consumption in the column was calculated by subtracting the measured DO concentration at sampling port SP14 from the DO concentration at SP0 0.5 d before. The DOM consumption was determined from the difference of DOC concentrations at SP14 and SP0.

4.2.4 Analytical methods

DOC concentrations were measured with a Shimadzu TOC-V CPH (Shimadzu Corporation, Kyoto, Japan). Nitrate and the other major ions were analyzed by means of a Metrohm 761 Compact IC (Metrohm Schweiz AG, Zofingen, Switzerland). Ammonium was measured with a Spectrophotometer Varian Cary 50 Bio (Varian BV, Middelburg, The Netherlands). The POC concentrations in sediment samples were determined by subtracting the inorganic carbon fraction, measured with a CO_2 Coulometer CM5015 (UIC Inc., Joilet, USA), from the total carbon fraction, measured with a CNS analyzer Eurovector EA3000 (Hekatech GmbH, Wegberg, Germany).

4.3 Results and discussion

4.3.1 Hydraulic conditions and concentration profiles of redox-active compounds

The winter and the summer sampling campaigns were conducted during low-flow conditions. The daily mean discharge of the Thur River during the field sampling campaigns varied between 13.7 and 24.8 m^3/s in summer and between 5.4 and 6.1 m^3/s in winter (Fig. 4.3). The daily mean temperatures in the river ranged from 20.9 to 22.9°C in summer and from 5.9 to 6.7°C in winter (Fig. 4.3).

The groundwater residence times between the river and the piezometers were estimated based on a groundwater flow model as well as the analysis of EC time series (Chapter 3) and ranged from 0.5 d at the piezometer closest to the river (R050) to 13 d at the piezometer furthest from the river (R023) (Fig. 4.1c, Fig. 4.4). As the mean residence time in the column was 0.5 d, the column well represented the situation at piezometer R050. The column experiments additionally allowed resolving the microbially-mediated redox processes on a scale that was not accessible in the field system.
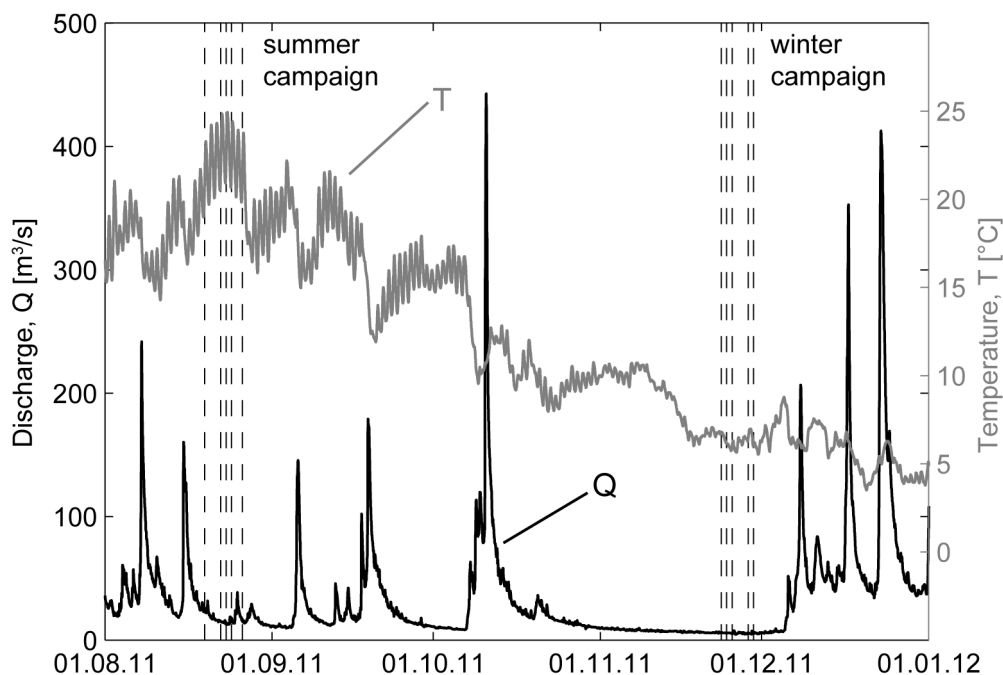
Fig. 4.3. Discharge (black line) and temperature (gray line) time series measured at the FOEN gauging station in Andelfingen covering the two detailed summer and winter sampling campaigns (August 19-26, 2011 and November 23-29, 2011). Each of the sampling days is shown as a dashed vertical line.

The temperature and the concentration profiles of selected redox-active compounds are shown in Fig. 4.4 for the sampling campaigns and in Fig. 4.5 for the column experiments. Most of the DO and DOM consumption in the field occurred between the river and the first piezometer (R050), both during summer and winter conditions. This observation indicates that most of the degradation processes took place within the first meters of the infiltration zone and shows that, in agreement with other studies (Bourg and Bertin, 1993; Brugger et al., 2001a; Sobczak and Findlay, 2002), the microbial activity was highest in this zone. For the piezometers further away from the river, an additional decrease in DO and DOC was observed in winter. However, considering the longer travel times to these piezometers, the corresponding degradation processes occurred much slower.
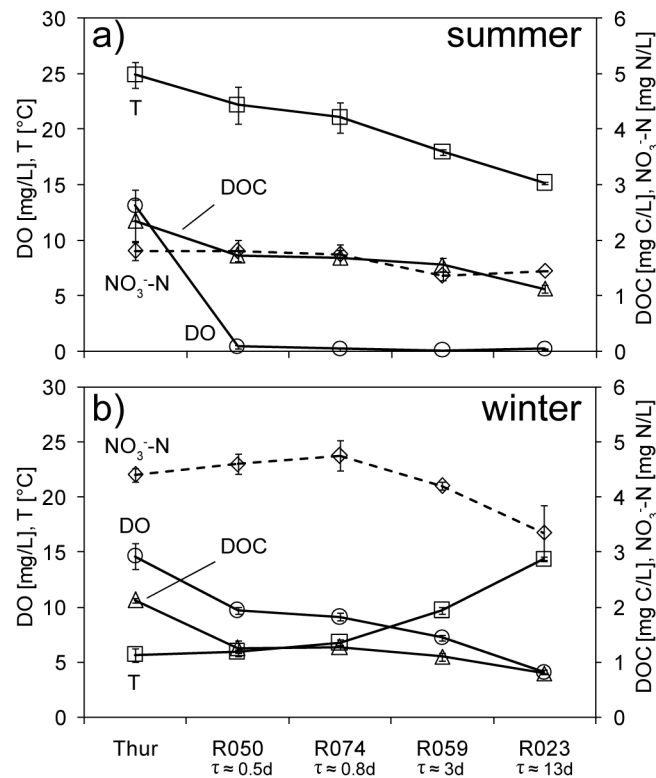
Fig. 4.4. Temperature and concentration profiles of DO, DOC and nitrate during (a) the summer and (b) the winter campaign. Mean and standard deviations are shown as symbols and error bars, respectively (n=5). Estimated groundwater residence times (τ) between the river and the piezometers are also indicated.

The DO concentration profiles for the column experiments revealed that the highest DO consumption rate occurred between the first two sampling ports. This is in accordance with other column experiments, for which the highest DO consumption rate was observed within the first centimeter of the column (von Gunten and Zobrist, 1993; von Gunten et al., 1994). At 20°C, the initial decrease of DO was followed by a linear decrease in the column, while at 5°C the DO concentration remained constant after the initial decrease (Fig. 4.5a). The linear decrease at 20°C suggests a zero-order degradation rate, which means that the DO consumption in the column was not limited by the substrates DO and NOM. The DO profile of the control experiment (performed after the 5°C experiment) was almost identical to the DO profile of the first experiment at 20°C (Supporting information: Fig. 4.11). This indicates that the column properties decisive for the bacterial degradation processes did not change during the operation period at 5°C.

We consider aerobic respiration of NOM as the only process responsible for the consumption of DO. Based on measured ammonium concentrations in river water, nitrification (oxidation of ammonium) potentially accounted for ≤2% of the DO consumption in the field campaigns and the column experiments, and can therefore be neglected. The removal of DOM during

river infiltration might be attributed to both microbial degradation and abiotic sorption processes (Brugger et al., 2001b). However, the summer and winter field sampling campaigns were conducted during relatively stable temperature and discharge conditions. It is therefore reasonable to assume that the sorption processes were in steady state and did not affect the removal of DOM. The same is true for the column system, which was equilibrated for ≥20 d before the measurements were taken. Therefore, we assume that microbial degradation processes dominated the abiotic sorption processes, which is in agreement with Sobczak and Findlay (2002).

The DO consumption between the river and the first piezometer (R050) was larger in summer than in winter and that between the column inlet and column outlet was larger at 20 than at 5°C. This is a clear indication of the temperature dependence of the microbially mediated degradation of NOM by aerobic respiration. In contrast, the consumption of DOM was similar during summer and winter conditions with about 0.7 mg C/L (Fig. 4.4) during the field sampling campaigns and about 0.3 mg C/L (Fig. 4.5) in the column experiments. Furthermore, the DOM was not consumed completely, both during the field sampling campaigns and in the column experiments. Only a fraction of about 30-50% of the total DOM was degraded, corresponding to the biodegradable DOM (BDOM). Similar values for the BDOM fraction were reported in several field studies (Sobczak and Findlay, 2002; Sharma et al., 2012). 50-70% of the DOM remained, presumably due to its recalcitrant nature.

During summer conditions, DO was nearly completely consumed at the first piezometer R050 (Fig. 4.4). Similarly, almost anoxic conditions were observed at the column outlet at 20°C (Fig. 4.5). However, denitrification was not observed either in the field, or in the column. Apparently, under summer conditions, there is enough nitrate available to act as a redox buffer preventing $Mn(IV)$- and $Fe(III)$-reducing conditions in the infiltration system.
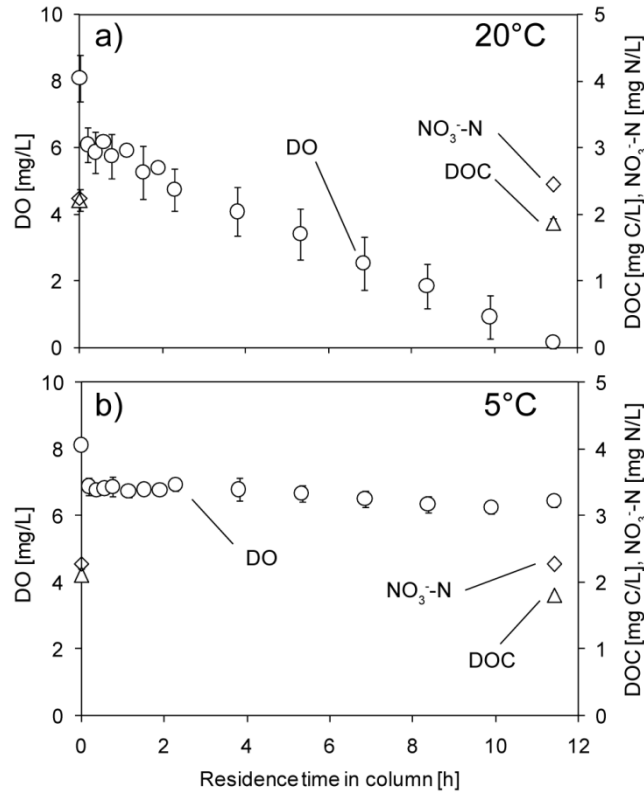
Fig. 4.5. Concentration profiles of DO, DOC and nitrate in the column at (a) 20°C and (b) 5°C. Each symbol represents a sampling port. The first data point corresponds to the sampling port at the inlet of the column (SP0), the last data point to the sampling port at the outlet of the column (SP14). Mean and standard deviations are shown as symbols and error bars, respectively (n=3).

4.3.2   Impact of temperature on DO and DOM consumption

4.3.2.1   Sampling campaigns and column experiments

To assess the impact of temperature on the aerobic NOM degradation, we compared the DO and DOM consumption between the river and the first piezometer (R050), and between the column inlet and outlet for summer and winter conditions. The resulting mean DO and DOM consumption for the field campaigns and column experiments are shown in Fig. 4.6. For a simplified version of aerobic respiration, one mole of DO (O_2) is used to oxidize one mole of organic carbon (CH_2O) (Eq. (4.1)):

$$CH_2O + O_2 \rightarrow CO_2 + H_2O \tag{4.1}$$

Accordingly, if DOM consumption would explain the entire DO consumption, the corresponding molar consumptions should be equal (bars in Fig. 4.6). However, during summer conditions (both in the field and in the column), DOM consumption explained only 10-20% of DO consumption (Fig. 4.6). The remaining 80-90% of the reduction capacity to

explain the DO consumption must therefore have been provided by other sources. POM in riverbed sediments and the column sand is an obvious source of additional reduction capacity (Brugger et al., 2001b; Sharma et al., 2012).

As mentioned in Section 4.3.1, DO consumption in the field and the column system was much smaller for lower than higher temperatures, while the DOM consumption remained at about the same level (Fig. 4.6) and did not seem to be significantly affected by temperature. As a result, DOM consumption accounted for larger fractions of 50% and 100% of the DO consumption at lower temperatures in the column and the field, respectively. Furthermore, the different behavior during summer and winter conditions suggests that the variability and temperature dependence of DO consumption are determined by the POM, rather than the DOM consumption.
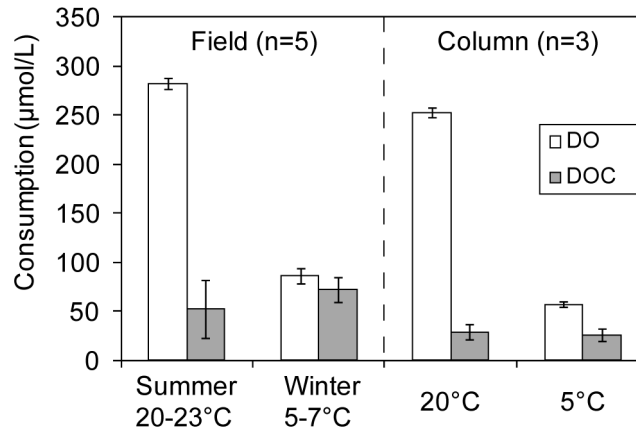

Fig. 4.6. Comparison of DO and DOM (expressed as DOC) consumption for the summer (20-23°C) and winter (5-7°C) field campaigns and for the column experiments at 20 and 5°C, respectively. The consumption refers to the concentration difference between the Thur River and the piezometer R050 in the field and between column inlet and outlet for the column experiments. Standard deviations are shown as error bars.

4.3.2.2 Periodic samplings

To test the dependence of the DO and DOM consumption on temperature more systematically, we compiled the corresponding data of all the samplings taken between 2008 and 2012 at the Thur River and the piezometer R050. We additionally calculated the POM consumption according to Eq. (4.2) assuming that the POM consumption corresponds to the difference between DO and DOM consumption. This implies that the consumption of DO (O_2) and DOM (CH_2O) is solely related to aerobic respiration (Section 4.3.1) and occurs at a molar ratio of one (Eq. (4.1)).

$$\Delta POC = \Delta DO - \Delta DOC \tag{4.2}$$

Fig. 4.10 (Supporting information) shows the DOM and the calculated POM consumption of all the 45 periodic samplings, including the two sampling campaigns of summer and winter 2011. Fig. 4.7 shows a plot of the DO consumption, the DOM consumption and the calculated POM consumption as a function of the daily mean river water temperature in scatter plots together with the calculated correlation coefficients. The DO consumption showed a high and significant correlation ($r = 0.74$, Fig. 4.7a) with the daily mean river water temperature. Thus temperature explained the variation in DO consumption to a high degree. However, DOM consumption was not correlated with river water temperature (Fig. 4.7b). This result coincides with the data shown in Fig. 4.6 and is in agreement with findings from Brugger et al. (2001b). Since the calculated POM consumption (Fig. 4.7c) is based on the difference between one highly-correlated parameter (DO consumption) and one uncorrelated parameter (DOM consumption), it is necessarily the case that POM consumption will also be highly correlated with temperature ($r = 0.7$).

This result supports the conjecture that the POM consumption is primarily responsible for the variability and temperature dependence of DO consumption, as stated in Section 4.3.2.1. The divergence between the temperature dependencies observed for DO and DOM consumption also have the consequence that DOM consumption accounts for a larger proportion of DO consumption at lower than at higher temperatures. At lower temperatures (<10°C), DOM consumption accounted for 50-100% of DO consumption, while at high temperatures (>15°C), DOM consumption accounted for 0-40% of DO consumption (Fig. 4.7). Correspondingly, the calculated POM consumption makes a more important contribution at high temperatures, suggesting that POM is the most important electron donor under these conditions.
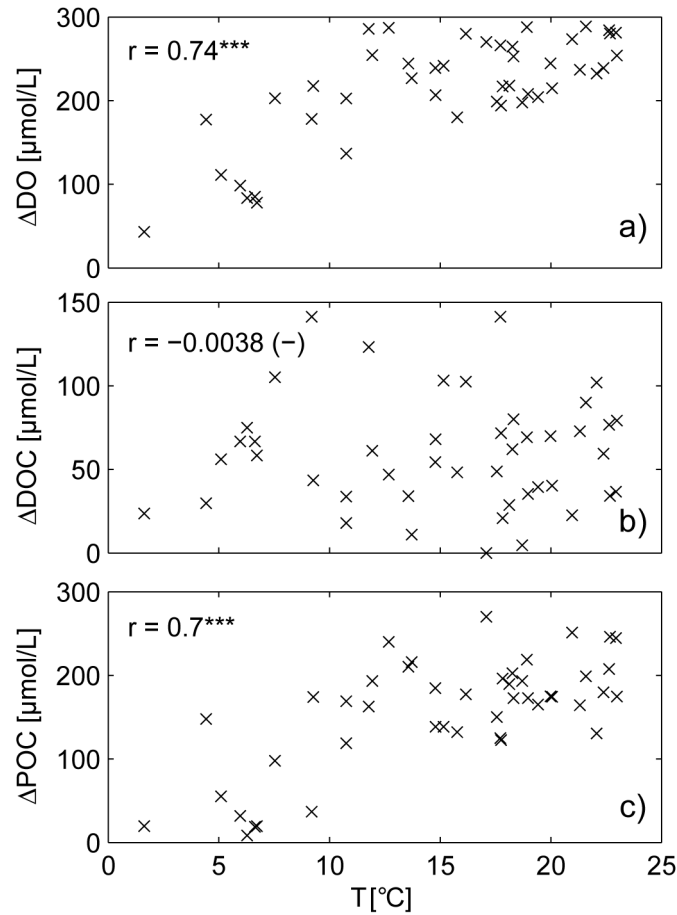
Fig. 4.7. Scatter plots between (a) DO consumption (ΔDO), (b) DOM consumption (ΔDOC), (c) calculated POM consumption (ΔPOC =ΔDO-ΔDOC) at the piezometer R050, and daily mean river water temperature (T). r is the correlation coefficient between two variables with the significance levels: *** = p<0.001, ** = p<0.01, * = p<0.05, (-) = p>0.05. p is the probability of two variables being uncorrelated.

4.3.2.3 Conceptual explanation

The fact that no correlation was observed between DOM consumption and temperature does not mean that this process is not temperature dependent. One conceptual explanation is based on the fact that consumption of the biodegradable fraction of DOM (BDOM) occurs generally at high degradation rates as it is present in a dissolved and bioavailable form. Even though the BDOM degradation rates might be lower at lower temperatures, bacteria most likely were able to completely consume the full BDOM fraction within the residence times of our field and column systems. Accordingly, on our scales of observation, the DOM consumption was limited by the amount of BDOM rather than by temperature-dependent rates. In contrast, POM consumption involves the cleavage of organic macromolecules into soluble monomers by extracellular hydrolytic enzymes (Egli, 1995; Pusch et al., 1998). Therefore, degradation of POM generally occurs at lower rates than degradation of BDOM (Greskowiak et al., 2006;

Sharma et al., 2012) and the temperature dependence of POM degradation could be resolved on the timescales of our experimental systems (field, column).

This conceptual explanation is based on the assumption that DOM resulting from hydrolysis of POM in bacterial biofilms does not contribute significantly to the DOM pool in the sampled groundwater, and hence did not affect the observed DOM consumption (Fig. 4.7b). In literature, the hydrolysis of POM is considered to be the rate-limiting step in POM degradation, which implies that the DOM resulting from hydrolysis undergoes fast biodegradation (Valentini et al., 1997; Henze et al., 1999; Vavilin et al., 2008). Furthermore, there is evidence that DOM uptake and transformation by bacteria is very efficient in biofilms (Pusch et al., 1998). Bacterial biofilms in sediments act thus as effective sinks of DOM that originated either from the river (as "transported/mobile substrate") or from the hydrolysis of POM ("stationary substrate").

4.3.3   Impact of discharge on DO and DOM consumption

The temperature dependence of DO consumption might be superimposed by a dependence on hydrologic conditions. High-discharge conditions or flood events are generally not considered to affect the redox conditions in the infiltration zone (Sprenger et al., 2011), but rather to increase the risk of a breakthrough of contaminants or pathogens at the pumping well due to shorter groundwater residence times (Schubert, 2002). However, it is well known that the suspended POM concentration in the river increases with river discharge, as a result of an increased mobilization of allochthonous and autochthonous POM (Meybeck, 1982). The contribution of periphyton (autochthonous POM) to the suspended POM pool in a river was found to positively correlate with discharge, because of the increased abrasive action at the riverbed (Uehlinger, 2006; Akamatsu et al., 2011). Furthermore, it has been observed that the POM import into gravelly riverbed sediments mostly occurred during flood events, which increased the POM concentrations and the microbial respiration rate in the riverbed sediments (Naegeli et al., 1995; Brunke and Gonser, 1997). Hence, the higher POM availability in the riverbed during high-discharge conditions might give rise to an increased DO consumption during river infiltration.

The overall correlation between DO consumption and the daily mean discharge (measured in Andelfingen) was small and not significant (Supporting information: Table 4.3). However, DO consumption increased with increasing discharge up to 60 m^3/s and leveled off at 200-300 µmol/L beyond this point (Fig. 4.8). As the data for discharges below 60 m^3/s covered a wide range of temperatures, DO consumption showed only a weak correlation with discharge

(r = 0.31). To compensate for the temperature dependence, we defined two temperature ranges, T<15°C (circles) and T>15°C (triangles). Following this separation, we found a significant correlation between DO consumption and discharge for the low-temperature range (r = 0.85). DOM consumption was not correlated with discharge (Supporting information: Table 4.3) suggesting that the increase in DO consumption is probably caused by an enhanced POM consumption, which supports the notion described above.

For the high-temperature range, the correlation between DO consumption and discharge was small and not significant. This result can be explained by the fact that DO consumption for the high-temperature range was already high (200-300 µmol/L) and nearly complete at low discharges. Hence, an increase in discharge could not lead to a significant increase in DO consumption.

Another process that might explain the increased DO consumption at higher discharges is the leaching of DOM from the soil and vegetation (root zone) at high groundwater tables. At our field site, this effect was found to be restricted to a zone dominated by the pioneer plant *salix viminalis* (willow bush) (Peter et al., 2012). The piezometer R050 was located close to the river, where the gravel-and-sand aquifer is covered by a relatively thin layer of alluvial fines (0.3 m) with no or only little grass vegetation. For this zone, the input of DOM from the soil and vegetation was found to be negligible (Peter et al., 2012).
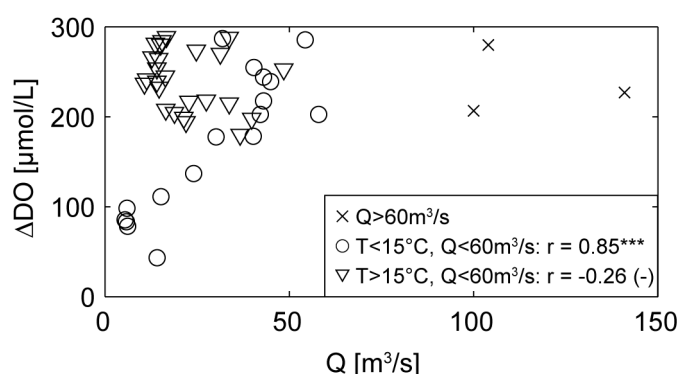
Fig. 4.8. Scatter plot between DO consumption at the piezometer R050 (ΔDO) and daily mean river discharge (Q). r is the correlation coefficient between the two variables with the significance levels: *** = p<0.001, ** = p<0.01, * = p<0.05, (-) = p>0.05. p is the probability of two variables being uncorrelated.

Low-discharge conditions are expected to promote the DO consumption as a result of increased groundwater residence times and higher loads of DOM in the river due to less dilution of wastewater effluent (Sprenger et al., 2011). In our observations, however, DO consumption did not reveal a significant increasing trend for decreasing discharges, regardless

of the considered temperature range (Fig. 4.8). Furthermore, the DOM consumption did not reveal any significant correlation with discharge, but was positively correlated with DOC concentrations in the river (Supporting information: Table 4.3). However, DOC concentrations in the river increased rather than decreased with discharge; the correlation was weak but significant. This suggests DOM sources other than wastewater treatment plants.

4.3.4   Implications for groundwater quality at riverbank-filtration systems

The latest climate change scenarios predict an increase in summer and winter air temperature of 4-5 K for NE-Switzerland by 2085. Furthermore, extreme events, such as summer heat waves, are expected to occur with a higher frequency and intensity (CH2011, 2011). River discharges are expected to decrease in summer and increase in winter. River water temperature, which is decisive for the degradation processes in the riverbed, is likely to increase by the same extent as air temperature, especially during low-flow conditions (FOEN, 2012a). During the hot summer of 2003, the mean river water temperature of the Thur River was 22°C for a period of 70-80 d. In the future, we might have to deal more frequently with extreme events of similar or longer duration and even higher mean river water temperatures.

According to our results, the calculated POM consumption showed a pronounced temperature dependence and accounted for most of the DO consumption during summer. Consumption of DO was enhanced during high-flow conditions, probably due to an increased import of POM into the riverbed. On our scales of observation, we could not identify any temperature dependence of the DOM consumption, which was rather limited by the fraction of BDOM. Moreover, the expectation that low-discharge conditions would lead to higher DOC concentrations in the river due to less dilution of wastewater effluents, and hence to an increased DOM and DO consumption during river infiltration, is not supported by our data.

Sprenger et al. (2011) assessed the vulnerability of riverbank-filtration systems to climate change (drought and flood scenarios) with respect to several water quality parameters (DOM, nutrients, pathogens). The vulnerability of a riverbank-filtration system to climate change with respect to the redox milieu in groundwater might depend on three major factors. (1) The hydraulic connection between the river and groundwater. If infiltration occurs through an unsaturated zone, which is aerated, complete DO depletion is not expected (Huggenberger et al., 1998; Hoehn and Scholtis, 2011). During infiltration in direct hydraulic connection to the groundwater table (saturated), which was the case at our field site, DO is not replenished and might become depleted, as observed during summer. (2) Based on our results, we consider the catchment characteristics as another decisive factor. Rivers in catchments without a retention

basin (e.g. a lake) have a more dynamic discharge regime and are likely to have a higher POM load, especially during flood events. (3) The grain-size distribution of the riverbed sediments. In gravelly riverbeds, the import of POM is possible to deeper layers, while in sandy or clogged riverbeds, the import of POM might be physically hindered (Brunke and Gonser, 1997). We therefore anticipate the highest vulnerability to climate change with respect to the redox milieu for riverbank-filtration systems at which infiltration occurs through a gravelly riverbed in direct hydraulic connection to the groundwater table and which are located in catchments without a retention basin.

For such riverbank-filtration systems, we consider future summer heat waves to be critical for the redox-related groundwater quality. A substantial increase in river water temperature during future heat waves will enhance the POM turnover, leading to a complete consumption of DO and potentially nitrate. As a consequence, Mn(II) and Fe(II) could be released, as observed during the hot summer 2003 (Hoehn and Scholtis, 2011). An additional POM input into the riverbed during flood events induces a higher consumption of DO and possibly nitrate, which may enhance the risk for Mn(III/IV)-/Fe(III)-reducing conditions in the infiltration zone.

The subsequent re-oxidation of Mn(II) and Fe(II) and precipitation of Mn(IV)- and Fe(III)(hydr)oxides can lead to clogging problems and deterioration of the drinking water quality (rusty water) at pumping stations of a drinking water supply. For the removal of dissolved Mn(II) and Fe(II), conventional pump-and-treat techniques can be applied, which are based on physical-chemical or biological processes (Mouchet, 1992). Alternatively, in-situ techniques can be used, in which the oxidation processes take place directly in the aquifer (Mettler et al., 2001).

4.4 Conclusions

We performed field investigations and laboratory column experiments to investigate the dynamics of redox processes that occur during river infiltration and their dependence on the climate-related variables temperature and discharge. The observations of the summer and winter sampling campaigns in the field could be successfully reproduced by column experiments. Particulate organic matter (POM) was identified as the main electron donor for dissolved oxygen (DO) consumption during summer conditions and both the DO and the calculated POM consumption revealed a pronounced temperature dependence. The DO consumption was enhanced during flood events, presumably due to an additional POM input into the riverbed.

In our field and column systems, DO was the most important electron acceptor. In summer (T>20°C), DO concentrations in groundwater were close to zero, but denitrification was not observed. Similarly, most of the Swiss aquifers fed by rivers are (sub)oxic under today's summer conditions and nitrate buffers the redox system before it becomes Mn(III/IV)- and Fe(III)-reducing. Therefore, currently there is no need to implement demanganation and deferisation. However, during future summer heat waves, an enhanced POM turnover could lead to a full consumption of DO and nitrate, enabling the release of Mn(II) and Fe(II). As the source, quality and quantity of POM and its input into the riverbed are very difficult to assess, it is nearly impossible to find direct intervention strategies.

We recommend long-term monitoring of the redox conditions at riverbank-filtration systems, which are characterized by an infiltration that occurs through a gravelly riverbed in direct hydraulic connection to the groundwater table, and by catchments without a retention basin. Long-term data will allow taking adequate measures in time, while accounting for the site-specific hydrogeological conditions.

Acknowledgments

4.5 Supporting information

Fig. 4.9. Discharge time series covering all the samples taken at the Niederneunforn field site between 2008 and 2012. Each sampling is shown as vertical dashed line.
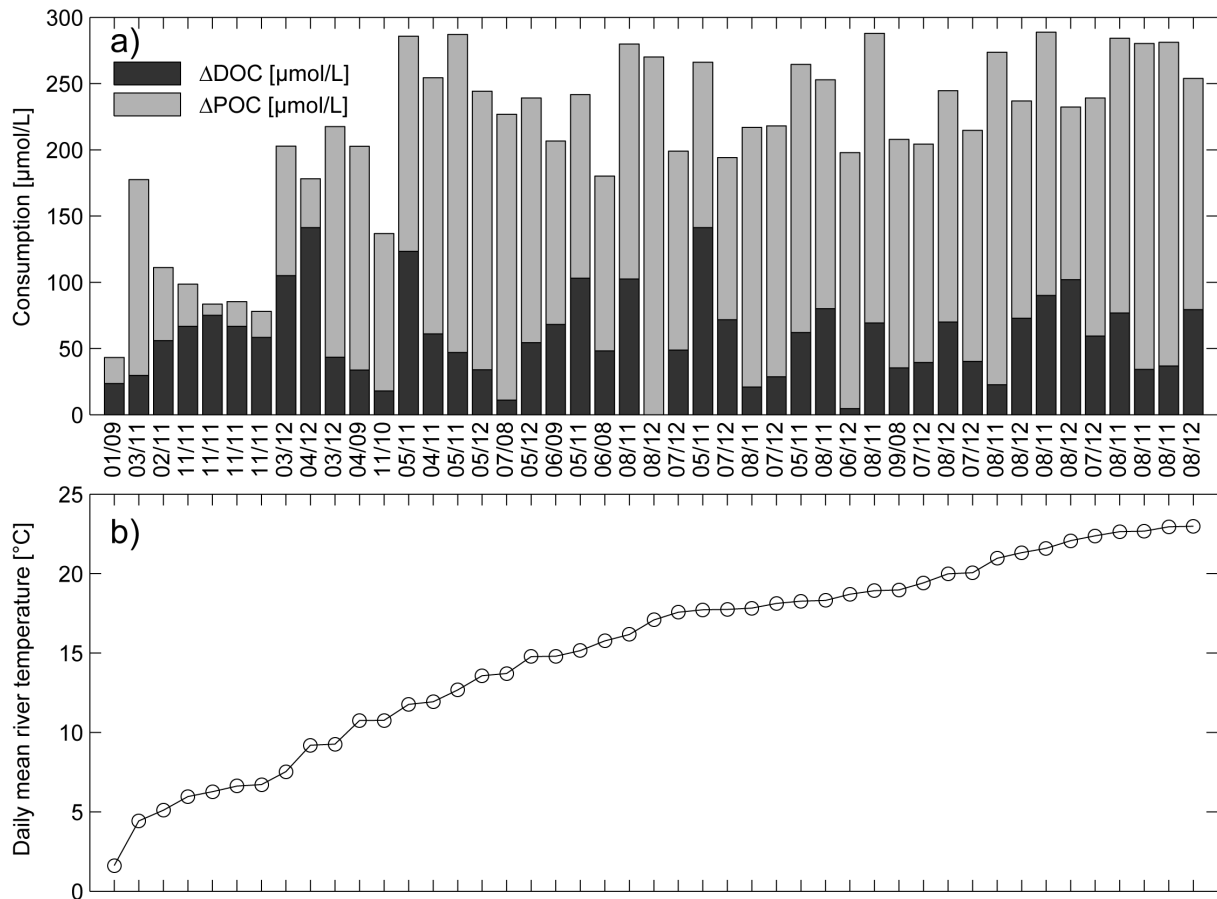
Fig. 4.10. (a) DOM consumption (ΔDOC) and calculated POM consumption (ΔPOC=ΔDO-ΔDOC) between the river and the piezometer R050 for the periodic samplings between 2008 and 2012 (n=45) including the sampling campaigns of summer and winter 2011. The DO consumption (ΔDO) corresponds to the sum of the dark and light gray bars. On the x-axis, the month and the year of each sampling are indicated. The data are sorted by increasing daily mean river water temperature, which is shown in (b) for each of the samplings.
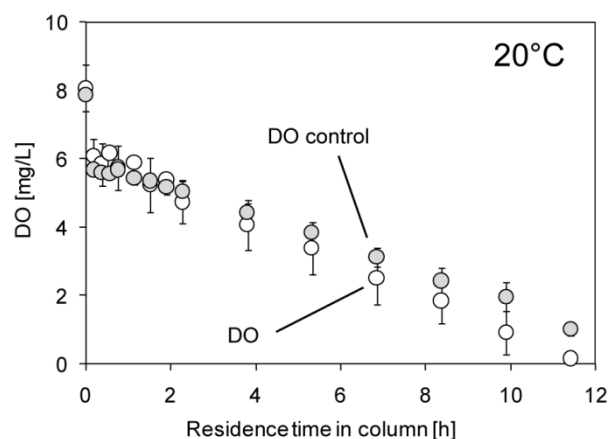
Fig. 4.11. DO concentration profiles in the column measured during the main experiment (white circles) and during the control experiment (gray circles) at 20°C. The control experiment was conducted after the experiment at 5°C. The mean and the standard deviations are shown as circles and error bars, respectively (n=3).

Table 4.1. Composition 1 of Thur River water used in the column experiments (collected on July 4, 2012).

DOC	pH[a]	El. conductivity[b]	Alkalinity[c]	NO_3^-	Na^+	Ca^{2+}	Mg^{2+}	PO_4^{2-} [d]	NH_4^+ [d]
[mg/L]		[μS/cm]	[mmol/L]	[mg N/L]	[mg/L]	[mg/L]	[mg/L]	[μg P/L]	[μg N/L]
2.1	8	407	4.08	2.2	11.9	68.0	12.1	35.5	11.6

[a]measured with a pH meter PHC 301, Hach Lange GmbH, Berlin, Germany
[b]measured with a Metrohm 712 Conductometer, Metrohm Schweiz AG, Zofingen, Switzerland
[c]measured with a Metrohm 809 Titrando, Metrohm Schweiz AG, Zofingen, Switzerland
[d]measured with a Spectrophotometer Varian Cary 50 Bio, Varian BV, Middelburg, The Netherlands

Table 4.2. Composition 2 of Thur River water used in the column experiments (collected on August 13, 2012).

| DOC	pH	El. conductivity	Alkalinity	NO_3^-	Na^+	Ca^{2+}	Mg^{2+}	PO_4^{2-}	NH_4^+
[mg/L]		[μS/cm]	[mmol/L]	[mg N/L]	[mg/L]	[mg/L]	[mg/L]	[μg P/L]	[μg N/L]
2.1	8	410	3.83	2.1	18.2	58.9	13.7	14.3	19.0

Table 4.3. Correlation coefficients between the parameters DO consumption (ΔDO), DOM consumption (ΔDOC), DOC concentration in the river (DOC river), calculated POM consumption (ΔPOC $=\Delta$DO-ΔDOC), daily mean river water temperature and daily mean river discharge for the periodic samplings at the piezometer R050 (n=45). Significance levels: *** = $p<0.001$, ** = $p<0.01$, * = $p<0.05$, (-) = $p>0.05$. p is the probability of two variables being uncorrelated.

	ΔDOC	DOC river	ΔPOC	Temperature	Discharge
ΔDO	0.15 (-)	0.35*	0.87***	0.74***	0.23 (-)
ΔDOC		0.61***	-0.35*	-0.0038 (-)	-0.066 (-)
DOC river			0.029 (-)	0.14 (-)	0.46**
ΔPOC				0.70***	0.25 (-)

Chapter 5

Modeling the dynamics of oxygen consumption during riverbank filtration by a stochastic-convective approach

Abstract

Dissolved oxygen (DO) is an important groundwater-quality parameter. In riverbank sediments, a strong decrease of DO over the distance of a few meters has frequently been observed. The consumption rates may vary in time, which puts the representativeness of common, sporadic DO measurements in groundwater, based on monthly or even yearly sampling, into question. We present a new modeling approach that allows efficiently estimating DO concentrations in alluvial groundwater from measured DO concentrations in the river under various temperature and discharge conditions. The model is based on the stochastic-convective reactive approach and assumes a time-invariant lognormal travel-time distribution of the streamline ensemble connecting the river and a groundwater observation well. DO consumption, resulting from aerobic respiration, is modeled by zero-order kinetics. The DO consumption rate depends on river temperature and discharge. While the temperature dependence of aerobic respiration is well known, the discharge dependence is probably related to an increased trapping of particulate organic matter (POM) within the riverbed during high-discharge events, thus enhancing the POM availability and DO consumption rate. We propose an empirical equation that quantifies the dependence between discharge and the DO consumption rate, which we infer from high-resolution DO time series measured in the Thur River (NE-Switzerland) and an adjacent observation well. The estimated parameterization at our field site suggests that an increasing discharge within the narrow window of 20-50 m^3/s enhances the DO consumption rate by a factor of 4. By considering the measured DO in the river and including the dependence of the DO consumption rate on both discharge and temperature, the model was able to capture the diurnal, short-term (days to

weeks), and seasonal dynamics of the observed DO within the alluvial aquifer. The temperature dependence of the DO consumption rate was found to be more important on a seasonal time scale, while the effect of discharge dominated the DO behavior during hydrological events extending over a few days to weeks. The presented modeling approach can be transferred to other riverbank-filtration systems to efficiently estimate DO concentrations in alluvial aquifers under various climatic and hydrologic conditions and, hence, assess the risk of approaching anoxic conditions in a changing climate.

5.1 Introduction

Drinking water originating from riverbank filtration provides considerable fractions (10-50%) of the overall drinking water production in several European countries (Tufenkji et al., 2002). The redox conditions in the infiltration zone are mainly controlled by microbial oxidation of natural organic matter (NOM), which leads to a consumption of terminal electron acceptors, such as oxygen, nitrate and Mn(IV)-/Fe(III)(hydr)oxides. Redox conditions have been observed to undergo seasonal variations due to the temperature dependence of NOM degradation (von Gunten et al., 1991; Massmann et al., 2006).

In the Swiss lowlands, the peri-alpine alluvial shallow gravel-and-sand aquifers are mostly oxic, which allows a minimal treatment of pumped groundwater before supplying it as drinking water to the distribution system. Under anoxic conditions, as observed in the hot summer of 2003 (Hoehn and Scholtis, 2011), the redox sequence proceeds to denitrification and eventually Mn(IV)-/Fe(III)oxide-reduction, leading to the occurrence of undesired dissolved species such as nitrite or Mn(II)/Fe(II) (Jacobs et al., 1988; Massmann et al., 2008). Additionally, it has been shown that degradation of micropollutants is sensitive to the presence or absence of oxygen (Greskowiak et al., 2006; Massmann et al., 2006; Maeng et al., 2010).

As a result of climate change, river temperatures as well as the frequency and intensity of heat waves are expected to increase, while river discharge is expected to decrease during summer months (CH2011, 2011; FOEN, 2012a). The higher microbial activity at increased temperatures and the longer groundwater residence times at lower discharge are supposed to increase the frequency of anoxic conditions in riverbank-filtration systems (Sprenger et al., 2011). To assess this risk, it is crucial to understand the dynamics of oxygen consumption during riverbank filtration as a function of temperature and discharge. While continuous monitoring of dissolved oxygen (DO) concentrations is routinely performed in rivers by environmental agencies, the monitoring of DO concentrations in groundwater is often

restricted to sampling on a monthly or even yearly basis. A quantitative understanding of the temperature and discharge dependence of DO consumption is therefore required, allowing for model-based estimates of DO concentrations in groundwater from those measured in the river.

Spatially explicit numerical reactive transport models have successfully been applied to simulate the dynamics of NOM degradation and DO consumption during river infiltration (Matsunaga et al., 1993; Horner et al., 2007; Sharma et al., 2012). Sharma et al. (2012) simulated the seasonal variation of groundwater DO concentrations by including a temperature-dependent NOM degradation rate. They also showed that discharge-related changes in the residence time caused changes in groundwater DO concentrations. However, spatially explicit numerical reactive transport models are often very complex and site specific, they have long run times and require a large data set for model setup and calibration.

In this study, we present a new semi-analytical model to predict DO concentrations in river-fed groundwater under various climatic and hydrologic conditions. The implementation of the model is easier and faster and model run times are shorter compared to spatially explicit numerical reactive transport models. The model is based on the stochastic-convective reactive approach (Simmons, 1982; Simmons et al., 1995) and incorporates a dependence of the DO consumption rate on river temperature and discharge. In former modeling studies, discharge was considered to affect groundwater residence times (Sharma et al., 2012) but not the degradation rate itself. We hypothesize that discharge fluctuations can also affect the NOM availability and hence, the DO consumption rate.

After an introduction to the theory of stochastic-convective reactive transport and the temperature and discharge dependence of DO consumption, we describe the model setup and its implementation for a riverbank-filtration system in NE-Switzerland at the peri-alpine Thur River. We then present a 9-month long high-resolution DO time series measured in the Thur River and an adjacent groundwater observation well. Based on these data, we test the dependence between discharge and the DO consumption rate and quantify this relationship by an empirical equation. We incorporate the estimated discharge and a literature-based temperature dependence of the DO consumption rate in the model formulation and simulate the 9-month long groundwater DO time series. We present the modeling results and discuss the model performance and the strengths and limitations of the modeling approach. Finally, we give advice for future applications of the model.

5.2 Theory

5.2.1 Stochastic-convective reactive transport

The transport system between the river and a groundwater observation well is conceptualized as ensemble of convective-reactive streamlines, each characterized by a distinct travel time. Diffusive exchange among the streamlines is not considered and dispersive effects are treated as a component of the randomness in the travel time probability-density function *(pdf)* of the streamline ensemble. Hence, the reactive processes are separated from physical transport (Simmons, 1982).

For each streamline, DO consumption is assumed to be solely related to aerobic respiration $CH_2O + O_2 \rightarrow CO_2 + H_2O$ and is described by zero-order kinetics:

$$\frac{dDO}{dt} = \frac{dc_{CH_2O}}{dt} = \begin{cases} -k_{eff} & \text{if } DO > 0 \\ 0 & \text{otherwise} \end{cases} \tag{5.1}$$

which is a good approximation to Michaelis-Menten kinetics, as typical half-saturation constants of aerobic respiration are small (0.03-0.3 mg/L according to Greskowiak et al. (2006) and Schäfer et al. (1998)). In Eq. (5.1), DO and c_{CH_2O} are molar concentrations of dissolved oxygen and NOM, respectively, and k_{eff} is the effective zero-order DO consumption rate, depending on the state of the system (temperature/discharge). If we assume CH_2O as the elemental composition of NOM and complete aerobic degradation, the consumption rates of DO and NOM are identical.

The DO concentration $DO(\tau)$ within each streamline with residence time τ is described by:

$$DO(\tau) = max\big(0, DO_{in} - k_{eff} \cdot \tau\big) \tag{5.2}$$

with DO_{in} being the input DO concentration of the river. Fig. 5.1 shows the normalized DO concentration distribution $DO(\tau)/DO_{in}$ for a set of streamlines with dimensionless travel times $\tau = [0, 5]$ for three different effective consumption rates (colored dashed lines).

The DO concentration at an observation well (DO_{out}) results from the stochastic-convective averaging of the concentration distribution $DO(\tau)$ over the travel-time *pdf* $g(\tau)$:

$$DO_{out} = \int_0^{\tau_{max}} g(\tau)\, DO(\tau)d\tau \tag{5.3}$$

in which τ_{max} is the maximal occurring travel time in $g(\tau)$. The bold solid colored lines in Fig. 5.1 indicate the normalized DO concentrations DO_{out}/DO_{in} at the observation well

resulting from the stochastic-convective averaging over the travel-time *pdf* (solid black line) for the different effective consumption rates.
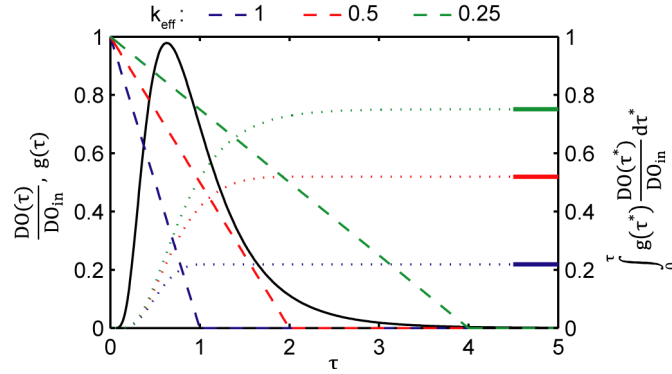

Fig. 5.1. Schematic illustration of the stochastic-convective averaging of the normalized concentration distribution $DO(\tau)/DO_{in}$ (colored dashed lines, Eq. (5.2)) over the travel-time *pdf* of the streamline ensemble $g(\tau)$ (black solid line) for three different effective consumption rates k_{eff}. The colored dotted lines represent the incremental integration to each τ according to the right axis label. The bold solid colored lines indicate the resulting normalized DO concentrations DO_{out}/DO_{in} at the observation well after full integration to τ_{max} (Eq. (5.3)).

The DO concentration $DO_{out}(t)$ at a certain observation well and a certain point in time t is described by convolution of the DO concentration distribution of the streamline ensemble with the travel-time *pdf* $g(\tau)$:

$$DO_{out}(t) = \int\limits_{0}^{\tau_{max}} g(\tau)\,max\big(0, DO_{in}(t - \tau) - k_{eff}(t - \tau) \cdot \tau\big)d\tau \tag{5.4}$$

In contrast to Eqs. (5.2) and (5.3), the DO concentrations along the individual streamlines are affected by time-dependent input DO concentrations $DO_{in}(t - \tau)$ and dynamic effective consumption rates $k_{eff}(t - \tau)$.

5.2.2 Effective DO consumption rate

The degradation of NOM during riverbank filtration is performed by microbes attached to the riverbed sediments (Pusch et al., 1998), mainly within the first meters of infiltration (Brugger et al., 2001a). NOM consists of dissolved organic matter (DOM) and particulate organic matter (POM). In contrast to DOM, POM is retained in the riverbed sediments by filtration. Chapter 4 of this thesis and other studies (Brugger et al., 2001b; Sharma et al., 2012) have highlighted that the degradation of POM accounted for most of the variability in DO consumption, while DOM degradation did not show a significant dependence on temperature

and discharge. In the following, we therefore consider POM as the main electron donor for DO consumption during riverbank filtration.

The rate of aerobic POM degradation, and hence the effective DO consumption rate k_{eff}, depend on temperature and POM availability (concentration and composition) (Pusch et al., 1998). The suspended POM concentration in the river water is known to increase with increasing discharge as a result of an increased mobilization of allochthonous (terrestrially-derived) and autochthonous (aquatically-derived) POM (Meybeck, 1982; Sugimoto et al., 2006; Besemer et al., 2009). The increase in autochthonous POM, which is generally highly biodegradable (Leenheer and Croue, 2003), was found to be related to the shearing off of periphyton due to the increasing abrasive action at the riverbed (Biggs and Close, 1989; Uehlinger, 2006; Akamatsu et al., 2011). Furthermore, it has been shown that the POM import into gravelly riverbeds mostly occurred under high-discharge conditions, which increased the POM concentration and the microbial respiration rate in the riverbed (Bretschko and Moser, 1993; Naegeli et al., 1995; Brunke and Gonser, 1997). Based on these observations, we hypothesize that discharge can be used as a proxy for the POM availability in the riverbed sediments, which in turn affects the effective DO consumption rate.

In order to separate the dependence of the effective consumption rate on temperature from that on discharge, we conceptualize k_{eff} as the product of a discharge-dependent consumption rate $k(Q)$ and a temperature factor f_T:

$$k_{eff}(t - \tau) = f_T(t - \tau) \cdot k\big(Q(t - \tau)\big) \tag{5.5}$$

which implies that k_{eff} is assumed to depend on the river temperature T and the discharge Q at the time of infiltration $t - \tau$.

The dependence of the DO consumption rate on discharge is not well established in the literature. Therefore, the assessment and quantification of this relationship constitutes an important part of this chapter (Sections 5.3.3 and 5.4.3). On the other hand, the temperature dependence of the POM degradation rate has been intensively studied. We apply the expression for the temperature factor f_T introduced by O'Connell (1990):

$$f_T(t - \tau) = e^{\alpha + \beta \cdot T(t-\tau)\left(1 - 0.5\frac{T(t-\tau)}{T_{opt}}\right)} \tag{5.6}$$

in which β and T_{opt} describe the temperature dependence, while α is a scale parameter. T_{opt} denotes the optimal temperature for degradation.

5.3 Materials and methods

5.3.1 Field site and data collection

The Niederneunforn field site is located in the Thur catchment in northeastern Switzerland (Fig. 5.2a). Because no retention basin (e.g. a lake) is located along the course of the river, its discharge is very dynamic, ranging from 3 to 1100 m^3/s, the average discharge being 47 m^3/s. The field site was instrumented with numerous observation wells during the interdisciplinary RECORD project (Schneider et al., 2011; Schirmer, 2013) in the context of river restoration measures realized in the year 2002 (Fig. 5.2b). A 3D groundwater flow and transport model was setup and calibrated against measured groundwater heads and experimentally determined groundwater travel times (Chapter 3). The groundwater flow field for low-flow conditions (Fig. 5.2b) indicates losing conditions along the main river channel.
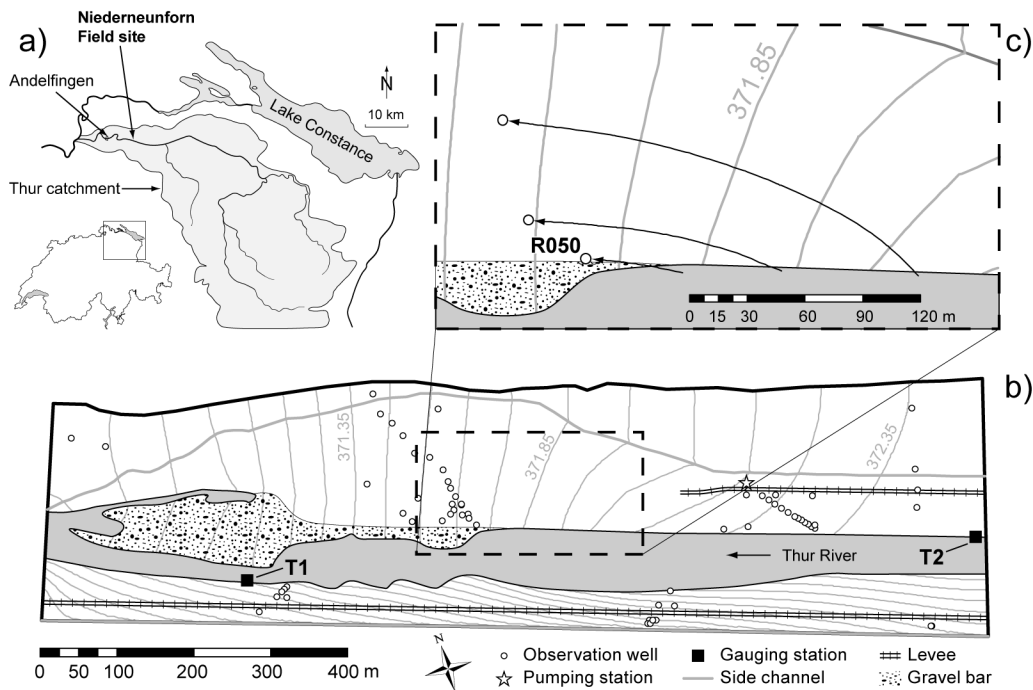
Fig. 5.2. (a) Thur catchment with indicated location of the Niederneunforn field site, NE-Switzerland. (b) Niederneunforn field site. The Thur River flows from right to left. Groundwater isopotentials at low-flow conditions (equidistance 10 cm) are taken from the 3D steady-state groundwater flow model of Chapter 3. T1 and T2 indicate the downstream and upstream gauging stations, respectively. (c) Enlargement of the area indicated by the dashed rectangle in (b). The black lines/arrows indicate the advective flow paths from the river to selected observation wells according to the groundwater flow model. Continuous DO measurements were conducted in the observation well R050.

To gain insight into the dynamics of DO consumption during river infiltration at the field site, we measured DO concentrations in the observation well R050 (Fig. 5.2c) at a temporal resolution of 15 min with an optical sensor (ROX/YSI 600OMS, YSI Inc., USA). The sensor was located in a depth of 2.3 m, in the center of the 2 m screen of the observation well. The groundwater table was always at least 1 m above the sensor.

DO concentrations in the river are routinely measured in Andelfingen (10 km downstream of Niederneunforn, Fig. 5.2a) by the Federal Office for the Environment at 10-min intervals using an optical sensor (SC100, Hach Lange GmbH, Germany). To validate the applicability of these data to our field site in Niederneunforn, we measured river DO concentrations at the gauging station T2 (Fig. 5.2b) with an optical sensor (LDO10115, Hach Lange GmbH, Germany) during three control periods, two in summer and one in winter. These control measurements of river DO concentrations revealed a good agreement between Andelfingen and Niederneunforn, including the phase and the amplitude of the diurnal fluctuations (Fig. 5.3).

Temperature and specific electrical conductivity (EC) were measured at the gauging station T1 (Fig. 5.2b) and in the observation well R050 at 15-min intervals (DL/N 70, STS AG, Switzerland). River discharge was measured at the gauging station T2 (Fig. 5.2b) at 15-min intervals by the Agency for the Environment of the Canton Thurgau. The data acquisition covered a period of 9 months, from August 2011 to April 2012. The groundwater DO time series contained a one-month gap in November 2011 and two smaller gaps in January and February 2012. Outliers in the data set were removed and intervals were equalized to 15 min.
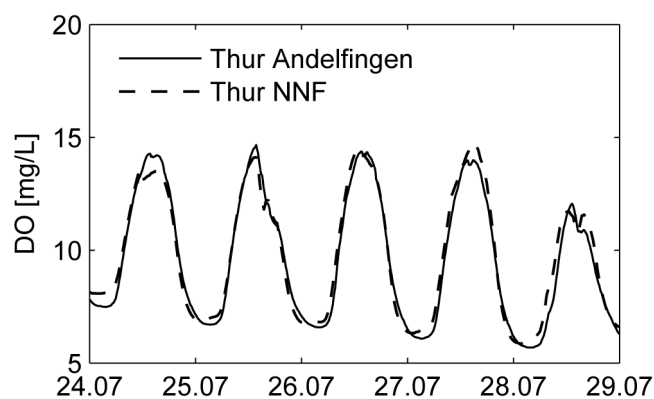

Fig. 5.3. Comparison of DO time series measured in the Thur River in Andelfingen (solid line) and in Niederneunforn (NNF, dashed line) during a five-day control period in summer 2012.

5.3.2 Estimation of travel-time pdf

The stochastic-convective reactive approach separates the physical transport from the reactive processes (Section 5.2.1). The travel-time *pdf* should therefore be obtained from a conservative tracer. Vogt et al. (2010a) propose to use fluctuations in the electrical conductivity (EC), which are transported from the river into the aquifer without retardation.

The transport of EC fluctuations from the river to an observation well can be described by convolution of the input EC signal $EC_{in}(t - \tau)$ with a travel-time *pdf* $g(\tau)$:

$$EC_{out}(t) = \int_{0}^{\tau_{max}} g(\tau)EC_{in}(t - \tau)\, d\tau + c \tag{5.7}$$

in which the offset c accounts for an increase in EC by the mineralization of groundwater.

We parameterized the travel-time *pdf* $g(\tau)$ by a lognormal *pdf* $LN(\tau; m, s)$, characterized by the mean m and standard deviation s. We assumed that the parameters of the travel-time *pdf* are time invariant, i.e. the travel-time *pdf* does not change over time. While discharge-related changes in travel time have been emphasized at other riverbank-filtration systems (Sharma et al., 2012), the assumption of a discharge-independent travel-time *pdf* seems to be reasonable at our field site. Previous studies at this site have shown that water level fluctuations in the river propagate into the aquifer quasi-instantaneously and that the change in head difference between the river and the groundwater is relatively small during flood events (Chapter 2, 3).

We estimated the mean m and the standard deviation s of the lognormal travel-time *pdf* at the observation well R050 by parametric deconvolution of the measured EC input and output signals in the river and the observation well, respectively. Deconvolution corresponds to the minimization of the following objective function L_{EC}:

$$L_{EC} = \int_{\tau_{max}}^{t_{max}} \left(EC_{out}(t) - \int_{0}^{\tau_{max}} LN(\tau; m, s)EC_{in}(t - \tau)\, d\tau + c \right)^{2} dt \tag{5.8}$$

All minimization problems described in this chapter were solved using the nonlinear least-square trust-region-reflective algorithm implemented as "lsqnonlin" function in MATLAB (Coleman and Li, 1996). To validate the resulting lognormal travel-time *pdf*, we additionally conducted a nonparametric deconvolution (Cirpka et al., 2007) of a 9-month long EC time series (April-December 2010). In contrast to parametric deconvolution, the nonparametric deconvolution does not assume a predefined shape of the travel-time *pdf*.

5.3.3 Discharge and temperature dependence of the DO consumption rate

To assess the dependence of the zero-order DO consumption rate k on river discharge (Section 5.2.2), we estimated k separately for seven periods of 10-20 d with different but relatively stable discharge conditions, by minimizing the following objective function L_{DO}:

$$L_{DO} = \int_{\tau_{max}}^{t_{max}} \left(DO_{out}(t) - \int_0^{\tau_{max}} g(\tau) \, max\big(0, DO_{in}(t-\tau) - k_{eff}(t-\tau) \cdot \tau\big) d\tau \right)^2 dt \quad (5.9)$$

with

$$k_{eff}(t-\tau) = f_T(t-\tau) \cdot k \quad\quad\quad (5.10)$$

in which the temperature factor f_T is given in Eq. (5.6) with parameters listed in Table 5.1 (Greskowiak et al., 2006).

Table 5.1. Comparison of different parameterizations of the temperature factor (Eq. (5.6)).

	Estimated	Literature
α [-]	-1.5	-1.5[a,b], -1.16[c], -3.43[d]
β [°C^{-1}]	0.19	0.18[a,b], 0.22[c], 0.19[d]
T_{opt} [°C]	26.3	35[a,b], 33.8[c], 36.9[d], 43±7[e]

[a]Greskowiak et al. (2006): used in this study, [b]Sharma et al. (2012), [c]O'Connell (1990), [d]Kirschbaum (1995), [e]Heitzer et al. (1991)

Based on the resulting consumption rates k of the seven periods at different discharges, we established a quantitative and empirical relationship $k(Q)$, see Section 5.4.3. This $k(Q)$ relationship was incorporated in the model formulation (Eqs. (5.4) and (5.5)) and the corresponding parameters were estimated by fitting the 9-month long DO time series (Eq. (5.9) combined with Eq. (5.5)).

To validate the parameterization of f_T (according to Eq. (5.6)) from Greskowiak et al. (2006), we estimated β and T_{opt} by fitting the DO time series of all the seven periods (Eq. (5.9) combined with Eq. (5.10)). The estimate for β was within the range of literature values, while the one for T_{opt} was unrealistically low (Table 5.1). The parameterization of Greskowiak et al. (2006) is in better agreement with other literature values. Furthermore, the estimated parameterization matched the one of Greskowiak et al. (2006) in the range of daily mean river temperatures covered by our data set (0-22°C, Fig. 5.4), which validates the parameterization

of Greskowiak et al. (2006) for our study. This parameterization has also been successfully applied by Sharma et al. (2012).
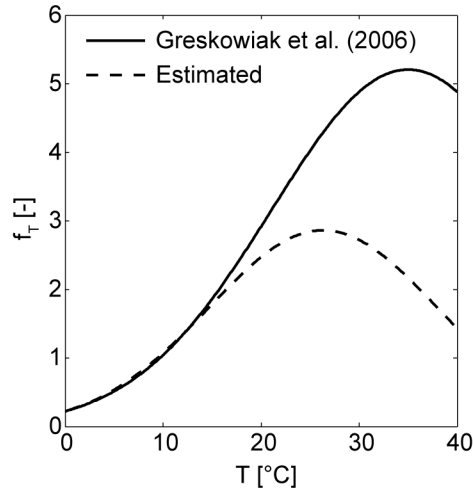

Fig. 5.4. Temperature factor (f_T) that accounts for the temperature dependence of the DO consumption rate (Eq. (5.6)). Solid line: parameterization of the temperature factor found by Greskowiak et al. (2006), which was adopted for this study. Dashed line: estimated temperature factor from our data.

5.4 Results and discussion

5.4.1 Description of measured data

The 9-month long river discharge time series covered a range of 5-450 m^3/s and was characterized by periods of low flow (<25 m^3/s) punctuated by flood events (Fig. 5.5a). The frequency of the floods was highest during December 2011 and January 2012. During snowmelt in March and April 2012, base flow was generally elevated to 40-50 m^3/s.

The DO concentrations in the river underwent strong diurnal fluctuations of up to 6 mg/L (Fig. 5.5b), resulting from the interplay of photosynthesis and respiration by periphyton (Reichert et al., 2009; Hayashi et al., 2012). The diurnal fluctuations revealed a repeated pattern of steadily increasing amplitude, truncated by floods. Complete reduction of diurnal fluctuations occurred after peak flows of >150 m^3/s, while partial reductions already occurred at discharges >30 m^3/s. These findings are consistent with those of Uehlinger (2006), who investigated the dynamics of gross primary production (GPP) in the Thur River and found that GPP reduction, resulting from periphyton removal from the riverbed, started at 30-50 m^3/s and was most significant during bed-moving floods (>150 m^3/s). Diurnal fluctuations were not present during December and January, partly due to the high frequency of flood events, and partly due to low temperatures and low solar radiation.
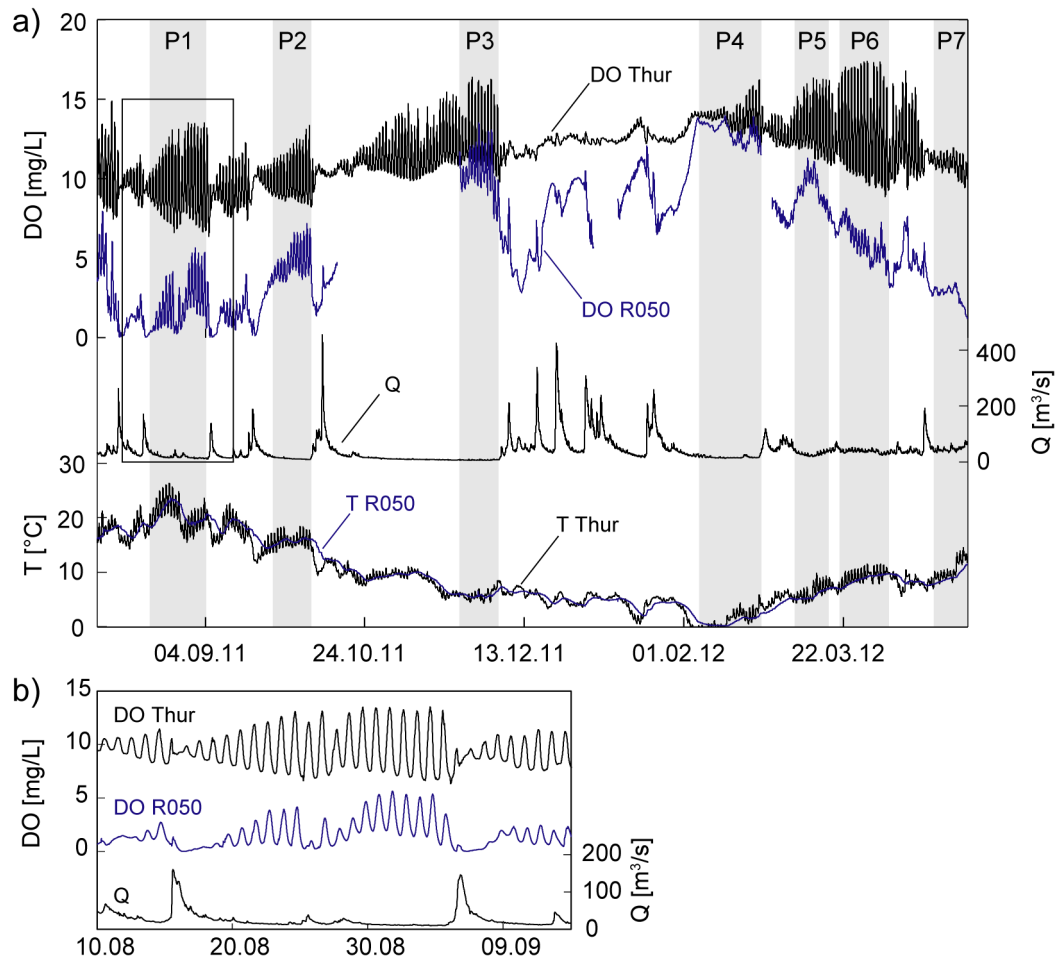
Fig. 5.5. (a) DO, discharge (Q) and temperature (T) time series in the Thur River and R050 during the 9-month long measurement period. The seven periods (P1-P7) used for the estimation of the consumption rates at different discharges are represented by gray bars. (b) Detailed plot of diurnal DO fluctuations in the river and in groundwater as a function of discharge for the 1-month long period delineated by the black rectangle in (a).

The diurnal DO fluctuations propagated from the river into the aquifer and could be resolved at the observation well R050 (Fig. 5.5b). As a result of the transport processes, the fluctuations were time shifted and had smaller amplitudes. The microbial degradation processes caused an overall decrease in DO concentrations. The DO consumption between the river and the observation well R050 showed a pronounced seasonal pattern, which reflects the temperature dependence of microbial POM degradation (Fig. 5.5a). During the temperature maximum in August 2011, groundwater DO concentrations varied between 0-4 mg/L. With decreasing temperatures in autumn and winter, the DO concentrations in groundwater increased up to nearly the level in the river itself, as observed during the temperature minimum in February 2012.

100

The seasonal pattern in groundwater DO concentrations was overlain by shorter-term variations that were related to river discharge (Fig. 5.5a, b). During flood events, the DO concentrations in groundwater dropped steeply and recovered again when river discharge declined. At first glance, this behavior is against intuition, as one would expect a breakthrough of higher DO concentrations during flood events due to higher infiltration velocities and shorter travel times. A similar pattern with decreasing DO concentrations at high discharges was observed in the riverbed of an upland stream in Scotland (Malcolm et al., 2006; Soulsby et al., 2009). However, at the Scotland site the drop in DO concentrations occurred after the peak flow and was explained by an upwelling of anoxic groundwater due to a reversal in the hydraulic gradient. This explanation does not apply to our field site, as losing conditions prevailed permanently. Furthermore, vertical DO profiles in the observation well R050 and adjacent wells did not reveal vertical differences in DO concentrations. This excludes that the observed drops in DO concentrations were caused by an uplift of older groundwater with lower DO concentrations during the rise of the groundwater table.

The conceptual explanation for the observed decrease in DO concentrations during high discharge is based on results from previous studies, as outlined in Section 5.2.2. First, suspended POM concentrations in rivers are known to be positively correlated with river discharge (Meybeck, 1982). Second, the POM import into gravelly riverbed sediments was found to occur mostly under high-discharge conditions (Naegeli et al., 1995; Brunke and Gonser, 1997). Finally, the increased POM availability in the riverbed allowed for faster POM degradation and faster DO consumption (Naegeli et al., 1995). Therefore, the observed dynamics in DO consumption (Fig. 5.5) illustrates the need of accounting for dependence of the DO consumption rate on both temperature and discharge in the model formulation.

5.4.2 Travel-time pdf

We estimated the parameters of the lognormal travel-time *pdf* by deconvolution of the diurnal EC fluctuations (Section 5.3.2, Eq. (5.8)) that occurred during the low-flow conditions of periods P1 and P3 (Fig. 5.5, Fig. 5.6). The mean m and the standard deviation s were estimated jointly for both periods, while the offset c was estimated separately. The resulting lognormal travel-time *pdf* at the observation well R050, shown in Fig. 5.7 (dashed line), is characterized by a mean of 0.4 d and a standard deviation of 0.3 d. The maximal travel time τ_{max} was set to 2 d, in order to obtain a recovery rate of at least 99%. The offset c amounted to 36 µS/cm for both periods. When applying the estimated lognormal travel-time *pdf*, the model simulations (Eq. (5.7)) well reproduced the measured EC time series with Nash-

Sutcliffe model efficiencies (Mayer and Butler, 1993) of 0.9 and 0.8 for periods P1 and P3, respectively (Fig. 5.6).
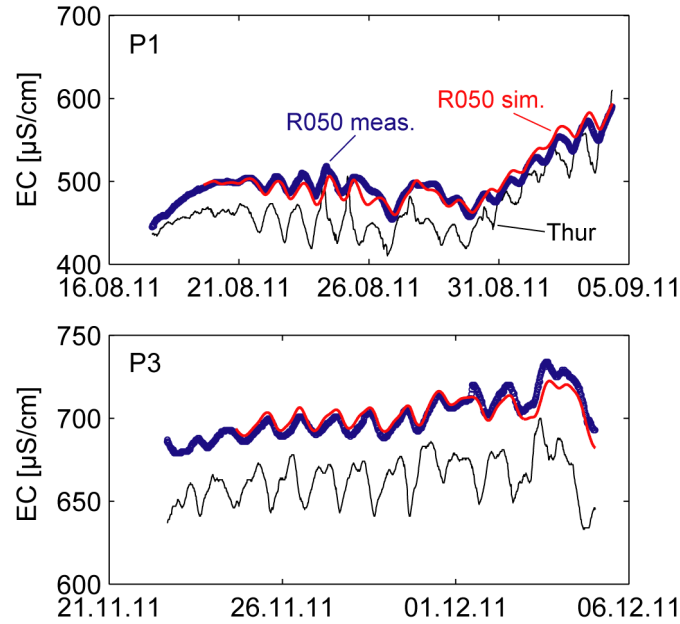

Fig. 5.6. Measured and simulated EC time series in groundwater at the observation well R050 for periods P1 and P3 (Fig. 5.5), using the estimated lognormal travel-time *pdf* (Fig. 5.7).

Fig. 5.7 additionally shows the statistical distribution of 1000 conditional realizations of the travel-time *pdf* resulting from nonparametric deconvolution of a 9-month long EC time series. Even though the 9-month long time series contained diurnal and event-driven EC fluctuations during low- and high-flow conditions, respectively, the nonparametric travel-time *pdf* did not show a shift to shorter travel times than the lognormal travel-time *pdf*; the modes were identical. This supports the use of a time-invariant travel-time *pdf* for our system, despite the strong discharge fluctuations. Furthermore, apart from the secondary peak, which may be an artifact caused by diurnal periodicity in EC time series (Vogt et al., 2010a), the lognormal travel-time *pdf* captured the main characteristics of the nonparametric travel-time *pdf*.
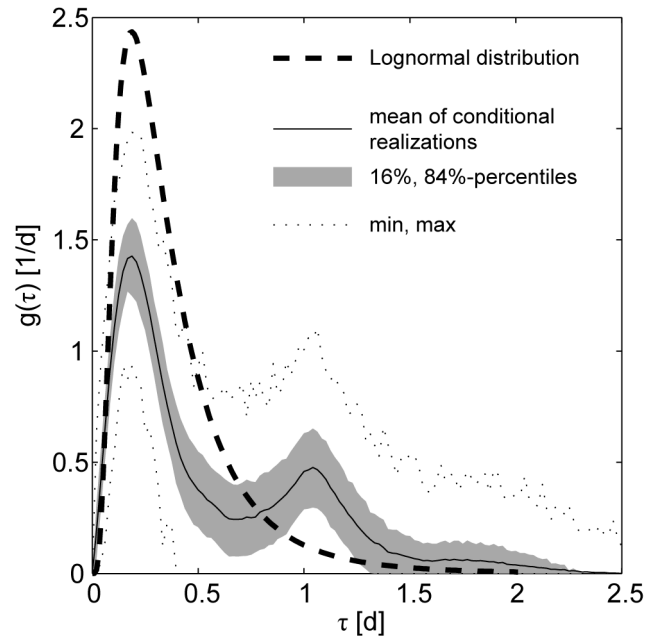
Fig. 5.7. Lognormal travel-time *pdf* at the observation well R050 (dashed line) resulting from deconvolution of the EC time series of periods P1 and P3 (Fig. 5.5, Fig. 5.6) according to Eq. (5.8). Additionally, the results from nonparametric deconvolution of a 9-month long EC time series are plotted. Solid line: mean of 1000 conditional realizations, gray area: 16 and 84 percentiles of the conditional statistical distributions, dotted lines: minimum and maximum values obtained in all realizations.

5.4.3   Quantifying the discharge dependence of the DO consumption rate

Fig. 5.8 plots the estimated zero-order DO consumption rates k (Section 5.3.3) for each of the seven separate periods against the corresponding mean discharge. These estimates of the DO consumption rates were compensated for the temperature dependence according to Eq. (5.10) and can be interpreted as effective DO consumption rates at a temperature of 10°C, at which the temperature factor f_T equals one (Fig. 5.4). The consumption rates remained on a level of 7-10 mg L^{-1} d^{-1} up to discharges of 20 m^3/s and steeply increased to 28 mg L^{-1} d^{-1} between 20 m^3/s and 50 m^3/s. These results confirm the dependence between the DO consumption rate and discharge, and suggest that discharge is a good proxy for the POM availability in the riverbed at our field site.
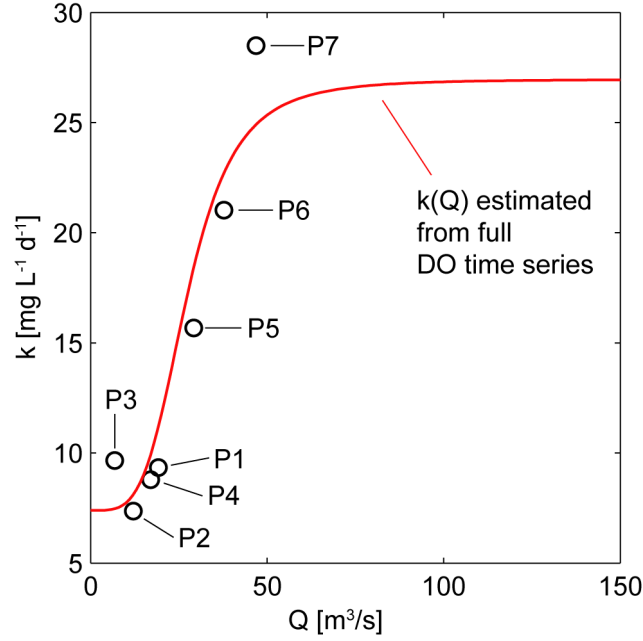
Fig. 5.8. Circles: estimated zero-order DO consumption rates k as a function of the mean discharge of each of the seven periods. Red line: estimated $k(Q)$ relationship (Eq. (5.14)) with parameters estimated by fitting the complete 9-month long DO time series (Table 5.2).

The DO consumption rates in Fig. 5.8 were estimated for separate periods of 10-20 d in length with different, but relatively stable discharge conditions (Fig. 5.5). An average estimation of the consumption rates for discharges >50 m^3/s was not feasible, as these discharges were related to flood events of short duration with fast changes in discharge. To estimate the consumption rate for a changing discharge within the full discharge spectrum, an empirical expression $k(Q)$ is required.

The concentration of suspended sediment and suspended POM in river water is usually described as a power function of river discharge (Meybeck, 1982; Hedges et al., 1986; Syvitski et al., 2000). If we assume that the POM import into the riverbed sediment is proportional to the POM concentration in the river, we may describe the discharge dependence of the substrate (POM) concentration S in the riverbed sediment by a power function as well:

$$S = aQ^b \tag{5.11}$$

The relation between the degradation rate and the substrate concentration $k(S)$ may be described by Michaelis-Menten kinetics:

$$k(S) = k_{max} \frac{S}{K_s + S} \tag{5.12}$$

104

in which k_{max} denotes the maximal degradation rate and K_s the half-saturation constant. Hence, even though the POM concentration (availability) in the riverbed might steadily increase with increasing discharge (Eq. (5.11)), we expect the DO consumption rates to level off at some point.

If we substitute Eq. (5.11) in Eq. (5.12) and reformulate the resulting equation, we can describe the discharge-dependent consumption rate by:

$$k(Q) = k_{max} \frac{Q^b}{K_Q^b + Q^b} \tag{5.13}$$

For an exponent $b > 1$, Eq. (5.13) describes an S-shaped curve, which increases from a level of zero for $Q \ll K_Q$ to a level of k_{max} for $Q \gg K_Q$. However, the estimated DO consumption rates (Fig. 5.8) indicate a level different from zero at low discharges (7-10 mg L^{-1} d^{-1}). We may address this by an offset at $Q = 0$, resulting in:

$$k\big(Q(t - \tau)\big) = C + A \left(\frac{Q(t - \tau)^b}{K_Q^b + Q(t - \tau)^b} \right) \tag{5.14}$$

in which C describes the minimum, and $C + A$ the maximum consumption rate, approached at $Q \gg K_Q$, respectively. The exponent b defines how fast the transition from C to $C + A$ occurs, and K_Q represents the discharge, at which the increase in k is the highest. As already stated in Section 5.2.2, it is assumed that the consumption rate depends on the discharge $Q(t - \tau)$ at the time of infiltration.

We incorporated the $k(Q)$ relationship of Eq. (5.14) in the model formulation (Section 5.3.3) and estimated the four parameters by fitting the 9-month long DO time series, which covered a discharge range of 5-450 m^3/s (Fig. 5.5). The resulting parameters are listed in Table 5.2 and the corresponding $k(Q)$ relationship is shown in Fig. 5.8. The resulting DO consumption rates remained at a level of 7 mg L^{-1} d^{-1} up to a discharge of 20 m^3/s, then increased steeply and leveled off at 27 mg L^{-1} d^{-1} at a discharge of 50 m^3/s.

The offset of 7 mg L^{-1} d^{-1} at low discharges may be explained by a consumption of POM that is either stored in the riverbed or imported from autochthonous sources. The steep increase in DO consumption rate above 20 m^3/s is probably related to an increased POM concentration in the river and the riverbed, partly due to the shearing off of periphyton (Section 5.4.1, Uehlinger (2006)). Even though the POM concentration (availability) in the river and the riverbed is likely to further increase at discharges >50 m^3/s (Eq. (5.11)), the DO consumption rate seems to be constrained by a microbial limitation (Eq. (5.12)).

Overall, the resulting $k(Q)$ relationship indicates that a discharge increase within the narrow window of 20-50 m^3/s enhances the consumption rate at our field site by a factor of about 4. It also shows that the effect of discharge on the DO consumption rate is already close to the maximum at a discharge of 50 m^3/s. The probability that the discharge Q at the Thur River exceeds 50 m^3/s is 30%. Typical situations are during snowmelt or short thunderstorms in the Thur catchment.

Table 5.2. Estimated parameters of the $k(Q)$ relationship (Eq. (5.14)) obtained by fitting the 9-month long DO time series (see Fig. 5.8).

	Estimated parameters
C [mg L^{-1} d^{-1}]	7.5
A [mg L^{-1} d^{-1}]	19.2
K_Q [m^3/s]	27.3
b [-]	4.3

The combination of the discharge dependence (Eq. (5.14), Fig. 5.8) with the temperature dependence (Eq. (5.6), Fig. 5.4) according to Eq. (5.5) allows the visualization of the effective DO consumption rate k_{eff} for a range of river temperatures and discharges (Fig. 5.9). Accordingly, the highest effective DO consumption rates at our field site occur at high temperatures and at discharges >50 m^3/s. The highest risk for the development of anoxic conditions in the infiltration zone of a riverbank-filtration system is usually anticipated for conditions of high river temperatures and low river discharges (Sprenger et al., 2011), assuming that low river discharges increase groundwater residence times. At our site, however, river discharge hardly affects groundwater residence times. Therefore, we anticipate the highest risk for the development of anoxic conditions in the infiltration zone at our site during summer heat waves combined with elevated discharges >50 m^3/s.
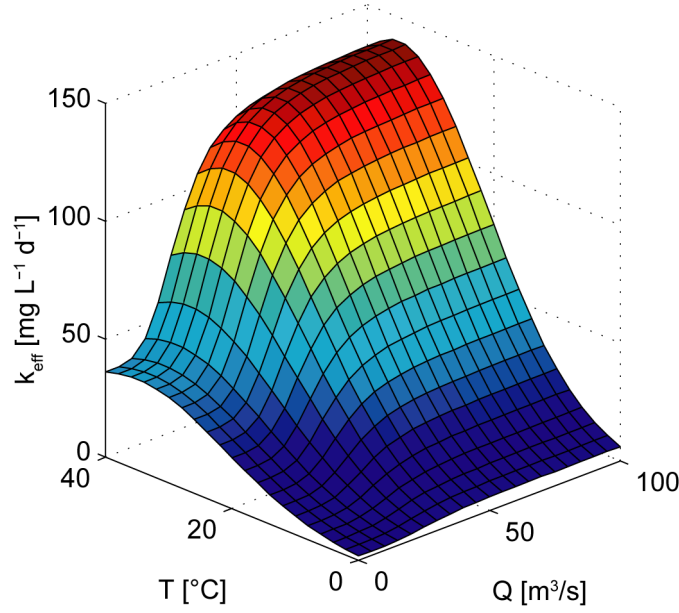
Fig. 5.9. Effective DO consumption rate k_{eff} (Eq. (5.5)) for a range of temperature and discharge conditions using the estimated parameter set for $k(Q)$ (Eq. (5.14), Table 5.2) and the literature-based parameter set for f_T (Eq. (5.6), Table 5.1).

5.4.4   Simulation of DO concentrations in groundwater

We applied the literature-based temperature dependence (Eq. (5.6), Fig. 5.4) and the estimated discharge dependence (Eq. (5.14), Fig. 5.8) of the effective DO consumption rate to simulate the 9-month long groundwater DO time series according to Eqs. (5.4) and (5.5). The simulated DO concentrations at the observation well R050 are plotted in Fig. 5.10 together with the measured DO concentrations at R050 and those measured in the Thur River. We additionally plotted the discharge time series, the discharge-dependent DO consumption rate $k(Q)$, the river temperature time series and the effective DO consumption rate $k_{eff}(Q,T)$.

The seasonal temperature variations led to a seasonal variation of the effective DO consumption rate k_{eff} that translated into a seasonal pattern in the simulated DO concentrations. The seasonal trend in k_{eff} was overlain by the effect of discharge. An increase in discharge above 20 m³/s caused a fast increase in k_{eff} and an associated drop in the simulated groundwater DO concentrations. The $k(Q)$ time series illustrates the fast increase of the consumption rate at increasing discharges, the truncation at a maximum of 27 mg L⁻¹ d⁻¹ above 50 m³/s, and the decrease during the recession of the flood event. The impact of discharge variations on k_{eff} was not only restricted to short periods of a few days. During the flood events in December 2011/January 2012 and during the snowmelt period in March/April 2012, discharge was above 40-50 m³/s during several weeks, which caused a persistent increase in k_{eff}.
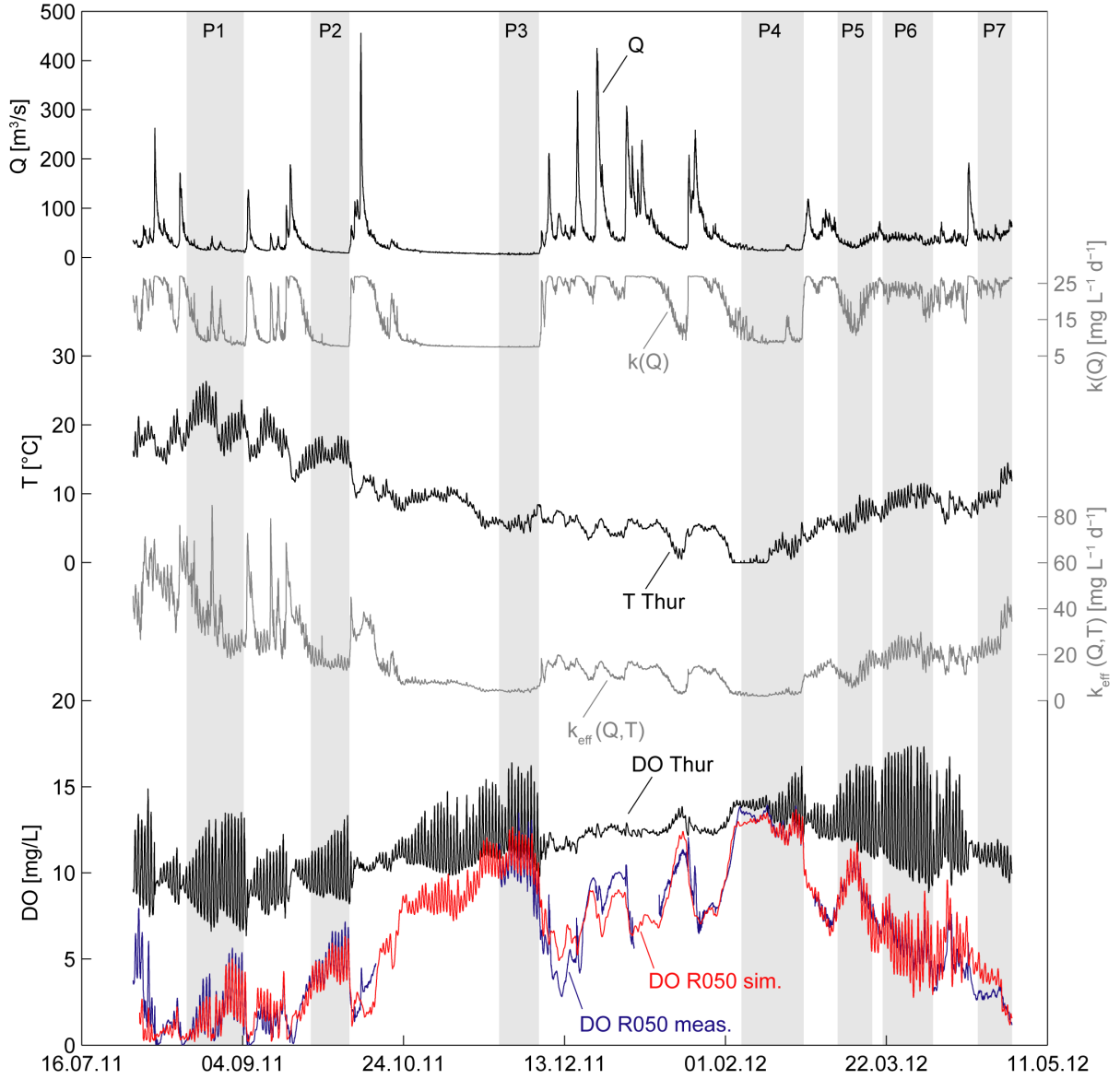
Fig. 5.10. Measured and simulated DO concentrations in groundwater at the observation well R050. The simulations were performed using the estimated parameter set for $k(Q)$ (Table 5.2) and the literature-based parameter set for f_T (Table 5.1). The figure additionally shows the time series of discharge (Q), the discharge-dependent DO consumption rate ($k(Q)$), the temperature (T) in the Thur River and the effective DO consumption rate ($k_{eff}(Q,T)$). The periods P1-P7, which are enlarged in Fig. 5.11, are delineated by gray bars.

The comparison of the simulated and the measured groundwater DO time series revealed a very good model performance, with a Nash-Sutcliffe model efficiency of 0.94. By accounting for both the temperature dependence and the discharge dependence of the DO consumption rate, the model captured the full dynamics in DO consumption during riverbank filtration on different temporal scales. The simulated groundwater DO concentrations tightly followed the measured DO concentrations across the complete temperature range (0-22°C) and the complete discharge range (5-450 m^3/s). The good model performance also validates the

proposed expression for the empirical $k(Q)$ relationship (Eq. (5.14)) and supports the underlying concept of using discharge as a proxy for the POM availability.

Fig. 5.11 shows the simulation results of the periods P1-P7 to assess the model performance on a daily to sub-daily time scale. For the periods P1-P4, the model successfully reproduced the DO time series in groundwater with respect to both the daily mean DO concentrations and the phase and amplitude of the diurnal fluctuations. The model also captured the depressions in groundwater DO concentrations during P1, which were related to two minor discharge events during this period (Fig. 5.10).

Besides an initial overestimation in P7, the model reasonably reproduced the daily mean DO concentrations in periods P5-P7 (March/April 2012). However, the amplitudes of the diurnal groundwater DO fluctuations were overestimated, especially in P6. This overestimation might be attributed to a bias in the input DO concentrations in the river, which were measured in Andelfingen, 10 km downstream of our field site (Section 5.3.1). While we demonstrated that the river DO concentrations in Andelfingen were representative for those at our field site during low-flow conditions (Section 5.3.1, Fig. 5.3), this may not be the case during long-lasting elevated discharges of 40-50 m^3/s that prevailed during the snowmelt period in March/April 2012.

The effective DO consumption rates k_{eff} ranged from 2 mg L^{-1} d^{-1} under low-flow conditions during winter temperatures (February, P4, Fig. 5.10) to 85 mg L^{-1} d^{-1} during a minor discharge event of 43 m^3/s at high summer temperatures (August, P1, Fig. 5.10). This range is within the spectrum of typical DO consumption rates of 0.05-96 mg L^{-1} d^{-1} (Matsunaga et al., 1993; Sharma et al., 2012). The seasonal temperature variations caused changes in k_{eff} by a factor of 10, while variations in the discharge caused changes by a factor of 4. On the seasonal time scale, the temperature-related changes in k_{eff} were therefore more important and accounted for 70% of the overall variability in k_{eff}. However, on the time scale of days to weeks, discharge-related changes in k_{eff} dominated its variability.
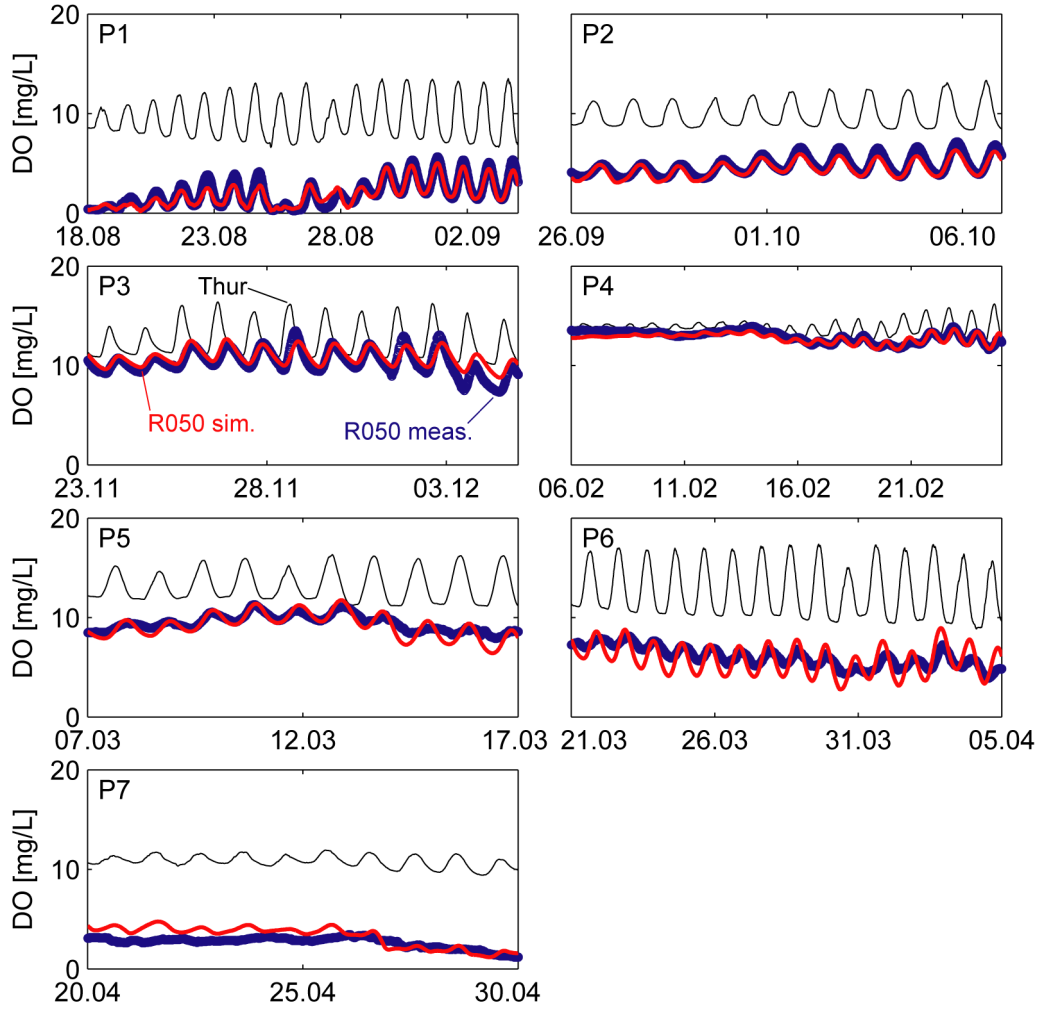
Fig. 5.11. Measured and simulated DO concentration time series in groundwater at the observation well R050 for the seven periods P1-P7 (Fig. 5.10).

5.4.5   Transferability of the model approach to other sites

The modeling approach proposed in this chapter may be applicable in other riverbank-filtration systems. Three main elements are required: The travel-time *pdf*, the temperature dependence, and the discharge dependence of the effective zero-order DO consumption rate. Once these elements are obtained, the model (Eqs. (5.4) and (5.5)) can be used to efficiently predict DO concentrations in groundwater from those measured in the river under various temperature and discharge conditions.

The travel-time *pdf* at an observation well may be obtained by deconvolution of a conservative signal, e.g. an EC or chloride time series measured in the river and the observation well. In this study, we have used a parametric deconvolution assuming a lognormal travel-time *pdf* (Section 5.3.2), but other parametric models such as the gamma distribution may be more appropriate at other sites. For our system, the assumption of a time-invariant travel-time *pdf* has shown to be reasonable despite very dynamic discharge

fluctuations (Section 5.4.2). At other riverbank-filtration systems however, the travel-time *pdf* might change as a function of discharge, which also affects predicted DO concentrations. A definition of a lognormal travel-time *pdf* with discharge-dependent parameters (m, s) is possible, but not straightforward.

To account for the temperature dependence of the effective DO consumption rate according to Eq. (5.5), we suggest to use the formulation of the temperature factor f_T proposed by O'Connell (1990) and the corresponding parameter values found by Greskowiak et al. (2006). This parameterization has been successfully applied in a previous modeling study and has been validated in the present study (Section 5.3.3).

The presented relationship between discharge and the DO consumption rate $k(Q)$ (Eq. (5.14)) is based on the concept of using discharge as a proxy for the POM availability in the riverbed. However, this concept will probably not be generally applicable, as the dynamics in the POM availability in the riverbed also depends on factors such as the catchment characteristics, the discharge regime and the grain-size distribution of the riverbed sediments (Naegeli et al., 1995; Brunke and Gonser, 1997; Pusch et al., 1998). Therefore, the inclusion of a discharge-dependent consumption rate $k(Q)$ in the functional form of Eq. (5.5) may not be adequate for all riverbank-filtration systems. We suppose that an increase in the POM availability and hence in the DO consumption rate with increasing discharge only occurs at riverbank-filtration systems with a gravelly riverbed. In coarse-sediment rivers, the import of POM to deeper layers is possible, while in sand-bottomed or clogged rivers, the import of POM is physically prevented (Brunke and Gonser, 1997).

The four parameters of the $k(Q)$ relationship according to Eq. (5.14) are site specific and need to be estimated by fitting measured DO time series in the river and in the observation well (Section 5.3.3). The parameterization obtained for our field site (Table 5.2) might only be applicable to riverbank filtration within the Thur Valley, which extends 30 km upstream from our field site (Fig. 5.2).

5.5 Conclusions

We have presented a new semi-analytical model to simulate the dynamics of dissolved oxygen (DO) consumption during riverbank filtration. The model implementation is fast and simple and model run times are short compared to spatially explicit numerical reactive transport models. Hence, the modeling approach provides an efficient tool to estimate DO

concentrations in groundwater from those measured in the river under various climatic and hydrologic conditions.

We have developed and implemented the model at a field site in northeastern Switzerland at the peri-alpine Thur River on the basis of a 9-month long high-resolution DO time series measured in the river and adjacent groundwater. The model successfully reproduced the seasonal, short-term (days to weeks) and diurnal variations in groundwater DO concentrations by considering the measured DO concentrations in the river and accounting for both the temperature and the discharge dependence of the zero-order DO consumption rate.

The good model performance validates the proposed empirical expression that quantifies the relationship between discharge and the DO consumption rate ($k(Q)$ relationship) and supports the underlying conceptual model. According to this conceptual model, high-discharge conditions increase the suspended POM concentration in the river. During river infiltration, POM is retained in the riverbed sediments within the first meters of infiltration. The higher POM import during high-discharge conditions increases the POM availability in the riverbed sediments, which allows for a faster POM degradation and a faster DO consumption within microbial biofilms. The estimated parameterization of the $k(Q)$ relationship from our data set revealed a steep increase of the DO consumption rates between 20-50 m^3/s and a leveling off beyond. As the POM availability in the riverbed is likely to further increase at discharges >50 m^3/s, the observed saturation may reflect the maximal DO consumption rate for the existing microbial community in the riverbed sediments.

High-discharge conditions can also reduce the residence time of infiltrated river water, which counteracts the effect of an increased POM availability on observed groundwater DO concentrations. At our field site, however, river discharge hardly affected groundwater residence times and therefore, the effect of a discharge-dependent DO consumption rate dominated the observed DO concentration dynamics in groundwater during high-discharge conditions.

Our results revealed that the combination of high river temperatures and elevated discharges of >50 m^3/s maximize the DO consumption rate and hence, the risk of anoxic conditions at our field site. Anoxic conditions at riverbank-filtration systems are of concern because of the appearance of undesired species as nitrite and dissolved Fe(II) and Mn(II). Furthermore, the redox state of the infiltration zone is decisive for the degradation of emerging micropollutants. Summer heat waves are expected to occur more frequently and more intensively in future due to climate change, increasing the risk of anoxic conditions in the infiltration zone. Our

modeling approach can contribute to a better assessment of this risk at individual riverbank-filtration systems and potentially reduces expensive long-term monitoring of groundwater DO concentrations.

Acknowledgments

Chapter 6

Conclusions and Outlook

6.1   Conclusions

The main objectives of this Ph.D. Thesis were to improve the understanding of physical and biogeochemical processes that occur during riverbank filtration, and the factors controlling them, by combining laboratory and field investigations as well as groundwater flow and reactive transport modeling. Moreover, this work aimed at developing tools that facilitate the model-based assessment of potential impacts of river restoration and climate change on river-recharged groundwater quality.

In the framework of river restoration, reductions in groundwater residence times as a result of riverbed widening and higher riverbed permeability may lead to a breakthrough of pathogenic bacteria or pollutants at the pumping well. To anticipate the effect of river restoration measures on residence times, a thorough understanding of the groundwater flow paths and flow velocities is indispensable. While methods based on the analysis of natural tracers provide direct estimates of the residence time, a calibrated numerical groundwater flow and transport model quantitatively links groundwater flow paths, flow velocities and residence times.

The surface water level distribution is an important prerequisite for modeling river-groundwater systems. In this thesis, two alternative interpolation methods were developed that are simpler and faster in their implementation compared to a hydraulic model, while still being able to account for typical hydromorphological features of dynamic (restored or natural) river sections, such as nonlinear longitudinal water level distributions, lateral water level gradients, disconnected river branches and hydraulic jumps. Both interpolation methods allow the definition of time-varying 1D or 2D surface water level distributions by combining continuous water level records at gauging stations with periodic water level measurements at fixpoints in between. The RM method applies a polynomial regression approach for the prediction of water levels at fixpoints as a function of the corresponding water levels at the determining gauging station, while the IM method uses a nonlinear interpolation approach between two gauging stations. Compared to a third reference method (RH), which is based on water level data from a 2D hydraulic model, the alternative methods proved to be accurate with respect to their water level predictions. The RM method benefits from the

straightforward implementation, but was found to provide reliable water level predictions only within the range of measurements made at the fixpoints. For the simulation of discharge conditions beyond the measured range, the use of the IM method is recommended instead.

To assess the impact of the method selection and the considered level of detail in the surface water level distribution on the simulated groundwater residence time, a 3D groundwater flow and transport model of the partly restored Niederneunforn field site was developed. Steady-state surface water level distributions were generated with both alternative methods (RM, IM) and the reference method (RH), as well as with two simplified versions of the IM method, and were assigned to the 1D side channel ($1^{st}/3^{rd}$ Type) and the 2D river (3rd Type) boundary conditions of the model. Model calibration against measured groundwater heads was performed for each of these model scenarios by an automated adjustment of selected transfer rates (conductance of colmation layer). Based on the calibration-constrained groundwater flow fields, groundwater age (groundwater residence time) was simulated according to the method of Goode (1996). This method is very convenient, as it provides a spatial distribution of groundwater age and accounts for advective and dispersive "age fluxes". Goode's method was successfully applied in this thesis and its application to other riverbank-filtration systems is recommended when simulating groundwater residence times.

To initially obtain a realistic groundwater residence time distribution at the field site, the transfer rates and the hydraulic conductivity distribution were jointly estimated by fitting both, measured groundwater heads and experimentally determined residence times from nonparametric deconvolution of EC time series. This procedure is highly recommended, as calibration against groundwater heads alone provides non-unique information on flow velocities and residence times.

The age predictions of the calibration-constrained groundwater flow fields using both alternative methods lay within a range of 30% compared to the reference RH model scenario. This error is small compared to the uncertainty of experimentally determined residence times of 60-80%, which confirms the predictive capability of the alternative methods when applied to real and complex river-groundwater systems. The simplification of the river water level distribution by neglecting lateral water level differences of 20-30 cm in the central part of the river caused moderate errors in groundwater age prediction of 40-80%. The additional simplification by assuming a linear longitudinal river water level distribution led to deviations in water levels of up to 50 cm and induced widespread errors in groundwater age of 200-500%.

Even though these specific errors in groundwater age prediction only apply to our field site, they emphasize the importance of an accurate (especially longitudinal) surface water level distribution for a reliable simulation of the groundwater flow field and groundwater residence times. To this end, the application of both alternative interpolation methods presented herein can be recommended, and may help to reliably assess the impact of river restoration measures on groundwater residence times and hence, to mitigate the conflict of interest between river restoration and drinking water protection.

In the context of climate change, the development of anoxic conditions in the infiltration zone of riverbank-filtration systems is of concern due to the mobilization of nitrite and especially Mn(II) and Fe(II), which would require additional treatment of the abstracted water. Climate models predict an increased frequency and intensity of summer heat waves, characterized by long-lasting periods of low discharges and high temperatures, which likely increase the risk for riverbank-filtration systems to become anoxic or even Mn(IV)- or Fe(III)-reducing. In this thesis, periodic and targeted (summer and winter) field sampling campaigns and column experiments simulating the field conditions were performed to improve the understanding of the dependence of dissolved oxygen (DO) and dissolved organic matter (DOM) consumption during riverbank filtration on the climate-related variables temperature and discharge.

The column experiments consistently reproduced the observations of the summer and winter field sampling campaigns. In both systems, DO consumption was found to strongly depend on temperature, while DOM consumption was essentially the same under summer and winter conditions. In summer, DOM consumption only explained 10-20% of DO consumption. The remaining 80-90% of the reduction capacity to explain the DO consumption is likely provided by particulate organic matter (POM) associated with the riverbed sediments.

These findings were confirmed by the results of 45 periodic field samplings that covered a wide temperature and discharge range over a period of five years. DO consumption was highly correlated with temperature, while the DOM consumption did not reveal a significant temperature dependence. Therefore, the variability and temperature dependence of DO consumption seemed to be explained by POM degradation to a large extent. The divergence between the temperature dependencies observed for DO and DOM consumption also have the consequence that POM is the most important electron donor under summer conditions. The importance of POM degradation for explaining the seasonal variability of the DO consumption during riverbank filtration has also been described in previous studies and presumably applies to most riverbank-filtration systems.

The periodic samplings also allowed for assessing the effect of discharge conditions on DO and DOM consumption. The general concept that low-flow conditions enhance DO and DOM consumption as a result of increased groundwater residence times and higher loads of DOM in the river due to less dilution of wastewater effluent is not supported by the results of this thesis. DO consumption increased rather than decreased with increasing discharge and DOM consumption did not reveal any significant correlation with discharge. It is hypothesized that the increased DO consumption at higher discharges is related to an increased import of POM into the riverbed. Furthermore, the DOC concentrations in the river increased rather than decreased with discharge, suggesting DOM sources other than wastewater treatment plants.

During summer conditions (T>20°C), groundwater DO concentrations at the field site were close to zero, but denitrification was not observed. Similarly, most peri-alpine aquifers fed by rivers are (sub)oxic under today's summer conditions. Therefore, currently there is no need to implement additional water treatment steps such as demanganation and deferisation. However, a substantial increase in river water temperature during future heat waves will enhance the POM turnover, leading to a complete consumption of DO and potentially nitrate. As a consequence, nitrite and possibly Mn(II) and Fe(II) could be released. In order to take adequate measures in time, the long-term monitoring of DO and other redox parameters in groundwater is recommended.

However, while continuous monitoring of DO concentrations is routinely performed in rivers by environmental agencies, the monitoring of DO concentrations in groundwater is often restricted to sampling on a monthly or even yearly basis. In this thesis, a new semi-analytical model was developed that allows efficiently estimating DO concentrations in river-fed groundwater from measured DO concentrations in the river under various temperature and discharge conditions on a weekly, daily or even sub-daily time scale.

The model is based on the stochastic-convective reactive approach. The transport system between the river and a groundwater observation well is conceptualized as ensemble of convective-reactive streamlines, whose travel times are assumed to be lognormally distributed and time invariant. The lognormal travel time probability-density function *(pdf)* for a selected observation well was obtained from parametric deconvolution of diurnal EC fluctuations measured in the Thur River and the observation well. For the Niederneunforn field site, the assumption of a time-invariant travel-time *pdf* has shown to be reasonable despite very dynamic discharge fluctuations. At other riverbank-filtration systems however, extending the model by a non-stationary formulation of the travel-time *pdf* might be required.

DO consumption during riverbank filtration is simulated by zero-order kinetics and the consumption rate depends on river temperature and discharge. The temperature dependence of aerobic respiration is well known. A literature-based expression was adopted and the corresponding parameters were successfully validated for the Niederneunforn field site. The same parameterization has also been validated in a previous modeling study at a different site (Sharma et al., 2012) and is presumably applicable to account for the temperature dependence of aerobic respiration at most riverbank-filtration systems.

The discharge dependence of the DO consumption rate is probably related to an increased trapping of POM within the riverbed during high-discharge events, thus enhancing the POM availability and DO consumption rate. An empirical equation that quantifies the discharge dependence was proposed ($k(Q)$ relationship). The inferred parameterization from high-resolution DO time series measured in the river and the observation well suggests an increase of the DO consumption rate by a factor of 4 within the narrow window of 20-50 m^3/s and a leveling off beyond. This finding agrees well with the observations of the periodic samplings; DO consumption increased up to a discharge of 60 m^3/s and leveled off beyond. Therefore, the highest risk for the development of anoxic conditions in the infiltration zone at the Niederneunforn field site is anticipated during summer heat waves combined with elevated discharges >50 m^3/s. Such discharges typically result from short thunderstorms in the Thur catchment.

By considering the measured DO concentrations in the river and accounting for both the temperature and the discharge dependence of the zero-order DO consumption rate, the model successfully reproduced the seasonal, short-term (days to weeks) and diurnal variations in groundwater DO concentrations with a Nash-Sutcliffe model efficiency of 0.94. The good model performance validates the proposed $k(Q)$ relationship and the underlying concept of using discharge as a proxy for the POM availability in the riverbed. However, this concept is probably not generally applicable and the inclusion of a discharge-dependent DO consumption rate in the model formulation might only be adequate for riverbank-filtration systems with a gravelly riverbed and within a catchment without retention basins (e.g. a lake). Rivers in catchments without retention basins typically have a dynamic discharge regime with strong, rapid and frequent discharge fluctuations, which favors the mobilization of POM. In gravelly riverbeds, the import of POM during high-discharge conditions is possible to deeper layers, while in sandy or clogged riverbeds, the import of POM might be physically hindered.

The presented modeling approach can be transferred to other riverbank-filtration systems. The literature-based temperature dependence of the DO consumption rate seems to be generally applicable and may be directly adopted in future model applications. On the other hand, the travel-time *pdf* and the discharge dependence of the DO consumption rate are site specific and need to be estimated case by case. Once these elements are obtained, the model can be used to efficiently estimate groundwater DO concentrations at riverbank-filtration systems under various climatic and hydrologic conditions and, hence, assess the risk of approaching anoxic conditions in a changing climate.

6.2 Outlook

The effectiveness of riverbank filtration depends on the interplay of physical and biogeochemical processes, both being subject to three-dimensional heterogeneity and temporal variability. This Ph.D. Thesis is one step towards a better understanding of these processes and their dependencies, and provides methods and models that may facilitate the characterization and risk assessment of riverbank-filtration systems within the context of a changing and challenging environment. However, the investigations and conclusions of this Ph.D. Thesis led to more questions and the developed tools may require further refinement and validation. Potential research questions and recommendations that may be applicable to future research projects are outlined below.

River restoration. The effect of river restoration measures on river-fed groundwater quality is not well understood yet. For instance, higher riverbed permeability is likely to reduce the residence time within the riverbed, which may lower the retention capacity for bacteria and pollutants. Conversely, an increased hyporheic exchange is considered to promote interstitial microbial activity, which in turn enhances the removal of organic matter and pollutants. Furthermore, the higher infiltration rate and the higher oxygen flux may help to maintain oxic conditions in the infiltration zone, thus being favorable for river-recharged groundwater quality as well. What is the relative importance of these contrasting effects? Does the enhanced microbial activity compensate or even dominate the shorter residence times with respect to the removal efficiency? Answering these questions would help to further mitigate the conflict of interest between river restoration and drinking water protection. Thereto, research projects that investigate hydraulic, microbiologic and biogeochemical aspects of river-groundwater systems before and after river restoration are highly recommended.

POM. In this thesis, the importance of POM as an electron donor under summer conditions is emphasized (Chapter 4). It has been shown that POM accounted for most DO consumption

under summer conditions and hence, will probably play an important role in the development of anoxic or even Mn(IV)-/Fe(III)-reducing conditions in a changing climate. Furthermore, DO consumption was found to increase with increasing discharge, which was attributed to an enhanced import of POM into the riverbed. The importance of POM as electron donor has been recognized in previous studies, but the factors controlling POM dynamics in riverbed sediments are highly variable and not well understood yet (Naegeli et al., 1995; Brunke and Gonser, 1997). Hence, it might be worthwhile to further investigate the source, composition and bioavailability of POM in river systems, as well as its retention, storage and consumption within the riverbed. A better assessment of the POM dynamics in riverbed sediments is a complex task due to the riverbed heterogeneity and variability, but may help to identify potential intervention strategies that allow reducing the POM availability and hence, the risk of anoxic and Mn(IV)-/Fe(III)-reducing conditions during future heat waves.

Further model application and validation. The presented alternative interpolation methods (Chapter 2) and the developed stochastic-convective reactive modeling approach (Chapter 5) were successfully – but exclusively – applied at the Niederneunforn field site. Using these tools at other riverbank-filtration systems would help to validate their applicability and versatility.

Interpolation methods. In this thesis, the application of the interpolation methods for simulating groundwater flow and transport at the field site was restricted to steady state (Chapter 3). However, the new interpolation methods are capable of generating time-varying 1D and 2D surface water level distributions (Chapter 2) and may be used for transient model simulations to assess the impact of water level fluctuations on key predictions at riverbank-filtration systems such as groundwater flow paths, flow velocities and residence times. In this context, it might be crucial to consider not only the change in water levels, but also in the lateral extent of the river. In their current implementation, the interpolation methods assume a constant river extent. Nevertheless, depending on the groundwater modeling code, accounting for a changing river width with changing river water levels is possible (e.g. in FEFLOW using the Interface Manager), but may require a considerable amount of work.

Non-stationary formulation of travel-time pdf. The current implementation of the stochastic-convective reactive model (Chapter 5) assumes a time-invariant travel-time *pdf*, implying that discharge does not affect groundwater residence times. While this assumption has shown to be reasonable at the Niederneunforn field site, other studies demonstrated a significant effect of discharge fluctuations on groundwater residence times (Sharma et al., 2012). To maximize

the applicability of the modeling approach, the inclusion of a non-stationary travel-time *pdf* in the model formulation is recommended. Relating the parameters of travel-time *pdfs* (e.g. the mean and the standard deviation of the lognormal distribution) to discharge is possible, but not straightforward and will require considerable effort.

Climate change scenarios. The stochastic-convective reactive modeling approach incorporates a quantitative description of DO consumption during riverbank filtration as a function of the climate-related variables temperature and discharge, and has the particular strength of very short model run times. Therefore, the modeling approach is well suited for long-term simulations of groundwater DO concentrations in river-recharged groundwater. Swiss climate models provide projections of temperature and precipitation for 30-year periods centered around 2035, 2060 and 2085 with a daily resolution, which can be transferred to a specific site either by the delta change method or statistical downscaling (CH2011, 2011). These climate projections – at least for temperature – can readily be applied as input to the stochastic-convective model, which would provide valuable information on the frequency and intensity (duration) of anoxic conditions at riverbank-filtration systems. However, it is recommended to extend the model formulation in order to include both DO and nitrate consumption during riverbank filtration. The inclusion of nitrate as a second electron acceptor in the model can be achieved with a minor programming effort and would allow for quantitatively determining the risk of Mn(IV)-/Fe(III)-reducing conditions in the infiltration zone of riverbank-filtration systems.

Bibliography

Akamatsu, F., Kobayashi, S., Amano, K., Nakanishi, S., Oshima, Y., 2011. Longitudinal and seasonal changes in the origin and quality of transported particulate organic matter along a gravel-bed river. Hydrobiologia 669 (1), 183-197.

Anderson, M.P., 2005. Heat as a ground water tracer. Ground Water 43 (6), 951-968.

Baumann, M., Jordan, P., Hoehn, E., Geisser, H., 2009. Ein neues Grundwassermodell für das Thurtal. Band 63 der Mitteilungen der Thurgauischen Naturforschenden Gesellschaft. Thurgauische Naturforschende Gesellschaft, Frauenfeld, 240 pp.

Besemer, K., Luef, B., Preiner, S., Eichberger, B., Agis, M., Peduzzi, P., 2009. Sources and composition of organic matter for bacterial growth in a large European river floodplain system (Danube, Austria). Org. Geochem. 40 (3), 321-331.

Biggs, B.J.F., Close, M.E., 1989. Periphyton biomass dynamics in gravel bed rivers: the relative effects of flows and nutrients. Freshwater Biol. 22 (2), 209-231.

Boulton, A.J., 2007. Hyporheic rehabilitation in rivers: restoring vertical connectivity. Freshwater Biol. 52 (4), 632-650.

Bourg, A.C.M., Bertin, C., 1993. Biogeochemical Processes during the infiltration of River Water into an Alluvial Aquifer. Environ. Sci. Technol. 27 (4), 661-666.

Bretschko, G., Moser, H., 1993. Transport and retention of matter in riparian ecotones. Hydrobiologia 251 (1-3), 95-101.

Brugger, A., Reitner, B., Kolar, I., Queric, N., Herndl, G.J., 2001a. Seasonal and spatial distribution of dissolved and particulate organic carbon and bacteria in the bank of an impounding reservoir on the Enns River, Austria. Freshwater Biol. 46 (8), 997-1016.

Brugger, A., Wett, B., Kolar, I., Reitner, B., Herndl, G.J., 2001b. Immobilization and bacterial utilization of dissolved organic carbon entering the riparian zone of the alpine Enns River, Austria. Aquat. Microb. Ecol. 24 (2), 129-142.

Brunke, M., 1999. Colmation and depth filtration within streambeds: Retention of particles in hyporheic interstices. Int. Rev. Hydrobiol. 84 (2), 99-117.

Brunke, M., Gonser, T., 1997. The ecological significance of exchange processes between rivers and groundwater. Freshwater Biol. 37 (1), 1-33.

Brunner, P., Cook, P.G., Simmons, C.T., 2009. Hydrogeologic controls on disconnection between surface water and groundwater. Water Resour. Res. 45, 13.

BUWAL, 2004. Groundwater protection guide. Bundesamt für Umwelt, Wald und Landschaft, Bern, pp. 141.

Cardenas, M.B., 2009. Stream-aquifer interactions and hyporheic exchange in gaining and losing sinuous streams. Water Resour. Res. 45, 1-13.

Cardenas, M.B., Wilson, J.L., Zlotnik, V.A., 2004. Impact of heterogeneity, bed forms, and stream curvature on subchannel hyporheic exchange. Water Resour. Res. 40 (8), 1-13.

CH2011, 2011. Swiss Climate Change Scenarios CH2011. C2SM, MeteoSwiss, ETH, NCCR Climate and OcCC, Zurich, pp. 88.

Cirpka, O.A., Fienen, M.N., Hofer, M., Hoehn, E., Tessarini, A., Kipfer, R., Kitanidis, P.K., 2007. Analyzing bank filtration by deconvoluting time series of electric conductivity. Ground Water 45 (3), 318-328.

Coleman, T.F., Li, Y., 1996. An Interior, Trust Region Approach for Nonlinear Minimization Subject to Bounds. SIAM J. Optimiz. 6, 418-445.

Derx, J., Blaschke, A.P., Blöschl, G., 2010. Three-dimensional flow patterns at the river-aquifer interface -- a case study at the Danube. Adv. Water Resour. 33 (11), 1375-1387.

Diem, S., Vogt, T., Hoehn, E., 2010. Spatial characterization of hydraulic conductivity in alluvial gravel-and-sand aquifers: a comparison of methods. Grundwasser 15 (4), 241-251.

Doetsch, J., Linde, N., Vogt, T., Binley, A., Green, A.G., 2012. Imaging and quantifying salt-tracer transport in a riparian groundwater system by means of 3D ERT monitoring. Geophysics 77 (5), B207-B218.

Doherty, J., 2005. Pest. Model-independant parameter estimation. Watermark Numerical Computing.

Doppler, T., Franssen, H.J.H., Kaiser, H.P., Kuhlman, U., Stauffer, F., 2007. Field evidence of a dynamic leakage coefficient for modelling river-aquifer interactions. J. Hydrol. 347 (1-2), 177-187.

DVGW, 2000. Richtlinien für Trinkwasserschutzgebiete. Deutsche Vereinigung des Gas- und Wasserfachs, DVGW, Bonn.

Eckert, P., Irmscher, R., 2006. Over 130 years of experience with Riverbank filtration in Dusseldorf, Germany. J. Water Supply Res. T. 55 (4), 283-291.

Eckert, P., Lamberts, R., Wagner, C., 2008. The impact of climate change on drinking water supply by riverbank filtration. Water Sci. Technol.: Water Supply 8 (3), 319-324.

Egli, T., 1995. The ecological and physiological significance of the growth of heterotrophic microorganisms with mixtures of substrates. In: Jones, G.N. (Ed.), Advances in Microbial Ecology. Plenum Press, New York, pp. 305-386.

Engeler, I., Hendricks Franssen, H.J., Müller, R., Stauffer, F., 2011. The importance of coupled modelling of variably saturated groundwater flow-heat transport for assessing river-aquifer interactions. J. Hydrol. 397 (3-4), 295-305.

European-Commission, 2000. Directive 2000/60/EC of the European Parliament and of the Council establishing a framework for Community action in the field of water policy. European Commission, Brussels, pp. 72.

124

FOEN, 2012a. Effects of climate change on water resources and watercourses. Synthesis report on the "Climate Change and Hydrology in Switzerland" (CCHydro) project. Federal Office for the Environment FOEN, Bern, pp. 76.

FOEN, 2012b. Groundwater protection zones in unconsolidated rocks. A module for the enforcement guide groundwater protection. Federal Office for the Environment FOEN, Bern, pp. 58.

FOEN, 2012c. Revitalization of water courses. Strategic planning. Federal Office for the Environment, FOEN, Bern, pp. 42.

Froyland, L., 2011. Characterizing the dynamics of groundwater flow in a losing stream. Master Thesis. Norwegian University of Science and Technology, Trondheim, pp. 58.

Gelhar, L.W., Welty, C., Rehfeldt, K.R., 1992. A critical review of data on field-scale dispersion in aquifers. Water Resour. Res. 28 (7), 1955-1974.

Goode, D.J., 1996. Direct simulation of groundwater age. Water Resour. Res. 32 (2), 289-296.

Green, T.R., Taniguchi, M., Kooi, H., Gurdak, J.J., Allen, D.M., Hiscock, K.M., Treidel, H., Aureli, A., 2011. Beneath the surface of global change: Impacts of climate change on groundwater. J. Hydrol. 405 (3-4), 532-560.

Greskowiak, J., Prommer, H., Massmann, G., Nützmann, G., 2006. Modeling seasonal redox dynamics and the corresponding fate of the pharmaceutical residue phenazone during artificial recharge of groundwater. Environ. Sci. Technol. 40 (21), 6615-6621.

Grünheid, S., Amy, G., Jekel, M., 2005. Removal of bulk dissolved organic carbon (DOC) and trace organic compounds by bank filtration and artificial recharge. Water Res. 39 (14), 3219-3228.

GSchG, 2011. Bundesgesetz über den Schutz der Gewässer, 814.20. Die Bundesversammlung der Schweizerischen Eidgenossenschaft, Bern, pp. 32.

GSchV, 2011. Gewässerschutzverordnung, 814.201. Der Schweizerische Bundesrat, Bern, pp. 68.

Harvey, J.W., Bencala, K.E., 1993. The effect of streambed topography on surface-subsurface water exchange in mountain catchments. Water Resour. Res. 29 (1), 89-98.

Hayashi, M., Vogt, T., Machler, L., Schirmer, M., 2012. Diurnal fluctuations of electrical conductivity in a pre-alpine river: Effects of photosynthesis and groundwater exchange. J. Hydrol. 450, 93-104.

Hedges, J.I., Clark, W.A., Quay, P.D., Richey, J.E., Devol, A.H., Santos, U.D., 1986. Compositions and fluxes of particulate organic material in the amazon river. Limnol. Oceanogr. 31 (4), 717-738.

Heitzer, A., Kohler, H.P.E., Reichert, P., Hamer, G., 1991. Utility of Phenomenological Models for Describing Temperature Dependence of Bacterial Growth. Appl. Environ. Microbiol. 57 (9), 2656-2665.

Henze, M., Gujer, W., Mino, T., Matsuo, T., Wentzel, M.C., Marais, G.V.R., Van Loosdrecht, M.C.M., 1999. Activated Sludge Model No.2d, ASM2d. Water Sci. Technol. 39 (1), 165-182.

Hiscock, K.M., Grischek, T., 2002. Attenuation of groundwater pollution by bank filtration. J. Hydrol. 266 (3-4), 139-144.

Hoehn, E., Cirpka, O.A., 2006. Assessing residence times of hyporheic ground water in two alluvial flood plains of the Southern Alps using water temperature and tracers. Hydrol. Earth Syst. Sc. 10 (4), 553-563.

Hoehn, E., Meylan, B., 2009. Measures to protect drinking-water wells near rivers from hydraulic engineering operations in peri-alpine flood-plains. Grundwasser 14 (4), 255-263.

Hoehn, E., Scholtis, A., 2011. Exchange between a river and groundwater, assessed with hydrochemical data. Hydrol. Earth Syst. Sc. 15 (3), 983-988.

Horner, C., Holzbecher, E., Nützmann, G., 2007. A coupled transport and reaction model for long column experiments simulating bank filtration. Hydrol. Process. 21 (8), 1015-1025.

Huggenberger, P., Hoehn, E., Beschta, R., Woessner, W., 1998. Abiotic aspects of channels and floodplains in riparian ecology. Freshwater Biol. 40 (3), 407-425.

IPCC, 2007. Fourth Assessment Report: Climate Change 2007: Impacts, Adaptation and Vulnerability. Summary for Policy-Makers. Intergovernmental Panel on Climate Change, IPCC, New York.

Jacobs, L.A., Von Gunten, H.R., Keil, R., Kuslys, M., 1988. Geochemical changes along a river-groundwater infiltration flow path: Glattfelden, Switzerland. Geochim. Cosmochim. Ac. 52 (11), 2693-2706.

Kalbus, E., Reinstorf, F., Schirmer, M., 2006. Measuring methods for groundwater - Surface water interactions: A review. Hydrol. Earth Syst. Sc. 10 (6), 873-887.

Käser, D.H., Binley, A., Heathwaite, A.L., 2013. On the importance of considering channel microforms in groundwater models of hyporheic exchange. River Res. Appl. 29 (4), 528-535.

Käser, D.H., Binley, A., Heathwaite, A.L., Krause, S., 2009. Spatio-temporal variations of hyporheic flow in a riffle-step-pool sequence. Hydrol. Process. 23 (15), 2138-2149.

Kirschbaum, M.U.F., 1995. The temperature dependence of soil organic matter decomposition, and the effect of global warming on soil organic C storage. Soil Biol. Biochem. 27 (6), 753-760.

Kuehn, W., Mueller, U., 2000. Riverbank filtration - An overview. J. Am. Water Works Ass. 92 (12), 60-69.

Lautz, L.K., Siegel, D.I., 2006. Modeling surface and ground water mixing in the hyporheic zone using MODFLOW and MT3D. Adv. Water Resour. 29 (11), 1618-1633.

Leenheer, J.A., Croue, J.P., 2003. Characterizing aquatic dissolved organic matter. Environ. Sci. Technol. 37 (1), 18A-26A.

Maeng, S.K., Ameda, E., Sharma, S.K., Grützmacher, G., Amy, G.L., 2010. Organic micropollutant removal from wastewater effluent-impacted drinking water sources during bank filtration and artificial recharge. Water Res. 44 (14), 4003-4014.

Malcolm, I.A., Soulsby, C., Youngson, A.F., 2006. High-frequency logging technologies reveal state-dependent hyporheic process dynamics: implications for hydroecological studies. Hydrol. Process. 20 (3), 615-622.

Massmann, G., Greskowiak, J., Dünnbier, U., Zuehlke, S., Knappe, A., Pekdeger, A., 2006. The impact of variable temperatures on the redox conditions and the behaviour of pharmaceutical residues during artificial recharge. J. Hydrol. 328 (1-2), 141-156.

Massmann, G., Nogeitzig, A., Taute, T., Pekdeger, A., 2008. Seasonal and spatial distribution of redox zones during lake bank filtration in Berlin, Germany. Environ. Geol. 54 (1), 53-65.

Matsunaga, T., Karametaxas, G., von Gunten, H.R., Lichtner, P.C., 1993. Redox chemistry of iron and manganese minerals in river-recharged aquifers: A model interpretation of a column experiment. Geochim. Cosmochim. Ac. 57 (8), 1691-1704.

Mayer, D.G., Butler, D.G., 1993. Statistical validation. Ecol. Model. 68 (1-2), 21-32.

Mettler, S., Abdelmoula, M., Hoehn, E., Schoenenberger, R., Weidler, P., von Gunten, U., 2001. Characterization of iron and manganese precipitates from an in situ ground water treatment plant. Ground Water 39 (6), 921-930.

Meybeck, M., 1982. Carbon, nitrogen, and phosphorus transport by world rivers. Am. J. Sci. 282 (4), 401-450.

Mouchet, P., 1992. From conventional to biological removal of iron and manganese in France. J. Am. Water Works Ass. 84 (4), 158-167.

Murdoch, P.S., Baron, J.S., Miller, T.L., 2000. Potential effects of climate change on surface-water quality in North America. J. Am. Water Resour. As. 36 (2), 347-366.

Naegeli, M.W., Hartmann, U., Meyer, E.I., Uehlinger, U., 1995. POM-dynamics and community respiration in the sediments of a floodprone prealpine river (Necker, Switzerland). Arch. Hydrobiol. 133 (3), 339-347.

O'Connell, A.M., 1990. Microbial decomposition (respiration) of litter in eucalypt forests of south-western Australia: an empirical-model based on laboratory incubations. Soil Biol. Biochem. 22 (2), 153-160.

OcCC, 2005. Heat Summer 2003. OcCC/ProClim, Bern, pp. 28.

Park, J.H., Duan, L., Kim, B., Mitchell, M.J., Shibata, H., 2010. Potential effects of climate change and variability on watershed biogeochemical processes and water quality in Northeast Asia. Environ. Int. 36 (2), 212-225.

Pasquale, N., Perona, P., Schneider, P., Shrestha, J., Wombacher, A., Burlando, P., 2011. Modern comprehensive approach to monitor the morphodynamic evolution of a restored river corridor. Hydrol. Earth Syst. Sc. 15 (4), 1197-1212.

Peter, S., Koetzsch, S., Traber, J., Bernasconi, S.M., Wehrli, B., Durisch-Kaiser, E., 2012. Intensified organic carbon dynamics in the ground water of a restored riparian zone. Freshwater Biol. 57 (8), 1603-1616.

Pusch, M., Fiebig, D., Brettar, I., Eisenmann, H., Ellis, B.K., Kaplan, L.A., Lock, M.A., Naegeli, M.W., Traunspurger, W., 1998. The role of micro-organisms in the ecological connectivity of running waters. Freshwater Biol. 40 (3), 453-495.

Reichert, P., Uehlinger, U., Acuna, V., 2009. Estimating stream metabolism from oxygen concentrations: Effect of spatial heterogeneity. J. Geophys. Res.-Biogeosci. 114, 15.

Sacher, F., Brauch, H.J., 2002. Experiences on the fate of organic micropollutants during riverbank filtration. In: Ray, C. (Ed.), Riverbank filtration: understanding contaminant biogeochemistry and pathogen removal. Kluwer, Dordrecht, pp. 135-151.

Schäfer, D., Schäfer, W., Kinzelbach, W., 1998. Simulation of reactive processes related to biodegradation in aquifers - 2. Model application to a column study on organic carbon degradation. J. Contam. Hydrol. 31 (1-2), 187-209.

Schäppi, B., Perona, P., Schneider, P., Burlando, P., 2010. Integrating river cross section measurements with digital terrain models for improved flow modelling applications. Computers and Geosciences 36 (6), 707-716.

Schirmer, M., 2013. Das RECORD-Projekt - Flussrevitalisierung, eine ökologische Massnahme in einem komplexen Umfeld. Aqua und Gas 3, 22-28.

Schneider, P., Vogt, T., Schirmer, M., Doetsch, J., Linde, N., Pasquale, N., Perona, P., Cirpka, O.A., 2011. Towards improved instrumentation for assessing river-groundwater interactions in a restored river corridor. Hydrol. Earth Syst. Sc. 15 (8), 2531-2549.

Schubert, J., 2002. Hydraulic aspects of riverbank filtration - Field studies. J. Hydrol. 266 (3-4), 145-161.

Schwarzenbach, R.P., Giger, W., Hoehn, E., Schneider, J.K., 1983. Behavior of organic-compounds during infiltration of river water to groundwater - field studies. Environ. Sci. Technol. 17 (8), 472-479.

Senhorst, H.A.J., Zwolsman, J.J.G., 2005. Climate change and effects on water quality: a first impression. Water Sci. Technol. 51 (5), 53-59.

Sharma, L., Greskowiak, J., Ray, C., Eckert, P., Prommer, H., 2012. Elucidating temperature effects on seasonal variations of biogeochemical turnover rates during riverbank filtration. J. Hydrol. 428, 104-115.

Simmons, C.S., 1982. A stochastic-convective transport representation of dispersion in one-dimensional porous-media systems. Water Resour. Res. 18 (4), 1193-1214.

Simmons, C.S., Ginn, T.R., Wood, B.D., 1995. Stochastic-convective transport with nonlinear reaction: Mathematical framework. Water Resour. Res. 31 (11), 2675-2688.

Sobczak, W.V., Findlay, S., 2002. Variation in bioavailability of dissolved organic carbon among stream hyporheic flowpaths. Ecology 83 (11), 3194-3209.

Sontheimer, H., 1980. Experience with riverbank filtration along the rhine river. J. Am. Water Works Ass. 72 (7), 386-390.

Soulsby, C., Malcolm, I.A., Tetzlaff, D., Youngson, A.F., 2009. Seasonal and inter-annual variability in hyporheic water quality revealed by continuous monitoring in a salmon spawning stream. River Res. Appl. 25 (10), 1304-1319.

Sprenger, C., Lorenzen, G., Hulshoff, I., Grutzmacher, G., Ronghang, M., Pekdeger, A., 2011. Vulnerability of bank filtration systems to climate change. Sci. Total Environ. 409 (4), 655-663.

Storey, R.G., Howard, K.W.F., Williams, D.D., 2003. Factors controlling riffle-scale hyporheic exchange flows and their seasonal changes in a gaining stream: A three-dimensional groundwater flow model. Water Resour. Res. 39 (2), SBH8-1 - SBH8-17.

Sugimoto, R., Kasai, A., Yamao, S., Fujiwara, T., Kimura, T., 2006. Short-term variation in behavior of allochthonous particulate organic matter accompanying changes of river discharge in Ise Bay, Japan. Estuar. Coast. Shelf Sci. 66 (1-2), 267-279.

Syvitski, J.P., Morehead, M.D., Bahr, D.B., Mulder, T., 2000. Estimating fluvial sediment transport: The rating parameters. Water Resour. Res. 36 (9), 2747-2760.

Toride, N., Leij, F.J., van Genuchten, M.T., 1995. The CXTFIT Code for Estimating Transport Parameters from Laboratory or Field Tracer Experiments, Version 2.0. Research Report No. 137, US Salinity Laboratory, Riverside, CA, pp. 131.

Tufenkji, N., Ryan, J.N., Elimelech, M., 2002. The promise of bank filtration. Environ. Sci. Technol. 36 (21), 422A-428A.

Uehlinger, U., 2006. Annual cycle and inter-annual variability of gross primary production and ecosystem respiration in a floodprone river during a 15-year period. Freshwater Biol. 51 (5), 938-950.

Valentini, A., Garuti, G., Rozzi, A., Tilche, A., 1997. Anaerobic degradation kinetics of particulate organic matter: A new approach. Water Sci. Technol. 36 (6-7), 239-246.

Vavilin, V.A., Fernandez, B., Palatsi, J., Flotats, X., 2008. Hydrolysis kinetics in anaerobic degradation of particulate organic material: An overview. Waste Manage. 28 (6), 939-951.

Vogt, T., Hoehn, E., Schneider, P., Freund, A., Schirmer, M., Cirpka, O.A., 2010a. Fluctuations of electrical conductivity as a natural tracer for bank filtration in a losing stream. Adv. Water Resour. 33 (11), 1296-1308.

Vogt, T., Schneider, P., Hahn-Woernle, L., Cirpka, O.A., 2010b. Estimation of seepage rates in a losing stream by means of fiber-optic high-resolution vertical temperature profiling. J. Hydrol. 380 (1-2), 154-164.

von Gunten, H.R., Karametaxas, G., Keil, R., 1994. Chemical Processes in Infiltrated Riverbed Sediments. Environ. Sci. Technol. 28 (12), 2087-2093.

von Gunten, H.R., Karametaxas, G., Krahenbuhl, U., Kuslys, M., Giovanoli, R., Hoehn, E., Keil, R., 1991. Seasonal biogeochemical cycles in riverborne groundwater. Geochim. Cosmochim. Ac. 55 (12), 3597-3609.

von Gunten, U., Zobrist, J., 1993. Biogeochemical changes in groundwater-infiltration systems: Column studies. Geochim. Cosmochim. Ac. 57 (16), 3895-3906.

Woessner, W.W., 2000. Stream and fluvial plain ground water interactions: Rescaling hydrogeologic thought. Ground Water 38 (3), 423-429.

Wondzell, S.M., LaNier, J., Haggerty, R., 2009. Evaluation of alternative groundwater flow models for simulating hyporheic exchange in a small mountain stream. J. Hydrol. 364 (1-2), 142-151.

Woolsey, S., Capelli, F., Gonser, T., Hoehn, E., Hostmann, M., Junker, B., Paetzold, A., Roulier, C., Schweizer, S., Tiegs, S.D., Tockner, K., Weber, C., Peter, A., 2007. A strategy to assess river restoration success. Freshwater Biol. 52 (4), 752-769.

Wroblicky, G.J., Campana, M.E., Valett, H.M., Dahm, C.N., 1998. Seasonal variation in surface-subsurface water exchange and lateral hyporheic area of two stream-aquifer systems. Water Resour. Res. 34 (3), 317-328.

Zwolsman, J.J.G., van Bokhoven, A.J., 2007. Impact of summer droughts on water quality of the Rhine River - a preview of climate change? Water Sci. Technol. 56 (4), 45-55.